UNIVERSITÀ
DEGLI STUDI
DI PADOVA

Sede Amministrativa: Università degli Studi di Padova

Dipartimento di Biologia

SCUOLA DI DOTTORATO DI RICERCA IN: Bioscienze e Biotecnologie
INDIRIZZO: Neurobiologia
CICLO XXVIII

Alzheimer's disease mouse models based on presenilin-2 N141I: an in vivo study of spontaneous electrical activity by means of hippocampal extracellular recordings

Direttore della Scuola: Ch.mo Prof. Paolo Bernardi
Coordinatore d'indirizzo: Ch.ma Prof.ssa Daniela Pietrobon

Supervisore: Dott.ssa Cristina Fasolato

Dottorando: Roberto Fontana

INDEX

TABLE OF FIGURES

ABBREVIATIONS

Aβ	amyloid-β
Aβo	amyloid-β oligomers
Ab	antibody
AD	Alzheimer's disease
APP	amyloid-β precursor protein
BOLD-fMRI	blood-oxygen-level dependent functional magnetic resonance imaging
CA	*Cornu Ammonis*
Ca^{2+}	calcium ion
DG	dentate gyrus
DOX	doxycycline
ECG	electrocardiogram
EEG	electroencephalogram
ER	endoplasmic reticulum
FAD	familial Alzheimer's disease
FS	fast-spiking
fMRI	functional magnetic resonance imaging
GFAP	glial fibrillary acidic protein
hAPP	human amyloid-β precursor protein
HC	histochemistry
HF	hippocampal formation
HFO	high-frequency oscillations
HG	high gamma
hPS	human presenilin
HRR	hippocampal respiration-induced rhythm
IHC	immunohistochemistry
LFP	local field potential
LTP	long term potentiation
mo	molecular layer
MCI	mild cognitive impairment
MRI	magnetic resonance imaging
MS-DBB	medial septum/diagonal band of Broca
p	p-value
PAC	phase-amplitude coupling
PBS	phosphate buffer solution
PET	positron emission tomography
PIB-PET	Pittsburgh compound B – positron emission tomography
PLC	phospholipase C
PS	presenilin

PS1	presenilin-1
PS2	presenilin-2
PS1KO	presenilin-1 knockout
PS2KO	presenilin-2 knockout
pl	polymorphic layer
SG	slow gamma
sg	*stratum granulosum*
SO	slow oscillation
so	*stratum oriens*
sp	*stratum pyramidalis*
sr	*stratum radiatum*
TEA	transient epileptic amensia
TBS	Tris-buffered solution
VGCC	voltage-gated calcium channel
wt	wild type

1 SUMMARY

Alzheimer's disease (AD) is a neurodegenerative pathology that affects an increasing number of elderly people. It is characterized by progressive impairment in cognition and memory and it is the most frequent cause of dementia, being responsible for 60 to 70 % of the cases over 65 years (World Health Organization, 2015).

The major neuropathological hallmarks of the disease are the deposition of neurofibrillary tangles and senile plaques, primarily in hippocampus, entorhinal cortex and neocortex, and a widespread neuronal loss (Hardy and Selkoe 2002).

AD is divided in sporadic and familial (FAD) forms. FAD is caused by highly penetrating mutations in three genes involved in amyloid-β (Aβ) metabolism: the Aβ precursor protein (*APP*), the presenilin1 (*PSEN1*) and the presenilin2 (*PSEN2*) (Bertram and Tanzi 2011).

The earliest pathological changes are believed to take place in the hippocampal formation and entorhinal cortex (Squire, Stark, Clark 2004). These regions are part of the medial temporal lobe and are fundamental for the encoding of new memories as well as for the fixation of recent ones. Moreover, they are among the first targets of the pathology in terms of tissue abnormalities and neuro-physiological alterations; these latter well correlate with memory deficits, being early symptoms of the disease (Sperling, Mormino, Johnson 2014; Squire, Stark, Clark 2004).

The most prominent network activity patterns in the hippocampus are field potential oscillations in the theta (4 – 12 Hz) and gamma (30 – 100 Hz) frequency bands. Theta and gamma oscillations are considered to play a pivotal role in memory as their properties, namely the amplitude, the frequency and the degree of their coupling, change during memory processes; moreover, they are predictive of learning performance (Lisman and Jensen 2013).

Several brain oscillations have been shown to interact, a phenomenon known as cross-frequency coupling (CFC) (Canolty and Knight 2010). One particular type of interaction consists in the phase of a slower oscillation modulating the amplitude of a faster one, hence the name phase-amplitude CFC (PAC). The PAC of theta on gamma oscillations in the hippocampus has drawn a growing interest since it has proven to be a physiological feature remarkably suited for predicting memory performance (Axmacher et al. 2010; Tort et al. 2009). Most notably, theta-gamma decoupling in the hippocampus impairs memory performance (Shirvalkar, Rapp, Shapiro 2010).

Further, a characteristic of brain electrophysiological signals is the "1/f" behavior of the frequency-domain power spectrum, meaning that the amplitude of each frequency component decays as a function of the frequency. Along with other features, the steepness of the decay has recently been shown to be informative about network activity.

At present, there are no therapies to reliably revert or stop AD. A biomarker (or a combination of biomarkers) for a non-invasive early diagnosis of the pathology – i.e. before the emergence of the cognitive deficits – would improve the efficacy of current and future strategies to contrast the progression of the disease (Sperling and Johnson 2013a).

Notwithstanding, FAD mutations of presenilin 1 (PS1) and, in particular of presenilin 2 (PS2) were shown to determine calcium (Ca^{2+}) homeostasis impairment, a common feature in AD

(Zampese et al. 2011a). In particular, Ca^{2+} defects due to PS2-N141I appear to occur independently of Aβ load (Kipanyula et al. 2012). However, at the brain network level, outcomes due to the mutant PS2 have not been explored.

The aims of this work were (i) the assessment of the effects of the PS2-N141I FAD mutation on the above-mentioned aspects of the hippocampal network activity and (ii) the identification of novel potential electrophysiological markers of the preclinical phase of AD. To these ends, we employed two FAD mouse models, PS2.30H and B6.152H, which express the human PS2-N141I mutation respectively alone or in combination with the human APP Swedish mutation (Ozmen et al. 2009; Richards et al. 2003).

We investigated the local field potential (LFP) signal in the dentate gyrus (DG) region of the hippocampus in the condition of urethane anesthesia. Through the exploitation of frequency and time-frequency methods, we extracted several signal features, including amplitude, spectral steepness and theta-higher frequencies PAC. The temporal evolution of these features was assessed by investigating three age points, namely 3, 6 and 12 months. Additionally, we characterized our transgenic lines for three known molecular and histological biomarker of the disease. We quantified the degree of $A\beta_{42}$ load at each time point while the presence of amyloid plaques and astrogliosis was addressed at 3 and 6 months of age.

At 6 months of age, we report a significant power increase of slow-gamma (SG, 25 – 40 Hz) and high-gamma (HG, 40 – 90 Hz) oscillations in the PS2.30H line and of beta (10 – 25 Hz) and SG oscillations in the B6.152H line. Gamma oscillations and, more generally, a broadband power increase are generated by local network activity and are linked to active computation (Buzsáki and Wang 2012). The enhancement of beta and gamma power that we observe in our models likely reflects neuronal hyperactivity, consistently with similar observations in both sporadic and familial AD as well as in several AD mouse models (Stargardt, Swaab, Bossers 2015). In our mouse lines, this is the first time that the condition of neural network hyperactivity is described, although *in vitro* neuronal Ca^{2+} hyperexcitability was previously reported (Kipanyula et al. 2012). In B6.152H mice, hyperactivity was timed with the appearance of amyloid plaques and astrogliosis, whereas in PS2.30H mice no molecular or histological biomarker significantly differed from the wt (wild-type) line at any investigated age. The observed hyperactivity is possibly due to the expression of the mutant PS2, rather than to the Aβ load which we probed to be profoundly different in the two AD mouse lines.

Only in the B6.152H line we found a more complex pattern of alterations. In addition to the broadband power increase, we report an enhancement of theta-beta and -SG PAC in this line at 6 months. Moreover, B6.152H mice displayed a steeper power spectrum slope compared to wt mice at 3 and 6 months of age. Both the overcoupling and the steeper spectral slope are ascribable to a condition of neuronal hyper-synchronicity, though with notable differences (Voytek and Knight 2015). Remarkably, we found that the difference between B6.152H and wt mice in terms of steepness was strongest at 3 months of age and diminished with ageing. Therefore, although further investigation will be required to validate this finding, hippocampal network hyper-synchronicity appears to be a promising early marker of the disease, at least in the context of a high Aβ load.

2 RIASSUNTO

La malattia di Alzheimer (AD, *Alzheimer's disease*) è una patologia neurodegenerativa che colpisce un numero crescente di anziani. E' caratterizzata da progressivo indebolimento delle funzioni cognitive e della memoria ed è la causa più comune di demenza, essendo responsabile del 60 – 70 % dei casi al di sopra dei 65 anni (World Health Organization, 2015).

I principali elementi neuropatologici caratteristici della malattia sono la deposizione di ammassi neurofibrillari e placche senili, *in primis* in ippocampo, corteccia entorinale e neocorteccia, e una diffusa perdita di neuroni.

L'AD si divide nelle forme sporadica e familiare (FAD, *familial AD*). La FAD è causata da mutazioni ad alto grado di penetranza a carico di tre geni coinvolti nel metabolismo della β-amiloide (Aβ, *amyloid-β*): Aβ precursor protein (*APP*), presenilin1 (*PSEN1*) e presenilin2 (*PSEN2*) (Bertram and Tanzi 2011).

Si ritiene che i primi cambiamenti patologici abbiano luogo nella formazione ippocampale e nella corteccia entorinale (Squire, Stark, Clark 2004). Queste regioni fanno parte del lobo medio-temporale e sono fondamentali per la codifica di nuovi ricordi, così come per la fissazione di quelli recenti. Esse, inoltre, rientrano tra i primi bersagli della malattia in termini di alterazioni istologiche e neuro-fisiologiche; queste ultime correlano bene con i deficit mnemonici e sono considerate sintomi precoci della malattia (Sperling, Mormino, Johnson 2014; Squire, Stark, Clark 2004).

In ippocampo l'attività di network più evidente è data dalle oscillazioni dei *field potentials* nelle bande di frequenza theta (4 – 12 Hz) e gamma (30 – 100 Hz). Si ritiene che le oscillazioni theta e gamma giochino un ruolo centrale nei processi di memoria, in quanto le loro proprietà, ovvero l'ampiezza, la frequenza e il loro grado di accoppiamento, cambiano durante i processi mnemonici; inoltre, esse sono predittive della prestazione di apprendimento (Lisman and Jensen 2013).

E' dimostrato che molte oscillazioni cerebrali interagiscono tra di loro, un fenomeno noto come *cross-frequency coupling* (CFC) (Canolty and Knight 2010). Una particolare tipologia di interazione consiste nella modulazione esercitata dalla fase di un'oscillazione più lenta sull'ampiezza di un'altra più veloce, da cui il nome CFC fase-ampiezza (PAC, *phase-amplitude CFC*). In ippocampo, il PAC delle oscillazioni theta sulle gamma ha attratto un crescente interesse, in virtù del fatto che ha dato prova di essere un aspetto fisiologico notevolmente adeguato per predire la prestazione mnemonica (Axmacher et al. 2010; Tort et al. 2009). In particolare, la perdita di *coupling* in ippocampo compromette il processo di apprendimento (Shirvalkar, Rapp, Shapiro 2010).

Inoltre, una caratteristica dei segnali elettrofisiologici cerebrali è il comportamento "1/f" dello spettro di potenza nel dominio della frequenza, nel senso che l'ampiezza di ogni componente in frequenza decade in funzione della frequenza. Assieme ad altre caratteristiche, la rapidità di decadimento dello spettro di potenza (*steepness*), misurata come pendenza della funzione in una rappresentazione semilogaritmica, si è rivelata particolarmente informativa dell'attività di network.

Allo stato attuale, non esistono terapie efficaci per arrestare o far regredire l'AD. Un marcatore (o una combinazione di marcatori) per una diagnosi precoce non invasiva della patologia – cioè prima della comparsa dei deficit cognitivi – migliorerebbe l'efficacia delle strategie attuali e future per contrastare la progressione della malattia (Sperling and Johnson 2013a).

Inoltre, è stato provato che le mutazioni FAD della presenilina 1 (PS1) e della presenilina 2 (PS2) sono in grado di alterare l'omeostasi del calcio (Ca^{2+}) intracellulare, una caratteristica comune nell'AD (Zampese et al. 2011a). Recentemente, è stato poi dimostrato che gli effetti della PS2-N141I sull'omeostasi del Ca^{2+} sono precoci ed indipendenti dai livelli di Aβ (Kipanyula et al. 2012; Zampese et al. 2011a) Tuttavia, gli effetti della PS2 mutata a livello del network cerebrale non sono stati ancora esplorati.

Gli obiettivi di questo lavoro erano (i) la valutazione degli effetti della mutazione FAD PS2-N141I sugli aspetti sopracitati dell'attività di rete ippocampale e (ii) l'identificazione di nuovi potenziali marcatori elettrofisiologici della fase preclinica dell'AD. A tal fine, abbiamo impiegato due modelli murini di FAD, PS2.30H e B6.152H, che esprimono la mutazione umana PS2-N141I, rispettivamente da sola o in combinazione con la mutazione Svedese dell'APP umana (Ozmen et al. 2009; Richards et al. 2003).

Abbiamo studiato il *local field potential* (LFP) nella regione del giro dentato (DG, *dentate gyrus*) in ippocampo, nella condizione di anestesia con uretano. Attraverso metodi di analisi in frequenza e tempo-frequenza, abbiamo estratto diverse caratteristiche del segnale, tra cui l'ampiezza, la pendenza spettrale e il PAC tra oscillazioni theta e a frequenze maggiori. L'evoluzione temporale di queste caratteristiche è stata valutata analizzando tre età, ovvero 3, 6 e 12 mesi. Inoltre, abbiamo caratterizzato le nostre linee transgeniche per tre noti marker molecolari ed istologici della malattia. Abbiamo quantificato il livello di $A\beta_{42}$ ad ogni punto temporale, mentre la presenza di placche amiloidi e di astrogliosi è stata investigata a 3 e 6 mesi di età.

A 6 mesi di età, riportiamo un significativo aumento della potenza delle oscillazioni *slow-gamma* (SG, 25 - 40 Hz) e *high-gamma* (HG, 40 - 90 Hz) nella linea PS2.30H e delle oscillazioni beta (10 - 25 Hz) e SG nella linea B6.152H. Le oscillazioni gamma e, più in generale, un aumento di potenza ad ampio spettro, sono generate dall'attività del network locale e riflettono processi di computazione attiva (Buzsáki and Wang 2012). L'aumento della potenza nelle oscillazioni beta e gamma che osserviamo nei nostri modelli riflette, probabilmente, iperattività neuronale, coerentemente con osservazioni simili riportate nelle forme sia sporadica che familiare dell'AD, così come in diversi modelli murini di AD (Stargardt, Swaab, Bossers 2015). Nelle nostre linee, questa è la prima volta che la condizione di iperattività neurale di network è descritta, anche se *in vitro* era stata precedentemente riportata ipereccitabilità neuronale basata sul Ca^{2+} (Kipanyula et al. 2012). Nei topi B6.152H, l'iperattività coincide temporalmente con la comparsa delle placche amiloidi e dell'astrogliosi, mentre nei topi PS2.30H nessun marcatore molecolare o istologico risulta significativamente diverso dalla linea wt (*wild-type*) a qualunque delle età indagate. L'iperattività osservata è probabilmente dovuta all'espressione della PS2 mutata, piuttosto che al livello di Aβ, il quale si è rivelato essere profondamente diverso nelle nostre due linee modello dell'AD.

Solo nella linea B6.152H abbiamo trovato un pattern più complesso di alterazioni. Oltre all'aumento di potenza ad ampio spettro, riportiamo un incremento del PAC tra oscillazioni theta e beta e tra theta e SG in questa linea a 6 mesi. Inoltre, i topi B6.152H mostrano una forte pendenza del *power spectrum* rispetto ai topi wt a 3 e 6 mesi di età. Sia l'*overcoupling* che l'incremento della pendenza spettrale sono riconducibili ad una condizione di iper-sincronicità neuronale, anche se con differenze importanti (Voytek and Knight 2015). È da notare che la differenza tra topi B6.152H e wt in termini di pendenza spettrale è più marcata a 3 mesi di età e diminuisce con l'invecchiamento. Pertanto, anche se ulteriori indagini saranno necessarie per convalidare questa osservazione, l'ipersincronicità del network ippocampale sembra essere un promettente marcatore precoce della malattia, almeno nel contesto di alti livelli di Aβ.

3 INTRODUCTION

The study of the brain encompasses multiple levels, ranging from the molecular and biophysical mechanisms underlying single neurons function to the complex web of their interactions that drives cognition and consciousness. Importantly, brain is a complex system, which basically means (i) that all the different levels organize in a hierarchical fashion, where each-level behavior is molded from the activity of both the higher and the lower level and (ii) that the qualities of the activity at a given level do not merely result from the sum of the properties of the basic constituents of that level but also emerge as novelties from the interaction among them. From this perspective, brain functioning has necessarily to be addressed at multiple scales. For instance, we cannot fully understand cognition by only considering the operation of single neurons and their connections. Rather, we need to further look at neuronal network activity as a whole.

In particular, a number of neurological disorders, including AD, Parkinson's disease, schizophrenia, epilepsy and autism, are associated with various forms of cognitive impairment and, historically, their pathophysiology has been studied focusing on molecular, cellular and pharmacologic aspects.

Only recently, the fast development and improvement of techniques that allow the investigation of brain at a multi-scale level, on one hand, and the enrichment of the tool-box for signal processing and analysis on the other, have provided an unprecedented understanding of neuronal networks. This permits to investigate the functional network alterations that occur in neurological disorders, which represents a mesoscale bridging between the molecular/cellular aspects of the disorders and their effects on cognition.

In the introduction, we first provide an overview of the techniques for recording or imaging neuronal network activity in vivo as well as the information that is obtainable from such data. Next, we briefly present the hippocampus, the brain structure on which the present study is focused. Finally, we describe the AD, its pathological as well as diagnostic aspects and some of the major recent findings regarding network alterations in the disease.

3.1 FUNCTIONAL ACTIVITY OF THE BRAIN

3.1.1 Neural activity recording

Ideally, in order to investigate brain functioning, it should be possible to simultaneously assess neuronal activity at all spatial scales and with sufficient temporal resolution to adequately describe the fastest events. Unfortunately, none of the available technologies is able to simultaneously record the activity of a large number of neurons at the single-cell level and in the milliseconds timescale, as it is required for describing the action potentials (AP). Likewise, none of them is capable to continuously scale across all the different levels. All the approaches that are summarized here are a compromise between spatial and temporal resolution and each of them has advantages as well as limitations in addressing different aspects of brain activity.

The most direct and detailed way to gather information about brain functioning is the recording of the intracellular electrical activity of single neurons. The technique of choice for performing this task is the patch-clamp, where a glass pipette containing the recording electrode is brought in very tight contact with the cell membrane and the patch of membrane under the contact area is torn so that the electrode is in contact with the intracellular domain. The patch-clamping technique offers unparalleled spatial and temporal detail, however it is only exploitable for recording from few cells at the same time. Hence, its usage for the investigation of neuronal networks is often very limited and the technique is generally confined to the study of cellular and sub-cellular dynamics. Nevertheless, accumulating findings proved patch-clamp useful at the network scale when combined with other higher level approaches.

Neuronal electric activity – be it action potentials (APs), subthreshold fluctuations, or post-synaptic potentials (PSP) – consists in continuous changes of transmembrane potential. Such changes rely on current flow across the membrane and, thus, they mobilize ions to and/or from the extracellular milieu. Therefore, at this level, the electric potential recorded at a given point results from the linear sum of the electric fields generated by the ongoing activity of all the neurons surrounding the recording site. This type of recording is referred to as LFP, emphasizing the "local" nature of the acquired signal. Indeed, extracellular ionic current propagation is attenuated as a function of the distance from the source, owing to the resistance of the medium and the presence of cell membranes on the path. Importantly, fast events are more affected than slow events. It follows that, for instance, a PSP-induced current can travel further with respect to an AP-induced one.

Highly sensitive electrodes placed on the scalp of a subject exploit the same principle of the LFP as they detect the electric fields generated by the sum of the neuronal activities in a very large volume. This technique is called electroencephalography (EEG) and it allows the non-invasive simultaneous recording from a number of sites above the brain surface. The recorded signal is, however, affected by the distortion and the attenuation exerted by the meninges, the skull and the scalp as the current travels through them. The temporal resolution is ideally the same as in the intracellular recording but in practice only relatively slow activities reach the scalp electrodes.

Somehow in between the LFP and the EEG in terms of spatial resolution and invasiveness it is the electrocorticography (ECoG), which consists in the subdural application of a grid of electrodes over the brain, in direct contact with the cerebral cortex. The advantage with respect to the EEG is a large increase in spatial resolution and signal amplitude as well as a strong decrease of muscle artifacts. Nevertheless, the ECoG signal is largely confined to the cortex and this technique can hardly be exploited for investigating deep brain dynamics. Yet, the most important drawback of ECoG is invasiveness: although it is less harmful to the brain when compared to implanting LFP recording electrodes, the procedure requires a surgical operation, hindering its usage in humans for solely research purposes.

Owing to historical reasons, it is conventional the usage of the EEG, ECoG and LFP terms as I described above. In this work, we always refer to them accordingly. However, it is noteworthy that a strict definition of the EEG signal would trace it as a synonymous of extracellular-

recording. As such, the EEG notion would encompass both the ECoG and the LFP signals and, indeed, these latter are sometimes referred to as depth, micro- or intracranial EEG.

One of the fundamental principles in electromagnetism is the reciprocal behavior of electric and magnetic fields. It follows that it is possible to exploit the variations of magnetic field to infer the voltage changes due to neuronal activity. This is, indeed, the underlying principle of the magnetoencephalography (MEG). As in the EEG, MEG sensors are capable of monitoring brain signals from outside the head, ensuring non-invasiveness. In this case, sensors are superconducting quantum interference device (SQUID) which operate at -270 °C in order to detect the very weak magnetic signals that arise from the brain. Contrarily to electricity, magnetic signal propagation is not hindered by air, thus, MEG sensors do not even need to be attached to the subject's head. Yet, the major advantage of the MEG is the fact that the magnetic signal is spared from any distortion as it crosses the overlaying tissues, which is beneficial mainly to spatial resolution.

A more indirect approach is called functional magnetic resonance imaging (fMRI). This technique images the brain and returns a map of the active areas at a given moment. The principles and the assumptions on which fMRI is based are several. A strong magnetic field is applied to the subject's body so that the spin of every atom becomes aligned to the magnetic field. Then, a radio frequency (RF) pulse at the frequency specific for the atom of interest is applied. Consequently, the atom-containing molecules are perturbed from the preferred alignment and, once the RF pulse ceases, the atoms realign with the magnetic field releasing energy. This latter is detected from sensors placed around the head. In magnetic resonance imaging (MRI) the target atom is hydrogen and the procedure yields contrasted anatomical images, useful for structural investigation of the brain. The main type of fMRI, instead, targets hemoglobin. In particular, it exploits (i) the reduced magnetic susceptibility of oxygenated versus deoxygenated hemoglobin and (ii) the hemodynamic response – i.e. the modulation of blood and oxygen supply depending on the energetic demand in a given region. Accordingly, it is called blood oxygen level-dependent (BOLD) fMRI. Basically, when a neuronal ensemble becomes active, it triggers blood supply enhancement to support the increased energy consumption (functional hyperemia). Consequently, the relative area results enriched in oxygenated hemoglobin and the changing is monitored as a variation of magnetic resonance. When statistically significant, the changing is reported on the map of active areas.

Concerning the spatial resolution, the fMRI offers remarkably detailed information while providing a whole brain image, thus empowering to investigate brain function during cognitive tasks as well as while in "resting state". However, the two major drawbacks of this technique arise from its indirect nature: (i) the temporal resolution mainly depends on the physiological kinetics that regulates oxygenated blood recruitment. This type of kinetics is on the order of seconds; (ii) the blood supply to a given area increases in response to whatsoever neuronal activity. Hence, the exact nature of the activity responsible for the increased energetic demand – whether it is e.g. neuronal firing or synaptic activity – remains elusive and can only be inferred.

Positron emission tomography (PET) is yet another advanced imaging method capable of visualizing brain function. The technique roughly consists in the injection or inhalation of a

biologically active molecule carrying a radiolabeled compound. As this latter decays, positrons are emitted and, indirectly, gamma rays are produced and can be detected by the ring sensor of the PET scanner. Therefore, it is possible to monitor the dynamics of the tagged biological molecule, although with lower temporal and spatial resolution than in fMRI. Fluorodeoxyglucose (FDG), an analogue of glucose, is often used as tracer, providing spatial and temporal information on glucose uptake and thus, similarly to BOLD-fMRI, on the metabolic activity in a given area.

As a final comment, we wish to underlie that, despite its usage in clinical and research settings dating back to 1929 – when Hans Berger first described the EEG – the extracellular electrophysiology is still a developing field, in particular concerning signal analysis. For decades, EEG recordings were investigated by sole ocular assessment. Only recently, the advent of a handful of data processing tools, in conjunction with the development of ever-faster computers empowering to routinely exploit them, has opened new avenues for neural physiology and pathophysiology understanding.

(Adeli and Ghosh-Dastidar 2010; Buzsaki 2006a; Buzsáki, Anastassiou, Koch 2012; Sporns 2011)

3.1.2 Neuronal networks and brain oscillations

What bridges between the microscale of single neurons and synapses activity and the macroscale of cognition and consciousness is the integrated connection of the units into networks that dynamically organize on hierarchical levels. As described in the previous paragraph, different techniques are better suited for investigating brain activity and functioning depending on the targeted level of organization (Sporns 2011).

The emergent feature of single neurons is the AP. Various types of membrane ionic conductance feature distinct biophysical properties, accounting for either specific or nonspecific ionic flow and conditions and parameters of the flow. Yet, particular assortments of ion channels give rise to the autocatalytic all-or-none phenomenon, the AP, suited for reliably binary encoding and information transmitting. At the opposite extreme, the richness of psychological categories (James 1890), including perceptions and emotions, is the grand emergent feature of the cerebral cortex working as a whole.

From an intermediate magnification, one of the most striking phenomena that spontaneously emerges is rhythmicity, the result of integrated network activity of neurons and astrocytes, that is easily observable by means of extracellular electric signal recording.

The first brain electrophysiological oscillatory pattern was described in 1929 by Hans Berger (Berger 1929). He observed that, if a subject was in a relaxed state and with eyes closed, a marked oscillation of the EEG signal appeared, in particular in the occipital region. The oscillation had a period of approximately 100 ms – 10 Hz – and Berger called it “alpha”. In addition, when the subject opened the eyes, the alpha rhythm disappeared in favor of a faster, smaller amplitude one, that he named “beta”.

Since Berger’s seminal findings, the oscillatory features of the extracellular brain signal have been extensively studied (Steriade et al. 1990). Several other rhythms were described in distinct areas as well as during various cognitive states and were generally named with Greek letters. These include delta (or slow waves), theta, spindles and gamma. They added on Berger’s alpha

and beta. In 1974, the oscillatory classes where classified in a taxonomy mainly intended for clinical purposes (International Federation of Societies for Electroencephalography and Clinical Neurophysiology 1974).

Delta oscillations have a frequency range of 0.5-4 Hz and are predominant during deep sleep phases. Theta rhythms are prominent in the hippocampal formation and emerge during rapid eye movement (REM) sleep as well as in correspondence with various exploratory activities in the awake animal (Buzsáki 2002). Although clinical classification of theta oscillations defines their range as of 4-8 Hz (International Federation of Societies for Electroencephalography and Clinical Neurophysiology 1974), this rhythm is the most variable across species in terms of frequency (Buzsáki, Logothetis, Singer 2013). Alpha waves (8-13 Hz) are present during wakefulness particularly over the occipital cortex and increase during attention tasks (Ray and Cole 1985). Spindles are waxing and waning oscillations with a frequency between 7 and 14 Hz, occurring every 5-10 sec and lasting 1.5-2 sec. Differently from alpha waves, spindles mark the light stage of sleep. In particular, they were characterized in the transition from waking to sleep (Steriade and Deschenes 1984). Beta oscillation occur in the range of 12-30 Hz and are generally associated with active thinking and, in particular when recorded over the motor areas, with voluntary movement suppression. Gamma rhythm encompasses a broad range of frequencies, from 30 to 90 Hz in the traditional taxonomy. While it is found ubiquitously in the cerebral cortex, on the other hand it is a local network rhythm. Yet, notably, distant networks can display synchronized gamma oscillations under certain circumstances (Buzsáki and Wang 2012).

The characteristics of the oscillatory extracellular signal are determined by the proportional contribution of all the ongoing cellular electric activities, including APs, PSPs, subthreshold fluctuations, as well as on the properties of the tissue. Nevertheless, brain oscillations should not be diminished to epiphenomena or poorly revolved approximations of the overall neuronal activity. On the contrary, the rhythmic oscillation, in turn, provides “contextual constraints”, influencing single neuron activity. Network oscillations bias neuron membrane potential and, thus, favors or opposes firing in response to synaptic input, synchronizes neurons into assemblies and modulate synaptic plasticity (Buzsáki and Draguhn 2004).

3.2 THE HIPPOCAMPAL FORMATION

The hippocampal formation (HF), often simply called “hippocampus”, is a medial temporal lobe structure, located under the cerebral cortex. Its general definition includes the territories of DG, *Cornu Ammonis* (CA) – or hippocampus proper – and subiculum on the basis of the three layered architecture that they share. This is the HF designation that will be used here. Yet, the denomination ”hippocampal formation” is sometimes extended to the presubiculum, the parasubiculum and the entorhinal cortex (EC), in light of the involvement of all these districts in the declarative memory function. Indeed, although a definitive answer in regard to the function of the hippocampus has not yet emerged, a large deal of evidence indicates that the medial temporal lobe in general, and the HF in particular, are essential brain components for anterograde declarative (i.e., consciously recallable) memory formation as well as for consolidating information from working to long-term memory (Andersen et al. 2006; Squire,

Stark, Clark 2004). Clinical investigation of patients with brain damage against the hippocampal region, including the famous cases of H.M. (temporal lobe surgery), N.A. (accident) and R.B. (ischemia), report the impairment of anterograde declarative memories formation as a common trait along with an intact ability of procedural (or non-declarative) memory learning (Purves 2004). On the other hand, studies based on fMRI in humans show that the formation of new episodic memory is associated with DG, CA2 and CA3 activation, though this is not the case during memory retrieval (Kirwan and Stark 2004; Zeineh et al. 2003).

Nevertheless, it should be noted that the hippocampus has also been implicated in other functions, including processing of olfactory information (Kay and Lazzara 2010; Vanderwolf 2001), spatial navigation (Craig and McBain 2015) and time-space codification (Nielson et al. 2015). Therefore, the complete picture of hippocampal function is likely to be complex. L. R. Squire broadly defined the hippocampus function as follows: "The hippocampus is important in both spatial and nonspatial tasks where new information must be acquired and associated in ways that allow it to be used flexibly to guide behavior" (Squire, Stark, Clark 2004).

Figure 1, reports the main connectivity of the HF. The circuitry in largely, yet not only, unidirectional, with the EC serving as a major input provider. Neurons in the superficial layers II and III of the EC project, respectively, to the DG and CA3 and to the CA1 and subiculum regions. The granule cells of the DG are the main target of the EC layer II axons, these latter forming the so-called "performant-path". DG granule cells, in turn, send axons (or "mossy fibers") principally to the CA3 region, where the main recipient are the pyramidal cells. The outbound projections of CA3 pyramidal cells form the Schaffer collaterals which make synapses onto the pyramidal cells in the CA2 and CA1 regions. CA1 pyramidal cells project axons to the subiculum and, finally, this latter jointly with CA1 form the major output of the HF by sending axons back to the V layer of entorhinal cortex. Also, while the principal target of the cortical projections of the subiculum is the EC, the former constitutes the major output to the subcortical regions. (Andersen et al. 2006). Only the excitatory glutamatergic connections compose the hippocampal connectivity just described. Yet, in addition to the EC glutamatergic input, another widely studied drive to the

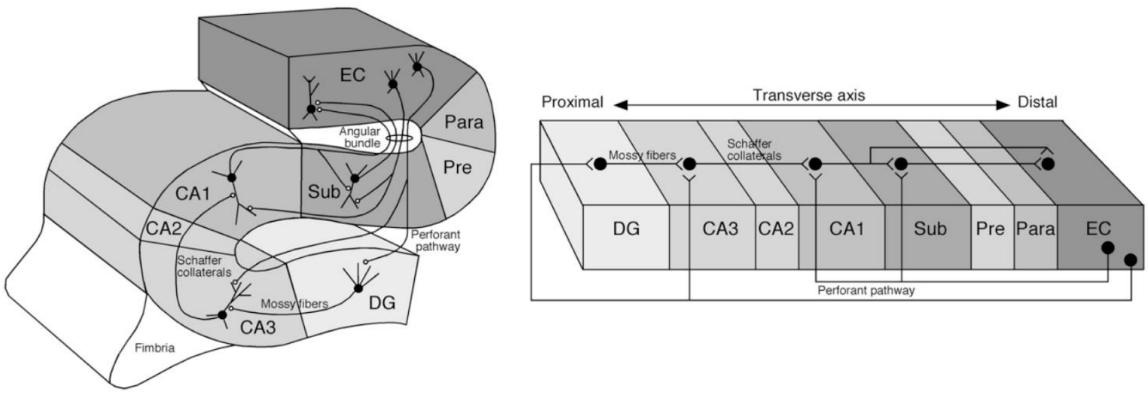

Figure 1. Hippocampal formation and main circuitry. The scheme describes the largely unidirectional connectivity in the hippocampus. Neurons in the superficial layers of the EC, which is the principal communication node between hippocampus and cortex, project to CA3 the DG through the perforant path. DG neurons form the mossy fibers and synapse onto CA3 neurons. Neurons in the CA3 subfield send axons to CA1 forming the Shaffer collaterals. CA1 neurons project to the subiculum and the deep layers of the EC. Efferences of the subiculum form synapses in the deep layers of the EC and form the principal output to the subcortical regions. Image adapted from (Andersen et al. 2006).

HF that we wish to mention is the cholinergic/GABAergic input from the medial septal nucleus and the nucleus of the diagonal band of Broca (MS-DBB) through the fimbria-fornix pathway onto the DG region. These input connections in the DG arising from this pathway are few compared to the performant path, nonetheless they play an important role in the generation of hippocampal theta oscillation (Andersen et al. 2006).

3.2.1 Theta-Gamma oscillations and memory

Theta and gamma oscillations are the principal oscillatory activities occurring in the hippocampus under physiological conditions (Bragin et al. 1995; Vanderwolf 1969). Both rhythms have been implicated in anterograde memory formation, working memory functioning and short-term memory retrieval (Lisman and Jensen 2013). In particular, theta power increased in successful memory encoding and in working memory retrieval (Kahana, Seelig, Madsen 2001; Lega, Jacobs, Kahana 2012) as well as during navigation (Vanderwolf 1969). In addition, the phase of the theta was shown to influence synaptic plasticity, with long-term potentiation (LTP) favored at the peak of the wave and depotentiation favored at the trough (Holscher, Anwyl, Rowan 1997). On the other hand, gamma power increases during memory encoding and correlates with successful subsequent recall (Sederberg et al. 2007a; Sederberg et al. 2007b). Furthermore, gamma power both remains high during the holding period in working memory tasks and positively correlates with memory load (Van Vugt et al. 2010).

Most notably, besides being present during memory storage, theta and gamma changes were capable to predict learning (Fell et al. 2011; Sederberg et al. 2007b) and retrieval performance (Lega, Jacobs, Kahana 2012).

Several brain oscillations have been shown to interact, a phenomenon known as CFC (Canolty and Knight 2010). The most commonly studied type of interaction consists in the phase of a slower oscillation modulating the amplitude of a faster one, hence the name PAC. The PAC of theta on gamma oscillation in the hippocampus has drawn a growing interest since it has proven to be a physiological feature remarkably suited for predicting memory formation (Axmacher et al. 2010; Lega et al. 2016) and recall (Shirvalkar, Rapp, Shapiro 2010). Most notably, theta-gamma decoupling in the hippocampus impairs memory performance (Shirvalkar, Rapp, Shapiro 2010). In this context, theta-gamma PAC is regarded as a bridge between local microscale neuronal ensembles and the systems-level macroscale network, allowing for dynamic network communication (Voytek and Knight 2015).

While the mechanisms governing the generation of APs are well understood, the dynamics at the basis of extracellular field oscillations have only partially been unveiled. Hippocampal theta rhythm is considered as a “consortium of mechanisms” (Buzsáki 2002), since it springs from the conjunction of intracellular and synaptic properties. Hippocampal theta depends on (i) intrinsic resonance properties of pyramidal neurons, (ii) interneurons-mediated inhibitory feedback and (iii) cholinergic inputs from the MS-DBB (Buzsáki 2002). Indeed, while MS-DBB lesions both abrogate theta oscillations in the hippocampus and impair memory (Winson 1978), the administration of muscarinic agonists to MS-DBB increases theta power (Lawson and Bland 1993) and favors learning (Markowska, Olton, Givens 1995). More recently, theta rhythm was alternatively proposed to be primarily relayed to the DG, in the HF, from the EC by means of

glutamatergic synaptic currents (Pernía-Andrade and Jonas 2014). Gamma oscillations, on the other hand, emerge as a result of the excitatory-inhibitory feedback connection between pyramidal cells and parvalbumin-expressing (PV) interneurons (Buzsáki and Wang 2012; Colgin and Moser 2010).

3.3 ALZHEIMER'S DISEASE

AD is an incurable neurodegenerative disease ultimately leading to death. It is the most common type of dementia (or major neurocognitive disorder) accounting for 60 to 70 % of the cases (World Health Organization, 2015). The Alzheimer's Association estimates the 11 % of Americans aged 65 or older to be affected (Alzheimer's Association, 2015). AD is generally characterized by cognitive symptoms including memory loss, difficulty completing familiar tasks, confusion, decreased or poor judgement, changes in mood and personality (Alzheimer's Association, 2015). Moreover, AD is largely associated with two neuropathological elements: the extracellular accumulation of amyloid plaques and the intracellular aggregation of neurofibrillary tangles (Selkoe 1991). Yet, the correspondence is not always consistent.

3.3.1 Historical background

AD is named after Alois Alzheimer's, who first described the pathology in his patient, Auguste Deter. He closely observed the clinical manifestations in her case for almost 5 years before she died and he investigated the neuropathology in her brain tissues after death. He reported progressive cognitive impairment – including reduced comprehension and memory – hallucinations, delusions and psychosocial incompetence along with the presence of evenly distributed miliary foci (later called senile plaques), neurofibrillary tangles and arteriosclerotic changes in the necroptic brain tissues (Alzheimer 1907; Maurer, Volk, Gerbaldo 1997).

Several other cases (Alzheimer 1911; Fischer 1907; Perusini 1909) were described shortly after Alzheimer's observations and AD started being considered a clinical-pathological entity, exhibiting a consistent correspondence between the clinical symptoms and histopathological traits, these latter in the form of senile plaques and neurofibrillary tangles. Although similar cases had been previously described in elderly people and acknowledged as senile dementia, Auguste D.'s relatively young age – 51 years at the time of her illness onset – was suggestive of a discrete disease, distinguishable from senile dementia occurring in the elders. This bias explains why AD was initially recognized as a rare presenile dementia (Ryan, Rossor, Fox 2015). Only several decades later, the continuum between AD and senile dementia became clearly apparent (Katzman 1976; Tomlinson, Blessed, Roth 1970). Finally, it was discovered that senile plaques derive from the extracellular deposition of Aβ protein (Glenner and Wong 1984) while intracellular aggregation of tau proteins is responsible for the neurofibrillary tangles (Goedert et al. 1988).

3.3.2 AD clinical diagnosis

The new unified picture paved the way to the definition of novel comprehensive clinical criteria (McKhann et al. 1984) for the diagnosis of AD that have since been in use (American

Psychiatric Association 2013). Probable AD is diagnosed when the following parameters are fully met:

- Established dementia;
- Deficits in at least two areas of cognition;
- Progressive worsening of memory and other cognitive functions;
- No disturbance of consciousness;
- Onset between ages of 40 and 90;
- Absence of systemic disorders.

Definitive diagnose requires histopathologic evidence in addition to the abovementioned criteria.

Although, there is no large consensus over the clinical stages of the disease, the American Psychiatric Association recognizes three levels of severity in AD, as any other dementia, that can be distinguished basing on the hindrance of daily living (American Psychiatric Association 2013):

- Mild: difficulties with instrumental activities;
- Moderate: difficulties with basic activities;
- Severe: fully dependent on caregivers.

Furthermore, the condition where a subject displays light but measurable cognitive decline, yet not satisfying the criteria for AD, has historically been called Mild Cognitive Impairment (MCI) (Petersen et al. 2001). MCI does not necessarily represent a prelude to AD, as only some 5 % of patients progress from MCI to AD each year. On the other hand, where the MCI involves memory problems - amnesic MCI (aMCI) - the risk of developing AD increases. For this reason, aMCI is sometimes referred to as preclinical AD or prodromal AD (Manly et al. 2008).

Recently these criteria were revised in order to account for the more complex picture that has meanwhile emerged (Jack et al. 2011) and that we summarize in the next paragraphs.

3.3.3 Genetics of AD

Families presenting patterns of AD suggestive of dominant autosomal transmission have long been known (Ryan, Rossor, Fox 2015). Yet, only in 1991 a linkage analysis in one of those families identified, on chromosome 21, the first fully penetrant dominant gene: *APP* (Aβ precursor protein) (Goate et al. 1991). Two other genes, *PSEN1* (presenilin 1) and *PSEN2* (presenilin 2), were discovered few years later on chromosome 14 and 1, respectively (Rogaev et al. 1995).

Mutations in one of these three genes invariably cause the disease – with the notable exception of two *APP* mutations providing protection against AD (Di Fede et al. 2009; Jonsson et al. 2012) – and account for the large majority of cases of autosomal-dominant inheritance. Additionally, two recessive pathological *APP* mutations are known (Di Fede et al. 2009; Tomiyama et al. 2008). The condition is known as FAD, with *PSEN1* mutations being responsible for most of FAD cases (Ryan, Rossor, Fox 2015) and *PSEN1* and *PSEN2* together accounting for 90% of FAD case (Honarnejad and Herms 2012).

While AD-linked mutations in *APP* and *PSEN*s account for the full penetrance of FAD, other genes were shown to be involved in modulating the probability of developing the disease, without necessarily determining it (Bertram and Tanzi 2011; Guerreiro and Hardy 2014). The strongest described genetic risk factor was identified in *APOE* (Apolipoprotein E) epsilon allele (*ApoE4*), which increase one's odds to develop AD by a 3- or 8- to 12-fold factor, depending on number of copies (Saunders et al. 1993).

Notably, FAD causing genes are associated with a form of AD that develops particularly early in life, generally in the late 40ies of an affected person but it could emerge as soon as in the 30ies or even late 20ies. This form of AD has been therefore named early-onset AD (EOAD) in distinction to the more common late-onset AD (LOAD).

Nevertheless, subjects carrying FAD genes sometimes develop the disease past the age 65 and, on the contrary, EOAD can be diagnosed in patients that do not present a strong AD-linked genetic background. Hence, while these categories are useful for practical research and clinical purposes, it important to note that AD exists in a continuum (Alzheimer's Association, 2015).

As a curiosity, we report that, after the rediscovery Auguste D.'s brain sections in Frankfurt (Graeber et al. 1998), the genetic basis of her EOAD was recently controversially debated. A first study reported a nucleotide substitution in exon 6 of *PSEN1*, possibly responsible for the EOAD (Muller, Winter, Graeber 2013), yet the conclusions were questioned by a following work that could not replicate the results (Rupp et al. 2014).

3.3.4 Pathogenesis

APP, *PSEN*s and *APOE* all code for proteins involved in the metabolism of Aβ (Hardy and Selkoe 2002). This latter is a 38-43 aminoacids-long peptide that, within the pathology, serves as building block of senile plaques (Glenner and Wong 1984; Masters et al. 1985), also called "amyloid" (starch-like) plaques. The two major isoforms of Aβ are $A\beta_{40}$ and $A\beta_{42}$, the latter being the most prone to aggregate.

APP encodes for Aβ precursor protein (APP) (Kang et al. 1987) which is a plasma membrane transmembrane glycoprotein. The sequential cleavage of APP performed by two proteolic enzymes, β-secretase first and then γ-secretase, determines the production of Aβ (see Figure 2). In particular, γ-secretase is a multimeric enzyme whose catalytic core is provided by presenilin. This exists in two isoforms, PS1 and PS2, which are encoded by *PSEN1* and *PSEN2*, respectively (Selkoe and Wolfe 2007). Alternatively, APP can be also cleaved by α-secretase at a different site generating a non-amyloidogenic peptide.

In 1992, the notion that Aβ is the molecular constituent of senile plaques, joint with the recent discovery of *APP* mutations being causative of AD, laid the foundation of the seminal amyloid cascade hypothesis (Hardy and Higgins 1992). The hypothesis posits that Aβ is the initiator, "the culprit", of the series of events leading to AD, including neurofibrillary tangles formation.

At the time of the hypothesis formulation, Aβ was thought to be noxious to the brain in the form of amyloid plaques. However, several lines of evidence oppose this view. First, neurofibrillary tangles seem to appear earlier than amyloid plaques, as suggested by the pioneering work of Braak and Braak (Braak and Braak 1998). Second, cognitive decline does not

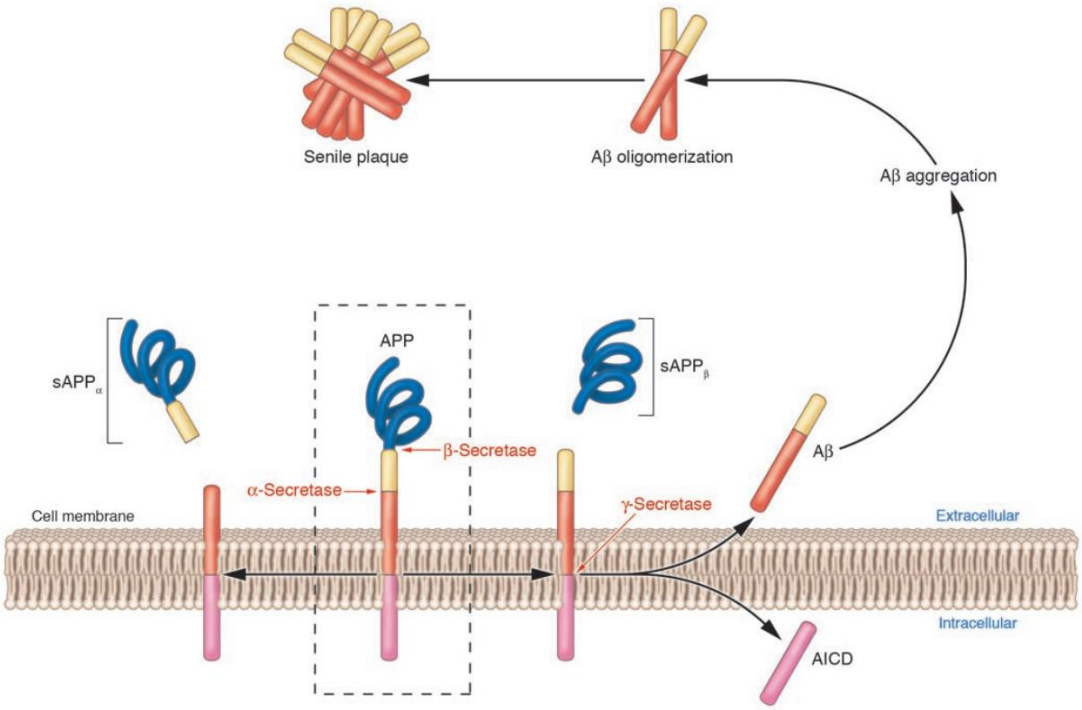

Figure 2. APP processing. The scheme recapitulates the two processing pathways that APP can undertake. The sequential cleavage operated by the β- and then the γ-secretase constitutes the Aβ producing pathway, which potentially leads to Aβo and amyloid plaques aggregation. The APP intra-cellular domain (AICD) is also released as a result of γ-secretase cleavage. Conversely, APP cleavage performed by the α-secretase results in non-amyloidogenic APP fragments. Image adapted from (Gandy 2005).

correlate with plaques deposition (Terry et al. 1991) – most strikingly, distributed plaques were reported in a subset of nondemented elders as well as many AD patients were found not to present plaques at a post mortem analysis (Price and Morris 1999). Third, neurological deficits independent of plaques were reported in mouse models (Lesné, Kotilinek, Ashe 2008).

The Aβ forms that are attracting the most interest for their potential responsibility in causing AD are $A\beta_{42}$ monomers and oligomers. The latter were shown to be increased in AD patients and to be the earliest component of amyloid plaques (Younkin 1995). In particular, the relative $A\beta_{42}$ concentration in relation to the $A\beta_{40}$ one – i.e. the Aβ42/ Aβ40 ratio – is increased in *PSEN*-based models of FAD in vitro (Bentahir et al. 2006). Accordingly, AD-causing mutations in *APP* and *PSEN*s affect APP processing and increase either the $A\beta_{42}$ level or simply the Aβ42/ Aβ40 ratio (Bentahir et al. 2006; Suzuki et al. 1994). On the other hand, Aβ aggregation, before ending in insoluble plaques, determines the formation of a wealth of intermediate soluble oligomers (Aβo). Aβo were observed in human AD brains (Shankar et al. 2008) as well as in AD models (Lesné et al. 2006) and, notably, they affect synaptic plasticity, dendritic spine density and memory (Lesné et al. 2006; Shankar et al. 2008).

In the past 24 years from the amyloid cascade formulation, the details of the hypothesis have been progressively readapted to account for the increasingly larger knowledge on the molecular, genetic and pathological aspects of the disease. Yet, the hypothesis has remained the best accepted model and has provided a valuable theoretical framework to research in the field. In the current formulation of the amyloid cascade hypothesis, $A\beta_{42}$ peptides form progressively larger aggregates, from soluble Aβo to insoluble plaques. Aβ aggregates, especially soluble Aβo,

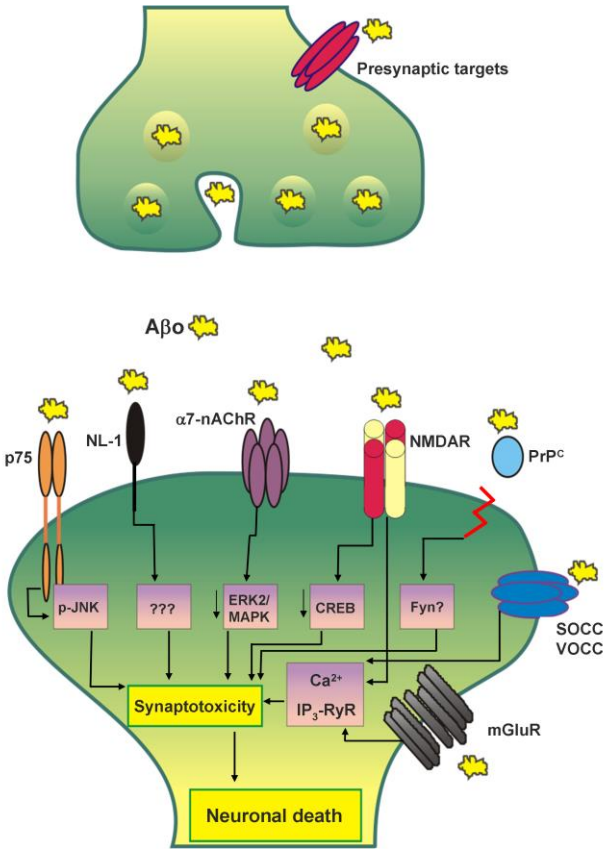

Figure 3 Effects of Aβ synaptic release. The illustration depicts the principal, yet not all, known pathways that are affected by Aβo at the postsynaptic level after its release from a presynaptic neuron. Image from **(Agostini and Fasolato 2016)**.

cause oxidative injury, gliosis and Ca^{2+} dysregulation ultimately resulting in synaptic loss and neuronal death.

Of note is the involvement in AD and pathological aging of alterations in Ca^{2+} homeostasis that was originally suggested by Khachaturian in the late '80 (Khachaturian 1987) and soon integrated in the amyloid cascade hypothesis (Hardy and Higgins 1992). The more recent discovery that presenilins (PSs) are not only involved in $A\beta_{42}$ production but are also directly responsible of Ca^{2+} alterations at multiple levels, including endoplasmic reticulum (ER), mitochondria and plasma membrane, substantiates and widens the original version of the Ca^{2+} hypothesis of AD, that was simply based on Aβ-induced Ca^{2+} defects (Honarnejad and Herms 2012).

Nowadays the amyloid cascade hypothesis is challenged because of a number of aspects that it fails to explain (Harrison and Owen 2016). Most notably, (i) biomarker studies suggest that about one third of elderly people without cognitive impairment show significant brain Aβ load; (ii) neurofibrillary tangles may appear earlier than amyloid plaques (Braak and Braak 1998; Price and Morris 1999); (iii) their topographic distribution differs from Aβ plaques deposition and neurodegenerative changes: neural loss is predominantly in the hippocampus and entorhinal cortex, whereas plaques are first found in frontal regions; (iv) clinical symptoms better correlate with tangles than Aβ burden; (v) $A\beta_{42}$ toxicity has been largely observed *in vitro*, and, most frequently at Aβ concentrations order of magnitudes higher than those found in the pathophysiology of AD (Fedele et al. 2015).

Yet, the strongest concern over the hypothesis probably arises from the failure of Aβ-targeting trials (Herrup 2015). Though, it is also argued that the unsuccessful results of the trials do not necessary imply the hypothesis to be wrong. It might rather be that it has not been properly tested because of insufficient target engagement or because the drugs may have been administered too late in the disease process (Golde, Schneider, Koo 2011).

AD pathology, additionally, includes the establishment of astrogliosis, a condition where astrocytes become reactive and release cytokines and other pro-inflammatory mediators, exerting a neuroinflammatory function (Steardo Jr et al. 2015). In this condition, astrocytes present a strong increase in the expression of glial fibrillary acidic protein (GFAP). Astrogliosis

generally precedes amyloid plaques deposition, though it is not clear at which stage its role in the development of the disease switches to disease advancing from being of benign defensive reaction. Nevertheless, astrogliosis has been proposed as a potential disease-modifying target, in light of the deleterious neurotoxic consequences of the sustained neuroinflammation arising from the self-perpetuating process of reactive gliosis (Rodríguez-Arellano et al. 2015; Steardo Jr et al. 2015).

Recently, a new interesting model accounting for the observations here recapitulated was proposed (Puzzo et al. 2015). It is reasoned that Aβ loss of function could result in a feedback enhancement of the dysfunctional peptide. In turn, high levels of Aβ would cause the inhibition of alpha7 nicotinic acetylcholine receptors (a7-nAchRs) determining synaptic dysfunction. However, a weak point of this model is that it requires Aβ to be loss of function towards inhibiting itself expression but, at the same time, capable of inhibiting a7-nAchRs. Moreover, it forgets to consider the other recognized Aβ targets, among which the most studied are the glutamate receptors NMDAR and mGluR5 (Wang et al. 2015).

Altogether, there is growing consensus that a reassessment of the framework is needed and that Aβ is unlikely to be the sole causative element of the disease (Herrup 2015).

3.3.5 Presenilins and Ca^{2+} homeostasis

PS1 and PS2 have become known for their role in Aβ processing, as the catalytic core of γ-secretase (Selkoe and Wolfe 2007). Yet, while γ-secretase is also involved in the proteolysis of a handful of substrates other than APP, including Notch (Hass et al. 2009), on the other hand, PSs per se intervene in several cellular processes ranging from signal transduction to tau phosphorylation and Ca^{2+} homeostasis (Honarnejad and Herms 2012).

As far as Ca^{2+} homeostasis is concerned, PSs are mainly implicated in ER Ca^{2+} signaling (Honarnejad and Herms 2012) and mitochondria-ER Ca^{2+} crosstalk (Zampese et al. 2011a). Notably, FAD-PS mutations, in vitro and in situ, enhance (Stutzmann et al. 2004) or reduce (Kipanyula et al. 2012) inositol trisphosphate receptor (IP_3R)-evoked Ca^{2+} responses as well as they increased Ryanodine receptors (RyR) expression and, thus, RyR-mediated Ca^{2+} response to caffeine (Kipanyula et al. 2012; Stutzmann et al. 2006). In addition to regulating protein levels, PSs directly modulate RyR channel opening probability (Hayrapetyan et al. 2008), this feature possibly bridging between FAD-PS mutations and RyR-mediated Ca^{2+} release dysregulation. Finally, FAD-PS2 mutations decrease ER Ca^{2+} content by dampening SERCA activity and slightly increasing passive ER Ca^{2+} leak (Brunello et al. 2009). In addition, they also increase mitochondrial Ca^{2+} uptake by favoring closer ER-mitochondria contact sites (Kipanyula et al. 2012). On the other hand, FAD-PS1 mutations cause ER Ca^{2+} overload by reducing ER Ca^{2+} leak thus indirectly favoring mitochondria Ca^{2+} uptake (Bezprozvanny 2009; Tu et al. 2006) but see (Shilling et al. 2012).

How the altered ER Ca^{2+} content/release and increased mitochondrial Ca^{2+} uptake cause the neuronal Ca^{2+} hyperactivity observed in FAD models in vitro and in vivo (see Neural hyperactivity) has to be explained yet (Busche et al. 2008).

It should be noted that, while PS1 and PS2 are highly homologue and share most of their known cellular functions (Honarnejad and Herms 2012; Lai et al. 2003), nevertheless several

important difference have been described, including (i) PS1 being a stronger Aβ producer and (ii) PS2, unlike PS1, being involved in the modulation of ER-mitochondria interaction (Shilling et al. 2012; Zampese et al. 2011a).

3.3.6 Current trend in AD diagnosis criteria

Since the definition of the still practiced criteria for AD diagnosis (McKhann et al. 1984), our knowledge on both the pathophysiology of AD, and the clinical manifestations that are timed to its progression, has largely increased. Studies showed that there is no tight correspondence between the clinical symptoms and the underlying pathology (Jack et al. 2011). Instead, as we saw in the former paragraph, a strong variability is observable: distributed plaques and a large number of tangles were reported in a subset of nondemented elders (Davis et al. 1999; Knopman et al. 2003; Price and Morris 1999) as well as cases of AD in the absence of a marked histopathology were described (Crystal et al. 1993; Riley, Snowdon, Markesbery 2002).

At the same time, it is recognized that a trend exists for strong cellular and tissutal alterations to be already present at the moment when the first symptoms are expressed (Golde, Schneider, Koo 2011). Interestingly, formation of, respectively, neurofibrillary tangles and amyloid plaques, seem to be independent events with the former appearing earlier and in the limbic structures, preferentially, and the latter appearing in the neocortex (Braak and Braak 1997; Price et al. 1991; Price and Morris 1999).

Moreover, there is now consensus that intra and extracellular deposits begin to accumulate long before the clinical disease becomes measurable. In particular, it was estimated that amyloid plaques accumulation may progress for some 10 to 20 years ahead of the clinical symptoms emergence (Benzinger et al. 2013; Villemagne et al. 2013).

These observations have two intertwined effects on the current view of the disease. First, AD has a long asymptomatic phase during which the brain is pathophysiologically affected, no matter the unaltered cognitive performance of the subject. Second, the cognitive symptoms are an ultimate result of the long going pathophysiological processes due to the disease and likely represent a late time point for a disease-modifying intervention. Hence, much emphasis should be devoted to the research targeting the changes and the mechanisms underlying the early stages of the pathology.

Indeed, the new criteria and guidelines for AD diagnosis, defined in 2011 (Jack et al. 2011), identify three stages of the disease: preclinical AD, MCI due to AD and dementia due to AD. Most notably, it is stressed the importance of counteracting the disease during its early phase. Moreover, while the diagnosis of MCI due to AD and AD dementia are mainly based on clinical assessment (American Psychiatric Association 2013), preclinical AD identification relies on biomarkers. Yet, the directions for preclinical AD diagnosis are presented as recommendations intended for research purposes. Their clinical employment is felt as premature and additional research on biomarkers is invoked.

3.3.7 Biomarkers

Biomarkers are parameters that describe the status of a given biological process. Brought down to the pathology, a biomarker is an indicator of the existence and/or progression of the disease.

A plethora of biomarkers has been developed in AD. They can be ascribed to different categories depending on the quality of the parameter – e.g. physiological, biochemical, anatomic – or the pathological stage that they are related to.

From the genetic perspective, *ApoE4* represents the strongest risk factor of developing AD (Saunders et al. 1993). However, as for amyloid plaques, ApoE4 does not provide information about the timing of clinical AD onset.

The histopathological biomarkers consist of the historic hallmarks of AD: aggregates deposition and neuronal degeneration. Indeed, although the concentration of plaques is no longer considered a significant indicator of the severity of the clinical disease, amyloid plaques presence increases the risk of developing AD by about four folds (Chen et al. 2014). Notably, Aβ deposits may be non-invasively detected and quantified by means of a PET scanning method, where compounds able to bind to the plaques – e.g. Pittsburgh compound B (PiB), a radioactive analog of thioflavins – are employed as PET tracer (see Neural activity recording). Conversely, neurofibrillary tangles proved to fairly correlate with the cognitive symptoms (Giannakopoulos et al. 2003). Further, neuronal degradation, assessed as hippocampal volume reduction (Gosche et al. 2002) or atrophy on structural MRI in the temporal lobe and parietal cortices (Sperling and Johnson 2013b), was shown to highly correlate with both MCI and AD. Finally, better than neuronal injury and neurofibrillary tangles deposition, synaptic loss appears to be the strongest correlate of the clinical symptoms (Terry et al. 1991).

Much work has been done in assessing biochemical biomarkers (Lista et al. 2014). These studies have focused on the cerebrospinal fluid (CSF) since it is in physical contact with the brain - conversely, blood is separated from the neural tissues by the blood-brain barrier (BBB) – and it is safe and relatively simple to access through a lumbar puncture. In particular, two biomarkers emerged from this approach. The first is the concentration of $A\beta_{42}$. Indeed, a 50 % lower level of $A\beta_{42}$ was consistently reported in AD patients' CSF (Andreasen and Zetterberg 2008; Blennow 2004), a phenomenon explained as complementary to Aβ aggregation in amyloid plaques (Strozyk et al. 2003). In addition, Aβ42/40 ratio was reported to decrease even more than Aβ42 per se in AD patients, owing to a slight increase of Aβ40 level (Schoonenboom et al. 2005). Moreover, CSF $A\beta_{42}$ has an accuracy of 65 – 75 % in predicting conversion from MCI to AD over 2 years (Mitchell, Monge-Argiles, Sanchez-Paya 2010). Conversely, a second indicator of AD is the high level of CSF tau. Combined analysis of $A\beta_{42}$ and tau levels in the CSF accounts for an 80 – 95 % of sensitivity in discriminating AD (Forlenza, Diniz, Gattaz 2010; Hampel et al. 2004; Mattsson et al. 2009).

However, it is important to note that CSF biomarkers alone, although compellingly accurate in discriminating AD and predicting MCI to AD conversion, are not sufficient to differentiate AD from other types of dementia (Lista et al. 2014). Likewise, it is worth noting that the predictive performance of $A\beta_{42}$ and tau levels drops when tested on unselected populations (Mattsson and

Zetterberg 2009). Additionally, CSF gathering is an invasive procedure and, though rarely, it may cause post-lumbar puncture headache (PLPH) (Zetterberg et al. 2010). Consequently, patients are sometimes concerned about discomfort during the procedure.

Finally, growing interest is now being attracted by the biomarkers of electrophysiological activity, including EEG and fMRI biomarkers. It is possible to extrapolate a wealth of parameters from the EEG signals by means of computer-aided tools ranging from time, frequency and time-frequency features to non-linear dynamics. Several are altered in AD. For instance, a clear peak of alpha activity in waking subjects with eyes closed is often missing in AD patients (Pucci et al. 1999). In addition, alpha and beta band slowing was reported (Dauwels, Vialatte, Cichocki 2010; Trambaiolli et al. 2011). Signal complexity is also reduced (Zhang et al. 2013). Likewise, coherence, as a measure of covariance between pairs of EEG signals, was consistently reported to be reduced in AD (Besthorn et al. 1997; Leuchter et al. 1987; Locatelli et al. 1998). Interestingly, the application of the machine-learning paradigm to exploit EEG coherence for AD diagnosis yielded encouraging results with sensitivity and specificity above 80 % (Trambaiolli et al. 2011).

Functional imaging studies employing fMRI have consistently reported a diminished activation in the hippocampal region in response to mnemonic tasks in AD patients (Ewers et al. 2011; Pihlajamaki, Jauhiainen, Soininen 2009). Interestingly, the opposite scenario is apparent in MCI patients. In this case, in fact, higher activation of the hippocampus in the course of the task has been generally described (Dickerson et al. 2005; Hämäläinen et al. 2007; Miller et al. 2008) and, most strikingly, the degree of the activation correlated with the probability of

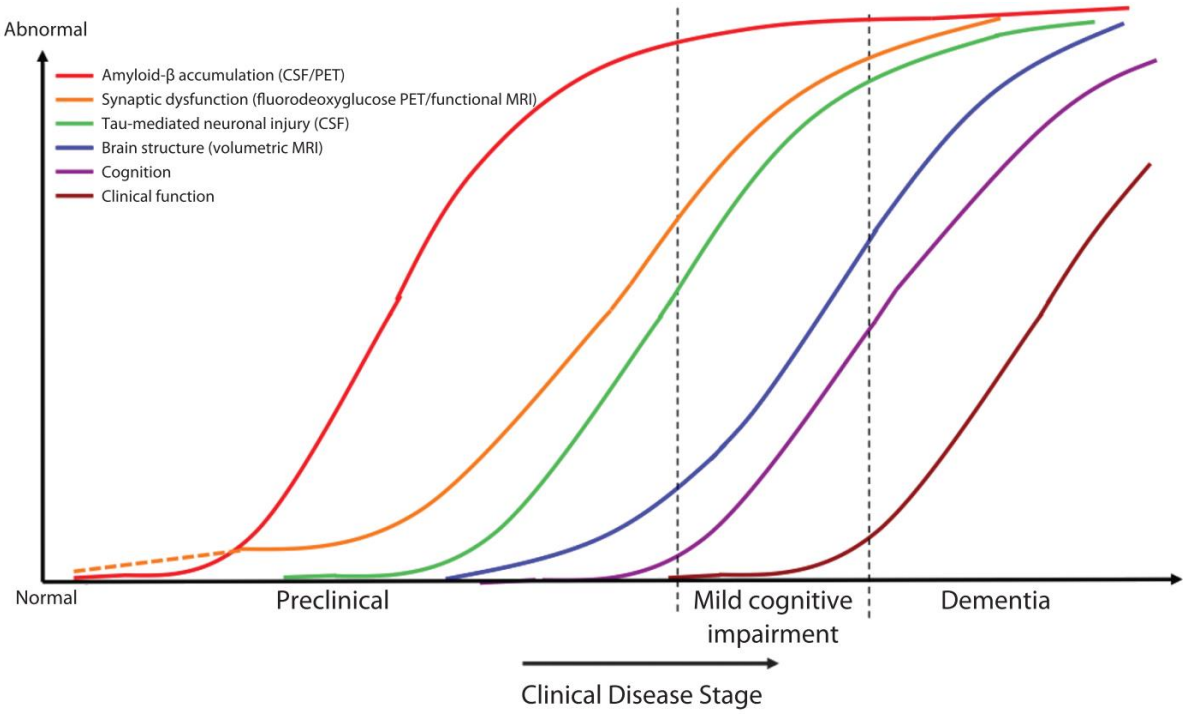

Figure 5. Current model of AD biomarkers dynamics. This simple illustration describes the current most accredited model of biomarkers appearance in AD. Accordingly, Aβ load (*red*), first in the form diffusible oligomers and then as insoluble aggregates, is the first process to start. Subsequently, synaptic dysfunction (*orange*) and neuronal injury (*green*) begin. By the time when the first cognitive symptoms of dementia (*purple*) are detected, these biomarkers have already reached very high levels and even brain atrophy and shrinkage (*blue*) are observable. Image from (Sperling and Johnson 2013a).

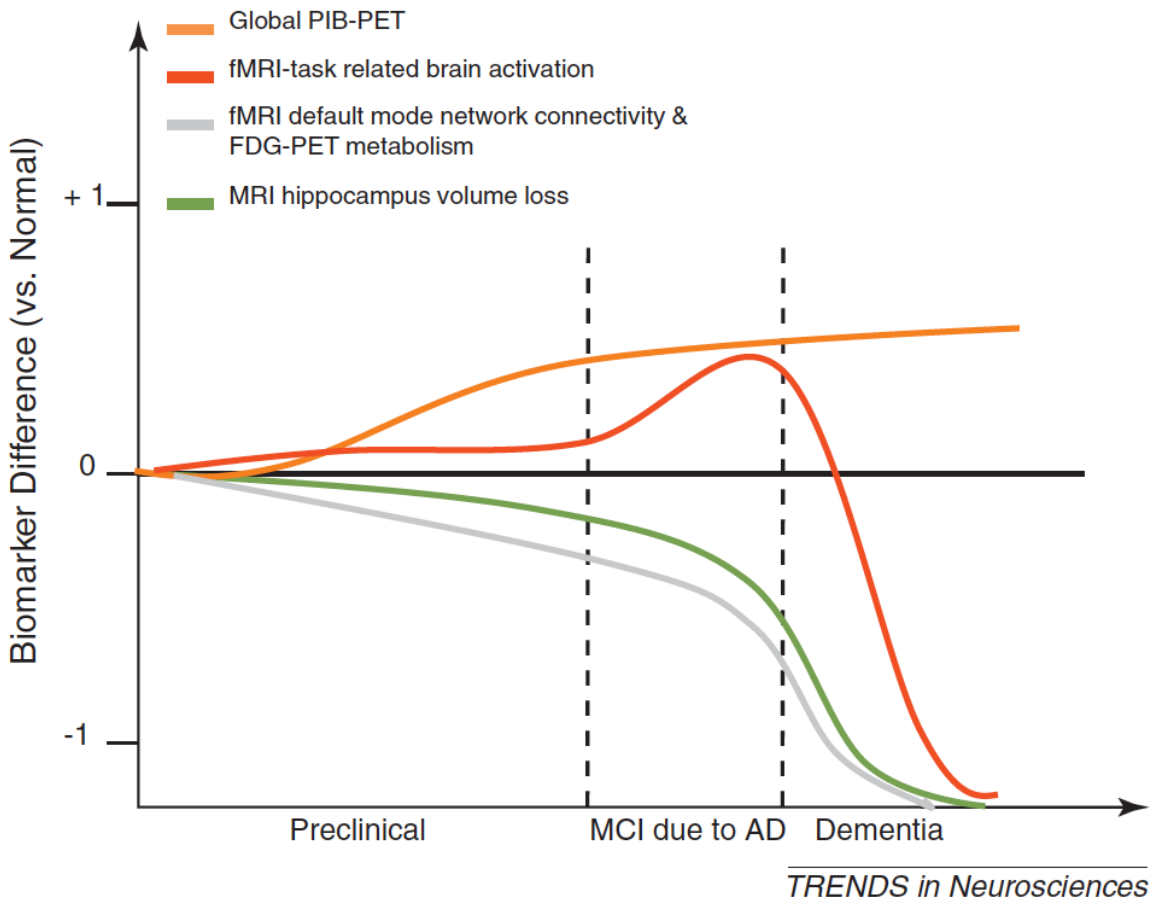

Figure 7. Model of the hypothetical progression of imaging biomarkers. The correlation between various imaging biomarkers and the different stages of the AD is illustrated in this scheme. Note, in particular, the slow increase of amyloid deposition (PIB-PET) that is believed to generally begin in the preclinical phase, long before the first symptoms, and the relatively rapid increase of task-driven brain activity (fMRI-task related brain activation) during the MCI phase followed by its decline after the onset of the overt AD phenotype. Image from (Ewers et al. 2011).

progression to AD in a longitudinal study (Miller et al. 2008). These studies strongly indicate the existence of a phase of hippocampal hyperactivity that precedes the overt clinical AD and that disappears with the emergence of this latter. Yet, it is still debated whether the hippocampal hyperactivity could be compensatory or disease-aggravating (Bakker et al. 2012; Ewers et al. 2011; Stargardt, Swaab, Bossers 2015).

Some of the biomarkers that we reported here, including $A\beta_{42}$ and tau CSF levels, were embodied, although only to a mere complementary purpose, in the revised criteria for AD diagnosis (American Psychiatric Association 2013; Jack et al. 2011).

The integrated analysis of neuropsychological, CSF, and MRI features performed better than each single approach in predicting conversion from MCI to AD over 2 years (Cui et al. 2011). This result suggests that success in developing early, preclinical diagnosis of ongoing AD pathology will be achieved only through combining the analysis of many biomarkers.

3.4 AD AND NETWORK DYSFUNCTIONS

AD is linked to the alteration of many network features spanning several scales of network complexity. It is possible to separate them in two major categories: alterations of oscillatory activity and neural hyperactivity.

3.4.1 Alterations of oscillations

EEG-assessed theta power increases in the frontal regions with the shrinkage of hippocampal volume in MCI and AD (Grunwald et al. 2001). Moreover, theta power is markedly increased in MCI patients that subsequently progress to AD (Jelic et al. 2000). Beta power decrease is similarly predictive of AD (Jelic et al. 2000) while theta/alpha power ratio results altered in correlation with AD-linked cerebrovascular damage (Moretti et al. 2007).

Whereas, alpha waves seem to disappear with the progression of the disease towards the most severe phases (Pucci et al. 1999; Smith 2005), beta oscillations parameters result well-suited for separating AD from MCI (Poil et al. 2013), in particular when considering the broadening of peak width and bandwidth in AD (Huang et al. 2000; Poil et al. 2013).

Finally, an overall slowing of the EEG, intended as shift of the power spectral density function towards lower frequencies, has long been known (Bennys et al. 2001; Rossini et al. 2006).

3.4.2 Neural Hyperactivity

Although Aβ causes depression of excitatory synapse (Palop et al. 2007; Shankar et al. 2007), its overall effect at the network level is of enhanced excitability (Palop and Mucke 2009). In accordance with increased network excitability, AD is linked to epilepsy as supported by the increased incidence of seizures in AD and the presence of seizures in the pedigree of many FAD families (Amatniek et al. 2006; Palop, Chin, Mucke 2006). In addition, epileptiform EEG activity was identified in several AD mouse models, including hAPPJ20 (Palop, Chin, Mucke 2006; Palop et al. 2007), hAPPJ9/FYN (Palop and Mucke 2009), Tg2576 (Chin et al. 2008) and hAPP/PS1 (Chin et al. 2008; Tanila, Minkeviciene, Dobszay 2008), PDAPP (Busche et al. 2015) and APdE9 (Minkeviciene et al. 2009). In this latter, network activity was further investigated *in vitro* and neuronal hyperexcitability was observed in cortical and hippocampal slices (Minkeviciene et al. 2009). Furthermore, hyperactive and hyperexcitable neurons were found both in the presence that in the absence of amyloid plaques in the APP23xPS45 mouse line (Busche et al. 2008; Busche et al. 2012). Remarkably, chronic administration of an antiepileptic drug, levetiracetam, to hAPPJ20 mice reduced neuronal hyperactivity and ameliorated the behavioral deficits as well as the synaptic plasticity impairment (Sanchez et al. 2012), whereas the reduction of Aβ levels by means of anti-Aβ immunotherapy worsened the phenotype of neuronal dysfunction by strongly increasing neuronal hyperactivity (Busche et al. 2015).

Neural AD-linked hyperactivity, in particular at the hippocampal level, has been consistently reported in humans as well (Celone et al. 2006; Dickerson et al. 2005). Importantly, the hyperactivity is observable in the putative early stages of the disease, namely in MCI patients displaying light symptoms (see Biomarkers) (Celone et al. 2006; Dickerson et al. 2005; Putcha et al. 2011; Stargardt, Swaab, Bossers 2015). Further, it is worth noting that hyperactivity has been also observed in cognitively intact elderly characterized by Aβ deposition (Buckner et al. 2005;

Oh et al. 2015; Sperling et al. 2009) or familial risk (Bassett et al. 2006). Finally, treatment of MCI patients with levetiracetam reduced hippocampal hyperactivity and improved memory performance in amnestic MCI (Bakker et al. 2012).

3.5 AD INVESTIGATION BY MEANS OF MOUSE MODELS

In 1991, the discovery of the existence of a gene, *APP*, whose pathogenic mutation provides a fully penetrant form of AD (Goate et al. 1991), gave rise to the possibility to investigate the molecular actors involved in the etiology of FAD and, likely, in the mechanisms underlying the AD.

Many mouse models have been and continue to be developed since then. Some are based on the knock-out of one or more of the genes responsible for the FAD, while many more are transgenic mice expressing FAD mutations.

Knock-out models are useful to gather information concerning broad physiological aspects as well as pathological pathways in which the wt and the mutant proteins could be involved, respectively. For instance, APP knock-out mice present decreased locomotor activity, while PS1 knock-out (PS1KO) mice die at the stage of embryos because of impaired somitogenesis and PS2 knock-out (PS2KO) mice display pulmonary fibrosis and hemorrhage. Finally, conditional PSs knock-out in adult mice was shown to progressively induce the classical hallmarks of the disease, including neurodegeneration (Shen and Kelleher 2007).

A large number of AD transgenic mouse models are in existence, each expressing a different combination of FAD mutations. However, none of the available model faithfully recapitulates all the aspects of AD pathogenesis. Conversely, each reproduces a specific assortment of AD features and is, thus, an incomplete model (Webster et al. 2014).The first AD mouse models that were developed, as well as the most used, are based on the expression of mutant human APP (hAPP). These animals appear to recapitulate the pre-dementia phase of the disease (Zahs and Ashe 2010). They generally exhibit amyloid plaques deposition as well as cognitive symptoms in an age-dependent fashion, with these latter occurring only in very old (18 – 24 months) mice (Duyckaerts, Potier, Delatour 2008).

On the contrary, the majority of models expressing mutated forms of human PS (hPS) do not display neurologic deficits nor plaques deposition. This is explained by the fact that the murine Aβ is less aggregating compared to the human one. Where both mutated hAPP and hPS are coexpressed in a double transgenic mouse, the production of $A\beta_{42}$ strongly increases and plaques deposition and cognitive symptoms are anticipated with the respect to the hAPP single transgenic mouse (Duyckaerts, Potier, Delatour 2008).

The expression of a mutated form of hAPP neither alone nor in combination with a mutated hPS is sufficient to cause any significant tau pathology. Therefore, in order to investigate the neurofibrillary component of AD, transgenic lines expressing variants of human tau protein are employed (Zahs and Ashe 2010). However, tau mutations do not cause AD but fronto-temporal dementia. In some of these lines brain atrophy is observed and only in such cases cognitive deficits emerge as well. Moreover, Aβ has been proved to potentiate the neurofibrillary

pathology in these lines, consistently with the hypothesis positing tau-related anomalies to be downstream to Aβ (Hardy and Selkoe 2002).

Altogether, mouse models represent a valuable tool for the research on AD. Notably, mice and humans have a high level of phylogenetic conservation in the architecture as well as in the circuitry and function of the hippocampus. Nevertheless, considering the failures of the clinical trial after the success of the therapies in murine setting, it is important to recognize that AD mouse models do not entirely recapitulate the AD phenotype. Firstly, since they are based on FAD mutations, they rather represent a model of the dominant autosomal forms of the disease. Secondly, considering the general lack of tau pathology and neurodegeneration, intended as neuronal loss, AD mouse model might, most commonly, reproduce preclinical stages of the disease (Zahs and Ashe 2010).

4 THE EXPERIMENTAL APPROACH

In view of the vast assortment of AD mouse models along with the corollary of specific features of their AD-like phenotype, a short introduction is required in order to present the characteristics of the AD models chosen for this study. In addition, the overview on our experimental setting is extended to include a review of the effects of urethane anesthesia on brain electrophysiological activity.

4.1 AD MOUSE MODELS BASED ON MUTANT PS2

Two FAD mouse models were employed in this study: the single transgenic line PS2.30H (Richards et al. 2003) which is homozygous for the human PS2-N141I mutation (Borchelt et al. 1996) and the double homozygous transgenic line B6.152H that presents the human *PSEN2* N141I (Volga/German) mutation in combination with the human *APP* KM670/671NL (Swedish) mutation (Ozmen et al. 2009). In these lines, the human PS2-N141I is under the control of the mouse prion protein promoter, while the human APP Swedish mutation is under the control of the Thy-1 promoter. Both transgenes are in homozygosity.

Although it is also active in thymocytes, lymphoid tissue and even some glial cells, the Thy-1 (also known as Thy-1.2) promoter has been modified (Caroni 1997; Vidal et al. 1990) to obtain a brain-specific neuronal promoter. The mouse prion promoter was suggested to be specific for neuronal cells (Maskri et al. 2004), however the cellular prion-protein is significantly expressed also in astrocytes (Lima et al. 2007; Moser et al. 1995), and, in astrocytes from PS2.30H mice, the over-expression of PS2 was also confirmed by Western blotting (unpublished data). For what concerns the pathological features, B6.152H mice present no plaques at 3 months, overt amyloid deposition at 6 months and heavy plaque deposition at 10 months of age (Ozmen et al. 2009). On the other hand, plaques deposition has never been assessed in PS2.30H mice. Further, B6.152H and PS2.30H lines present different Aβ load levels and Aβ42/Aβ40 ratios as early as 2-weeks of age (Kipanyula et al. 2012). Finally, due to PS2-N141 expression, both AD mouse models are characterized by similar precocious Ca^{2+} dysregulation, as it was demonstrated in neonatal primary neuronal cultures at 10-12 days *in vitro* as well as in acute brain slice preparations from 2-week-old mice (Kipanyula et al. 2012). In B6.152H mice, while cognitive impairment was detected by the Morris water maze only at 8 and 12 months of age, on the other hand an increase in LTP and post-tetanic potentiation in the DG has been reported as early as 3 months (Poirier et al. 2010). No reported study has characterized the PS2.30H line in terms of behavior yet. However, another model, expressing the PS2-N141I mutation under the control of the neuron-specific enolase (NSE) promoter, was proved to be cognitively impaired and to exhibit enhanced anxiety at 12- 18-months of age (Yuk et al. 2009).

Altogether, the PS2.30H and B6.152H lines are particularly suited to address the early effects of Ca^{2+} homeostasis alteration and Aβ load at the network level.

4.2 URETHANE ANESTHESIA

Urethane is an anesthetic that has long been used in neurophysiological research, in particular for investigating hippocampal oscillatory activities (Kramis, Vanderwolf, Bland 1975; Vandecasteele et al. 2014). Yet, its mechanisms of action are poorly understood. *In vitro* experiments on frog cells expressing recombinant neurotransmitter receptors, suggested that urethane exerts its action by weakly affecting multiple targets: it reduced the NMDA and the AMPA receptor-mediated excitatory currents by 10 % and 18 %, respectively, and enhanced GABA-A receptor-mediated inhibitory current by 23 % (Hara and Harris 2002). However, another *in vitro* study found no effect of urethane on PSPs, either excitatory or inhibitory in rat visual cortex acute slices. On the other hand, it reported a depression of pyramidal neurons firing rate due to shunting inhibition, operated by Ba^{2+}-sensitive K^+ leak currents (Sceniak and MacIver 2006).

Theta oscillations are a prominent hippocampal feature under urethane anesthesia (Buzsáki 2002). Nevertheless, hippocampal theta in the anesthetized animal has historically been distinguished from the awake animal theta on the basis of the pharmacological sensitivity to the muscarinic blocker atropine. While atropine exerts no substantial effect on theta oscillations in the awake behaving animal (Buzsáki et al. 1986), conversely it abrogates theta rhythm under urethane anesthesia (Kramis, Vanderwolf, Bland 1975).

Notably, urethane induces spontaneous sleep-like alternations of slow oscillations (SO) (0.2-1.2 Hz) and theta (3-4 Hz) dominated brain states (Pagliardini, Gosgnach, Dickson 2013). The name “slow oscillations” was preferred over “delta” (Wolansky et al. 2006) because of the similarity with the previously described cortical SO (Steriade, Nunez, Amzica 1993). Theta-dominated states are also accompanied by gamma (25-40 Hz) power increase. These alternations are reminiscent, respectively, of the rapid-eye movement (REM) and the slow-wave sleep (SWS) phases of the natural sleep cycle. Interestingly, the respiratory activity and the body temperature alternate in a similar fashion, further supporting the notion of urethane determining a sleep-like physiological state.

Recently, two hippocampal theta activities were reported to simultaneously exist in the mouse hippocampus under urethane anesthesia (Yanovsky et al. 2014). A generally faster one (3-6 Hz), called theta, that is sensitive to atropine and has the maximum power at the hippocampal fissure, and a slower one (2–5 Hz), that is atropine resistant and displays the maximum amplitude in the hilus of the DG. This latter rhythm was named “hippocampal respiration-induced rhythm” (HRR) by the authors, after two observations: (i) HRR has the same frequency of respiration and (ii) tracheotomy abrogates HRR. However, it is important to notice that both oscillations were investigated in response to noxious stimulation, which is known to trigger theta activity along with an increase of muscle tone, under urethane (Pagliardini, Gosgnach, Dickson 2013). Conversely, the spontaneous theta-dominated state is accompanied by muscle relaxation (Clement et al. 2008; Pagliardini, Gosgnach, Dickson 2013).

It is interesting to consider a wide-range and, to our knowledge uninvestigated, effect that urethane anesthesia could have on the oscillatory pattern. Urethane anesthesia is known to induce a drastic decrease of the mean frequency of hippocampal theta activity to 2 - 6 Hz (Kiss

et al. 2013; Pagliardini, Gosgnach, Dickson 2013; Yanovsky et al. 2014) from 6-9 Hz in the behaving animal (Buzsáki et al. 2003). At the same time, the frequencies of brain rhythms were described to be linked one to the other by a ratio corresponding to ~ 2.72 (e, Nepler's number) (Buzsáki, Logothetis, Singer 2013; Penttonen and Buzsáki 2003). Therefore, we reason that, along with theta, it is possible that all distinct oscillations were lowered after the effects of the anesthetic.

5 PURPOSE OF THE WORK

After the failure of Aβ-targeting therapies in clinical trials, one possible explanation is the fact that the treated patients had already fully developed the disease, as revealed by combined fMRI and cognitive assessment (Golde, Schneider, Koo 2011). At that point it is possible that Aβ-processing modifying drugs could exert very limited therapeutic effect, given that the associated neurodegeneration has already started. New clinical trials will require subjects at preclinical stages of AD, i.e. who show AD brain alterations and are likely to progress to MCI and AD during the trial period (Jagust 2016).

These discouraging results also highlight the urgency of early biomarkers that reliably indicate the undercover developing disease and that predict the overt onset of the first clinical symptoms with years of advance.

From this perspective, PET/CSF and brain volumetric biomarkers proved to be valuable tools for predicting MCI to AD conversion over 2 years. Yet, the moment when the brain has already started to shrink is anyhow likely to be very late, implying that a hypothetically effective disease-modifying therapy would yield no appreciable improvement because of the other detrimental mechanisms that have, meanwhile, established. Likewise, the alterations of brain oscillations were assessed in subjects already presenting symptoms of cognitive decline.

Conversely, the importance of AD mouse models lies in the possibility to address potential changes of oscillatory activity that precede the first symptoms.

Dysregulation of cellular Ca^{2+} homeostasis, Ca^{2+} hyperactivity and hyper-excitability appear to be among the first alterations observable in different AD mouse models (Camandola and Mattson 2011; Kipanyula et al. 2012; Stargardt, Swaab, Bossers 2015; Zampese et al. 2011b). In particular early neuronal impairment of physiological Ca^{2+} homeostasis has been described in the AD mouse models based on PS2-N141I (Kipanyula et al. 2012). Given that all FAD-linked mutations in PS2 determine profound alteration of Ca^{2+} signaling in mouse neuronal cells as well as in fibroblasts obtained by FAD patients, well before the onset of the cognitive decline (Giacomello et al. 2005; Zatti et al. 2006), it can be argued that addressing PS2 dependent hyperexcitability, in the absence or presence of Aβ accumulation, might help defining early markers of disease progression. In particular, we asked whether and from which stage of the disease it is possible to detect the effects of these modifications at the network level in the AD mouse lines PS2.30H and B6.152H, expressing the PS2-N141I in the absence or presence of hAPPswe respectively (Kipanyula et al. 2012).

For this purpose, we recorded *in vivo* the spontaneous LFP activity in the DG of mice under urethane anesthesia at different ages and investigated the oscillatory activity. To our knowledge, only few studies have addressed spontaneous hippocampal oscillatory activity in AD mouse models *in vivo* at early stages at the disease (Born et al. 2014; Ittner et al. 2014; Verret et al. 2012). Importantly, this is the first study addressing these aspects in a mouse model that does not express hAPP.

This work has been carried out in collaboration with Prof. S. Vassanelli (DBS) and Prof. G. Sparacino (DEI), of the University of Padua.

6 MATERIALS AND METHODS

6.1 ANIMALS

All experimental procedures were carried out in compliance with the Italian animal welfare regulations. The utmost care was taken to minimize animal suffering. Due to the system-level approach of this work, the *in vivo* techniques were a necessary choice. The electrophysiological recordings were obtained from 11, 8, 8 (3-month-old), 10, 12, 12 (6-month-old) and 7, 4, 5 (12-month-old) wt, PS2.30H and B6.152H mice respectively with a tolerance of 1 week for the 3-6 month groups and 2 weeks for the 12 month group; IHC and ELISA experiments were carried out with 3-4 animals per group. Females were chosen for all the experiments because in the human pathology women are most affected (Alzheimer's Association, 2015; Schmidt et al. 2008), and B6.152H follow this trend (Ozmen et al. 2009).

6.2 ACUTE ANIMAL PREPARATION

Mice were anesthetized by intraperitoneal injection of urethane (1.5-2 mg/g, U2500 - Sigma-Aldrich) dissolved in 0.9% NaCl physiological saline. In particular, the anesthetic effect was very variable and sensitive to small differences in dosage; hence, an initial dose of 1.2 mg/g was injected and additional doses (0.15 mg/g) were administered as necessary (Namgung, Valcourt, Routtenberg 1995). Absence of reaction to noxious stimuli (e.g. hind paw pinches) ensured the surgical plane of anesthesia. Body temperature was kept at 37 ± 0.5 °C by means of a servo-controlled heating pad (ATC1000 – World Precision Instruments, Inc.). Krebs solution (0.1 ml) was subcutaneously administered every two hours in order to maintain hydration levels.

The head was restrained in a stereotaxic frame and the skull was exposed. A hole was drilled at the site for inserting the recording electrode in the dentate gyrus region of the DG which was located according to (Huang et al. 2012) – about 2.4 mm posterior to bregma, 1.2 mm lateral to midline. The left hemisphere was selected provided that amyloid plaques and neurofibrillary tangles deposition is stronger in this hemisphere (Khan et al. 2014).

The cavity over the skull was filled with Krebs saline solution and a silver chloride reference electrode was dipped within.

Glass electrodes for local field potential (LFP) recording (0.9-1.6 MΩ tip resistance) were obtained from borosilicate capillaries (GB150T-10 – Science Products GmbH) pulled with a P-97 micropipette puller (Sutter Instrument Company) and were filled with Krebs saline solution.

In each animal, the LFP signal was serially acquired at three different depths from the meninges: 1.7 mm, 1.8 mm and 1.9 mm. These depths correspond to the molecular layer, the granule cell layer and the polymorphic layer of the DG.

Heart beat was monitored through electrocardiogram (ECG) recording. ECG positive and negative derivations were subcutaneously inserted in the forelimbs. A high accuracy temperature probe was leaned against chest wall, on the side of the body, to monitor respiration (IT-23, World Precision Instruments).

At the end of the electrophysiological experiment, mice were euthanized by excess of anesthesia and the brain was dissected. The left hemisphere was intended for histological investigations and was fixed in 4 % paraformaldehyde (PFA 4% in Tris-buffer saline, TBS: 150 mM NaCl, 50 mM Tris, pH adjusted to 7.4 with HCl). Conversely, the right-hemisphere cortex and hippocampus were snap-frozen in liquid nitrogen for molecular assays.

6.3 ELECTROPHYSIOLOGY

6.3.1 Data acquisition

The LFP signal was 10X amplified using an Axoclamp-2B amplifier with an HS-2Ax1LU headstage (Axon Instruments Inc.) in bridged mode. A custom-made amplifier provided further 10X amplification along with 4-pole butterworth low-pass filtering at 1 kHz. The ECG signal was 10X amplified and band-passed between 1 and 100 Hz by means of a DAM50 amplifier (World Precision Instruments). Respiration-induced movements of the chest wall were converted in voltage fluctuation by exploiting the piezoelectric properties of the temperature probe. Respiration signal was 100X amplified and band-passed between 0.1 and 100 Hz by means of a DP-301 amplifier (Warner Instruments).

All signal were digitalized at 10 kHz by means of a PCI-6071E I/O card (-0.5 – 0.5 V input range) combined with a BNC-2090 terminal block (National Instruments) in differential mode and recorded through a custom-made LabView (National Instruments) script. Each recording lasted from 15 minutes to two hours.

6.3.2 Signal processing

Analysis of the signals was performed offline in MATLAB (Mathworks). Custom-written and built-in scripts were employed.

Filtering was achieved through a zero-phase distortion filtering function (*filtfilt.m*) which processed the data in both the forward and reverse direction. Butterworth transfer function coefficients were employed (*butter.m*).

All signals were high-pass filtered at 0.05 Hz (3^{rd} order filter). Next, LFP, ECG and respiration signals were low-pass filtered (5^{th} order filter), respectively, at 250 Hz, 25 Hz and 10 Hz. Finally, they were down-sampled (*downsample.m*) to 500 Hz, 50 Hz and 20 Hz, respectively. LFP signals were further low-pass filtered at 10 Hz and down-sampled to 20 Hz for spectrograms computation in the SO and theta oscillations ranges.

6.3.3 Time-frequency analysis

In order to inspect the temporal fluctuations of frequency content in the recordings, LFP, ECG and respiration signals were time-frequency decomposed in the 0.1 - 10 Hz, 7 – 13 Hz and 1 – 5 Hz range, respectively, and the relative spectrograms were obtained. This was achieved employing a custom-written routine, based on a MATLAB built-in function (*cwtft.m*), that uses a fast Fourier transform algorithm to compute the Morlet continuous wavelet transform.

From each recording, as a result of the time frequency inspection, one 5-min window was selected and included for further analysis, provided that LFP theta activity, heart beat rate (HBR)

and respiration rate (RR) were stable throughout the entire window. Recordings that did not present time-windows fulfilling the inclusion criteria were discarded.

6.3.4 Spectral analysis

LFP power spectral density (PSD) was calculated for each 5-min window through the Welch estimate method (*pwelch.m*). The method divides the signal in overlapping sections, windows them with a Hamming windows and computes the periodogram for each window. Finally, the periodograms are averaged into the PSD estimate. Hamming windows of 2 sec were used with an overlap of 50 %.

The spectral power in the different wave band was obtained by computing the integral with the trapezoidal method (*trapz.m*) under the PSD curve in the relative frequency range.

6.3.5 Spectral steepness

PSD function steepness was evaluated as the slope coefficient of the PSD linear fitting. For each 5-min window the PSD function was interpolated (*polyfit.m*) with a least-squares line in the range 10 – 100 Hz.

6.3.6 PAC analysis

For theta-higher frequency PAC index analysis, each 5-min window was, first, bandpass filtered in the theta band (3^{rd} order filter) and in the specific higher frequency band band (6^{th} order filter) as described above. Next, the Hilbert transform (*hilbert.m*) was applied to each time-series obtained from filtering. Then, phase angle and amplitude time-series were extracted from the Hilbert transform of theta and the higher frequency filtering, respectively. Finally, theta-higher frequency PAC index was computed by means of the general linear model (GLM) as described (Penny et al. 2008). Basically, the amplitude of the faster oscillation is modeled by multiple regression and the index is the proportion of variance explained by the model.

6.3.7 Statistical analysis

Power spectra, band power, PSD slope and PAC indices obtained from the recordings at the three depths were averaged within animals to obtain grand mean quantifications for each animal. Those experiments where it was not possible to obtain one 5-min window from each depth, were discarded from the analysis.

Differences among means were tested by performing Kruskal-Wallis nonparametric test. Where Kruskal-Wallis test resulted in the existence of a pair of different populations, differences between means where tested with Mann-Whitney Rank Sum test.

The Mann-Whitney Rank Sum test was performed as an unpaired two-tailed test.

Statistical tests were carried out in GraphPad Prism. All data are expressed as mean ± SEM. The α level of significance was 0.05.

6.4 HISTOLOGY

To mark the position of the LFP electrode insertion (see Figure 6), at the end of the experiment the electrode was withdrawn, dipped in 1,1'-dioctadecyl-3,3,3',3'-tetramethylindocarbocyanine perchlorate (DiI) (0.05 % in DMSO) and then carefully reinserted to the same stereotaxic

coordinates of the mid depth. Next, the brain was dissected and the left hemisphere was fixed in 4 % PFA for 48 hours. After 3 times washing with TBS, the hemibrain was cut parallel to the sagittal plane with a vibratome (Leica VT1000 S), yielding 50 µm-thick slices. Finally, slices were either stained with toluidine blue and mounted by means of Mowiol mounting medium, or conserved for immunohistochemistry (IHC), see below. The electrode insertion site was visualized by epifluorescence microscopy using a ViCo microscope with a 4x objective (Nikon).

6.5 IMMUNOHISTOCHEMISTRY

6.5.1 Staining and acquisition

Mid-sagittal brain slices were cut from the left hemisphere as described above and conserved in TBS at 4 °C until employed (up to two weeks, maximum) for dorsal hippocampus immunostaining. For staining, slices were selected over a range of 400 µm, excluding the insertion site. Consistency of the selected anatomical position was ensured by ocular identification of several anatomical features in the first and last slice of the range, including the shape of the hippocampal section, the size of the left ventricle and caudoputamen and the thickness of the mid-brain region.

Immunostaining was performed on floating slices. Fist, slices were washed in TBS and incubated in 70% formic acid for 5 minutes to allow Aβ-antigen retrieval. Then, slices were incubated in permeabilizing/blocking buffer containing 0.2% TritonX-100 and 5% goat serum in TBS for 1 hour at room temperature (RT). Next, they were incubated overnight at 4 °C in the primary antibody (Ab1) solution, which consisted of the blocking buffer plus the Ab1s mouse anti-Aβ 17-24 (4G8, Covance, 1:1000) and rabbit anti-GFAP (Dako, 1:400). Then, slices were incubated in the secondary antibody (Ab2) solution, which consisted of the blocking buffer plus the Ab2s Alexa488-conjugated donkey anti-rabbit (Invitrogen, 1:1000) and Alexa555 conjugated goat anti-mouse (Invitrogen, 1:1000). Incubation in the Ab2 solution lasted 1 h at RT in the dark. Finally, slices were mounted on microscope slides by means of a Mowiol mounting medium and stored at 4°C until visualized via confocal microscopy. Every step described was separated from one other by 3 washes in TBS (5 min each).

Samples were imaged by means of the confocal laser microscope Leica SP5 with a 20X air objective. During acquisition, parameters for laser intensity and photomultiplier gain were kept constant.

6.5.2 Analysis

For astrogliosis quantification, we considered the average brightness level of GFAP labelling in the HF region. In each image, a region of interest (ROI) was traced encompassing the following regions: subiculum, DG, CA3 and CA1 (see Figure 11); for the cortex, a rectangular ROI of invariant size was drawn. Then, the average 8-bit pixel intensity (0-255) was computed for each ROI. Image analysis was performed in Fiji. Three slice for each mice were used to quantify the mean average value of the selected regions. The three lines were processed in parallel.

Statistical comparison of mean brightness intensities was carried out in GraphPad Prism. The unpaired two-tailed Mann-Whitney Rank Sum test was employed. All data are expressed as mean ± SEM. The α level of significance was 0.05.

6.6 ELISA

After brain extraction from the skull, the right hemisphere was dissected while kept in ice-cold HBSS (Ca^{2+} and Mg^{2+} free). The hippocampus and the cortex were isolated and placed in cryovials. These latter were snap-frozen in liquid nitrogen and stored at -80°C until employed for ELISA.

Total Aβ was extracted according to the following procedure designed to separate two fractions, the first one that was extracted by a RIPA solution containing SDS at high concentration (2%) and the second one that was extracted by a strong acidic solution. Briefly, the frozen tissue was thawed, weighted and diluted 1:5 weight/volume (w/v) in in RIPA buffer (50 mM Tris, 150 mM NaCl, 0.5% sodium deoxycholate, 1% Nonidet P-40, 2% SDS) also containing protease and phosphatase inhibitors (cOmplete, Mini, protease inhibitor cocktail, Roche; PhosSTOP, phosphatase inhibitor cocktail, Roche). Next, the tissue was cold homogenized by mechanical trituration through an insulin syringe. Then, the total volume was centrifuged (Beckman TLA-120.1 Rmax 3.89 cm – Tube, 343776 – 0.5 ml) at 50,000 rpm (109,000 g) for 1 h at 4°C. The supernatant was gathered, split in two aliquots constituting the "RIPA fraction" and stocked at -80°C until employed.

The remaining pellet was diluted 1/5 w/v in a solution of 70% formic acid (FA) in deionized water and resuspended through a micropipette. The FA fraction was left on ice for 30 min and, then, sonicated for 5 min at 4°C (485 W). It was subsequently centrifuged at 50,000 rpm for 1 h at 4°C, as above. The supernatant was split in aliquots constituting the "FA fraction" and stored at -80°C until employed.

At the moment of performing the ELISA assay, the RIPA fraction was diluted at least 1:10 in the assay standard diluent while an aliquot of the FA fraction was centrifuged and diluted 1:10 in a neutralization buffer (1 M Tris, 0.1 M NaCl, , pH adjusted to 7) also containing 0.025% phenol red to check for pH adjustment. The neutralized FA extract was assayed directly or upon further dilution according to the expected Aβ load.

The Wako assay 290-62601 was employed for the quantification of $Aβ_{42}$. This assay detects both the human and murine Aβ and is, hence, suited for the wt and the PS2.30H line, where only murine Aβ is produced, as well as for the B6.152H line, where human and murine Aβ are co-expressed.

6.6.1 Statistical analysis

Differences among average quantities of $Aβ_{40}$ and $Aβ_{42}$ were tested by performing Student's *t*-test, as an unpaired two-tailed test. Welch's correction was applied.

Statistical tests were carried out in GraphPad Prism. All data are expressed as mean ± SEM. The α level of significance was 0.05.

7 RESULTS

The consequences of FAD-PS2 mutations on Ca^{2+} homeostasis have been investigated in different model cells in vitro (Zampese et al. 2011a; Zampese et al. 2011b; Zatti et al. 2006) and specifically *in situ* for the AD mouse models based on the mutant PS2-N141I, expressed either alone or in combination with the APPswe mutation, respectively in the PS2.30H single transgenic and in the B6.152H double transgenic mouse lines (Kipanyula et al. 2012; Ozmen et al. 2009). Compelling evidence has been provided for dysregulation of neuronal Ca^{2+} homeostasis and Ca^{2+} hyperactivity in hippocampal slices as early as two weeks after birth, being effects that markedly precede the appearance of the classical hallmarks of AD, namely the surge of amyloid accumulation and deposition in brain tissues (Kipanyula et al. 2012; Ozmen et al. 2009).

Here, we addressed the network level outcomes of the PS2-N141I in the same mouse lines. In particular, we focused on the spontaneous oscillatory LFP activity of the DG, a brain region that is strongly and early affected by the disease in humans. We performed *in vivo* extracellular recordings in mice under urethane anesthesia while targeting 3 sites in the dorsal hippocampus, corresponding to the molecular, granule cell and polymorphic layers (ml, gc, pl) of the DG. Since the B6.152H line presents amyloid plaques deposition starting at 6 months of age (Ozmen et al. 2009), it seemed convenient to select this latter age as a reference time point. In addition, we investigated an early and a late time point, 3 and 12 months of age, respectively. The electrophysiological approach was corroborated by IHC and ELISA experiments in order to provide a molecular-histological framework to the brain activity observations.

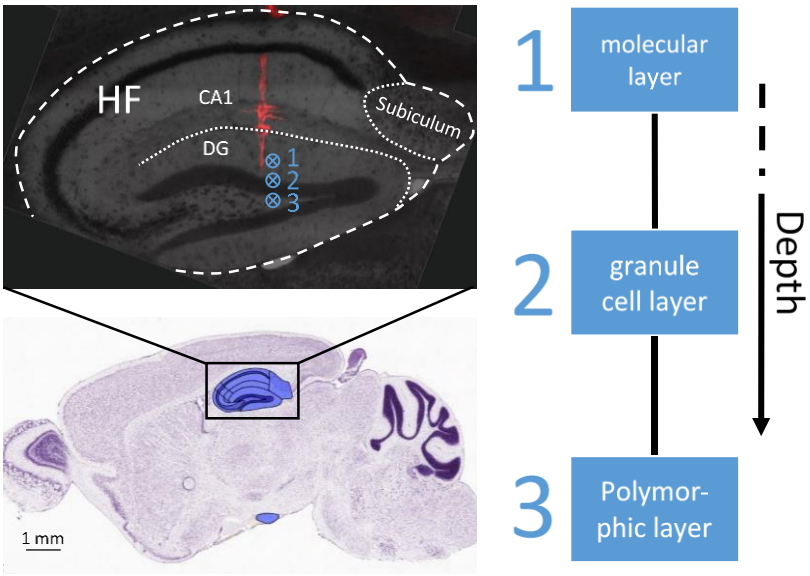

Figure 9. LFP recording sites. The LFP signal was recorded by means of an Ag/AgCl electrode inserted in the DG of the left-hemisphere dorsal hippocampus. In each experiment, the electrode was sequentially targeted to the three DG layer, as reported in the diagram on the right. The top-left image is a sagittal proximo-medial hippocampal slice illustrating the electrode insertion position, labelled at the end of the experiment by DiI and assessed through HC. The stereotaxic positions of targeted recording sites are also indicated. The bottom-left image is a whole brain sagittal slice from the Allen Mouse Brain volumetric Atlas 2012. The region of the HF is highlighted.

7.1 DEFINITION OF THE FREQUENCY BANDS

The LFP signal that we recorded presented two prominent rhythms, a slower oscillation, generally peaking at less than 1 Hz and a faster one at about 2.5 – 3 Hz (see Figure 7). These bands closely correspond, respectively, to the slow oscillations (~ 0.2 – 1.2 Hz) and the theta waves (~ 2 – 6 Hz) previously described in the hippocampus by other studies where mice under urethane anesthesia were employed (Pagliardini, Gosgnach, Dickson 2013; Yanovsky et al. 2014). Therefore, we defined slow oscillations the rhythm in the range of 0.1 – 1.4 Hz and theta the oscillations in the range 1.7 – 4.7 Hz. The particularly low inferior limit accounts for the many cases where theta activity had a near 2 Hz frequency or slightly lower.

Gamma band is classically confined approximately in the 30 – 90 Hz range (Buzsaki 2006a). However, this broad band has been recently shown to be further distinguishable in sub-bands, each accounting for a distinct mechanism of generation, on the basis of the degree to which the wave amplitude at each frequency is modulated as a function of a slower rhythm phase (Belluscio et al. 2012; Tort et al. 2010). Despite the lacking of a widely accepted convention over hippocampal gamma bands and nomenclature (Buzsáki and Wang 2012; Colgin and Moser 2010), at least two gamma ranges are generally acknowledged in the < 100 Hz spectrum. Accordingly, we defined a SG band as 25 – 40 Hz (Pagliardini, Gosgnach, Dickson 2013), a HG band as 40 – 90 Hz and an epsilon band as 110 -190 Hz (Belluscio et al. 2012; Buzsáki and Wang 2012; Freeman 2007; Scheffer-Teixeira et al. 2013). Finally, the beta band was defined between 10 and 25 Hz (Lowry and Kay 2007).

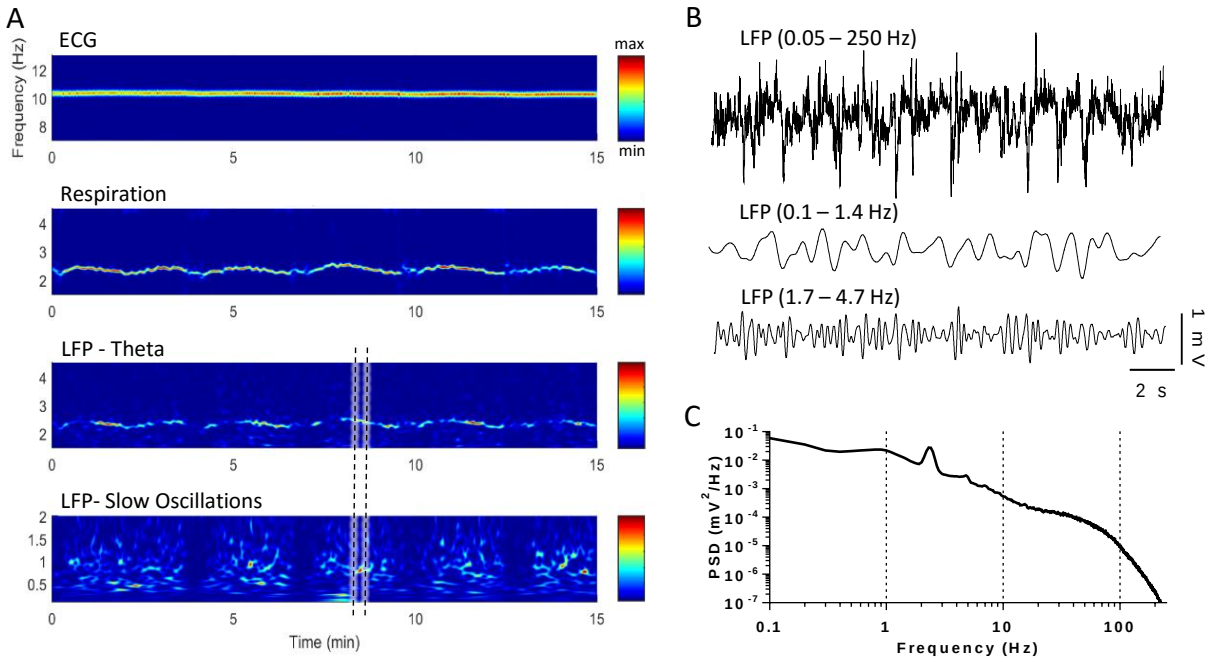

Figure 11. Frequency components of ECG, respiration and hippocampal LFP signals. A, Time-frequency spectrograms computed, respectively, from the ECG, respiration and hippocampal LFP traces simultaneously recorded in a 6–month-old wt mouse. Dashed lines indicate time window of the traces in B. **B**, LFP signal, from the time interval highlighted in A. The traces represent the same recording, yet broad-band, slow oscillation band and theta band filtered, respectively. **C**, Power spectrum computed from the same full-length LFP recording as in A. Slow oscillations and theta rhythm are prominent in the LFP signal. Theta oscillations and respiratory rhythm have the same frequency (2 – 3 Hz) and follow similar fluctuations of peak frequency and power. Slow oscillation power alternates coherently with that of theta.

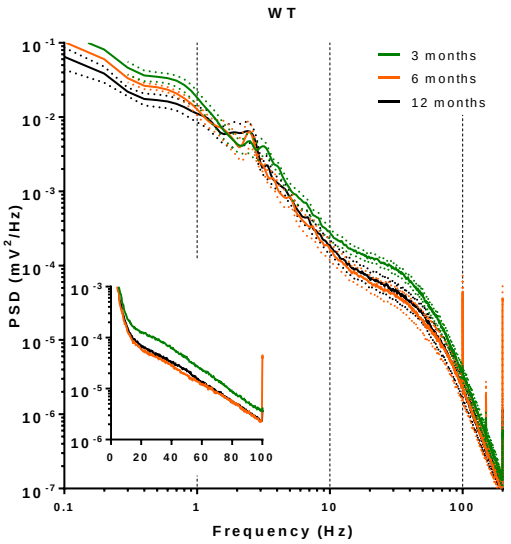
WT
3 months
6 months
12 months
PSD (mV²/Hz)
Frequency (Hz)

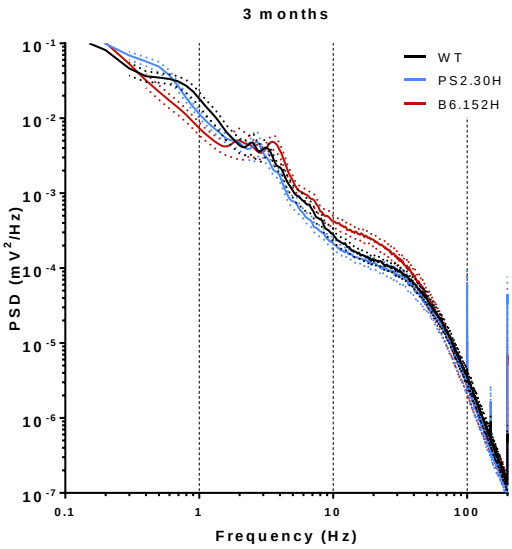
3 months
WT
PS2.30H
B6.152H
PSD (mV²/Hz)
Frequency (Hz)

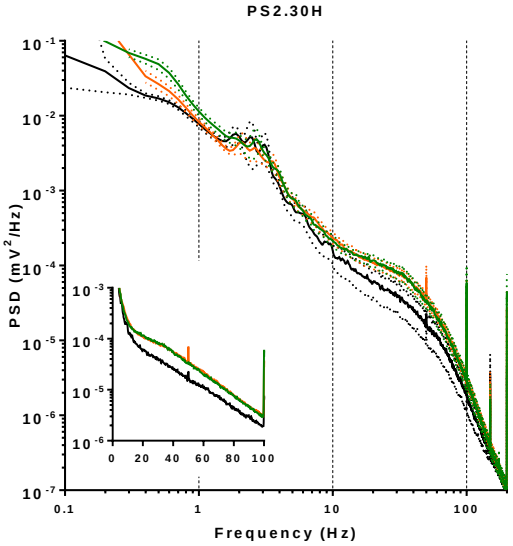
PS2.30H
PSD (mV²/Hz)
Frequency (Hz)

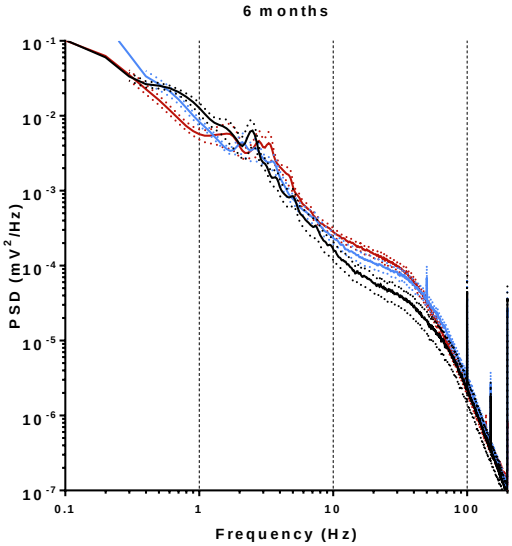
6 months
PSD (mV²/Hz)
Frequency (Hz)

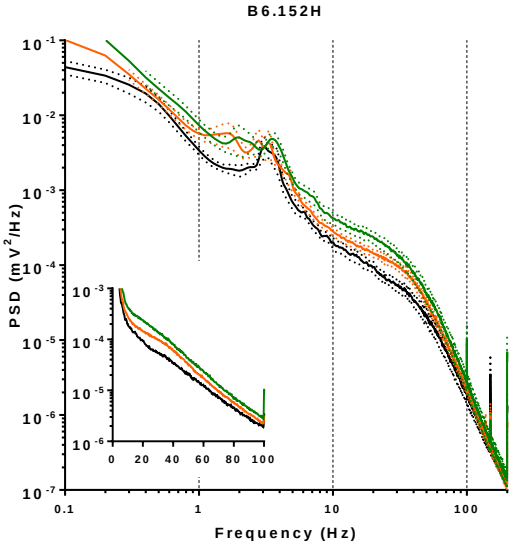
B6.152H
PSD (mV²/Hz)
Frequency (Hz)

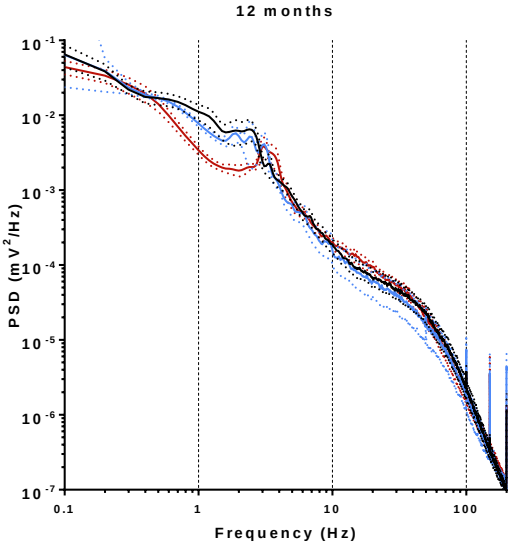
12 months
PSD (mV²/Hz)
Frequency (Hz)

Figure 13. Power spectral density compared by age and genotype. Left panels report the average PSD of each age-genotype group, compared within genotypes. A general trend to a decrease of spectrum offset is observable across genotypes. Right panels report the same power spectra as in the left panels but compared within different ages. A trend to a shift of SO power towards lower frequencies is appreciable at all ages. A "shoulder" of broad-band increased power is notable in the B6.152H line at 3 months of age as well as in both the PS2.30H and B6.152H line at 6 months of age roughly in the 10 – 45 Hz range. Spectra are represented in the "log-log" space. Inset-graphs in left panels are in semi-log representation, with the horizontal axis linearly scaled. Dotted lines represent ± SEM

7.2 HIPPOCAMPAL SLOW OSCILLATIONS, THETA AND RESPIRATION RHYTMS

Urethane anesthesia slowed mice respiration rhythm to 2 – 4 Hz (see Figure 7), consistently with other studies (Depuy et al. 2011; Yanovsky et al. 2014). Moreover, respiratory rhythm was entrained in a regular fluctuation, as described by Dickson's group (Pagliardini, Gosgnach, Dickson 2013).

Spontaneous theta oscillations in the LFP recordings reliably had the same frequency of respiration and followed its fluctuation, similarly to the recently described hippocampal oscillation induced by respiration – HRR (Yanovsky et al. 2014).

7.3 ALTERATION OF THE POWER SPECTRA DENSITY

We first asked whether the oscillatory pattern of the three lines was comparable across the three aging stages that we considered (3, 6 and 12 months). When the mean power spectra were computed for each group and plotted as the logarithm of the power density against the logarithm of the frequency (i.e. "log-log" plot) (see Figure 8, left panels), a tendency to an age-dependent overall decrease of the offset was observed in all genotypes. This phenomenon is better appreciable when power spectra are represented in the semi-log space (insets of Figure 8).

Next, in order to highlight alterations in the oscillatory activity of the three lines, we compared the mean power spectra of the animals by genotype at the different ages (see Figure 8, right panels).

Interestingly, the PSD decay function of B6.152H mice, represented in log-log, appears to be rotated at across the theta peak, when compared with that of wt mice. In fact, the slow oscillations are left-shifted towards lower frequencies and the SG activity is increased in power, the effect being stronger at 3 and 6 months on age.

We further investigated whether a broad-band alteration of the PSD function could underlay this observation. In particular, the slope coefficient has been described to be affected in several neurological diseases and disturbs, including Parkinson's disease and schizophrenia (Voytek and Knight 2015). Therefore, we evaluated the steepness of the power spectra by linear fitting the PSD curve, represented in semi-log, in the 10 – 100 Hz range (see Figure 9). We found that the PSD decay is significantly steeper ($p < 0.05$, Mann-Whitney rank-sum test) in both 3- (B6.152H, -0.257 ± 0.025; wt, -0.207 ± 0.020) and 6-month-old (B6.152H, -0.238 ± 0.024; wt, -0.199 ± 0.028) B6.152H mice compared to wt mice, although a tendency in the same direction is also noticeable at 12 months of age. Conversely, PSD steepness in PS2.30H mice was comparable ($p \geq 0.05$, Mann-Whitney rank-sum test) with wt mice at each considered age.

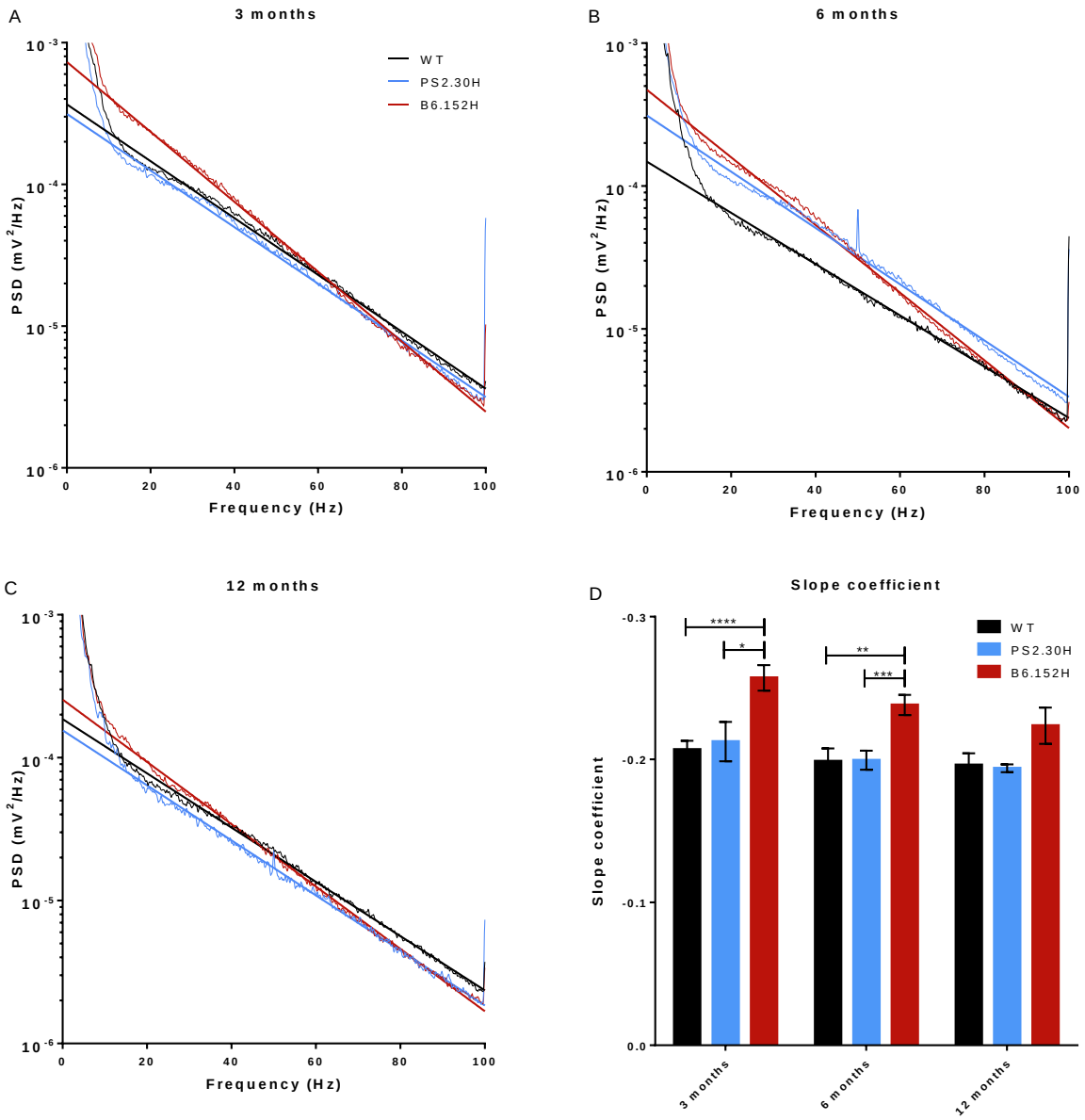

Figure 15. PDS linear fit. A-C, Mean power spectra of each age-genotype group as presented in the right panels of Figure 8 but limited to the ≤ 100 Hz frequencies and plotted in the semi-log space. Straight lines represent linear fitting computed in the range 10 – 100 Hz. SEM is not displayed for the sake of readability. **D**, Bar graph reporting the mean linear-fit slope coefficient for each age-genotype group. B6.152H mice present a significantly steeper decay at both 3 and 6 months of age with respect to the other mouse lines. The steepness appears to decrease with aging in B6.152H mice. Error bars represent ± SEM. *, $p < 0.05$; **, $p < 0.01$; ***, $p < 0.001$; ****, $p < 0.0001$. Mann-Whitney rank-sum test.

Taken together, these results indicate an overall alteration of DG network dynamics under urethane anesthesia, as inferable through the analysis of the PSD slope coefficient, in B6.152H, but not PS2.30H mice, as soon as 3 months of age.

7.4 Enhancement of beta and gamma power

Since the power spectrum appeared rotated in the lower frequencies (< 30 Hz), at least in the B6.152H line, we asked whether this could affect the power in the individual bands. Therefore, we obtained the power by computing the integral of the PSD function in each band (see Figure

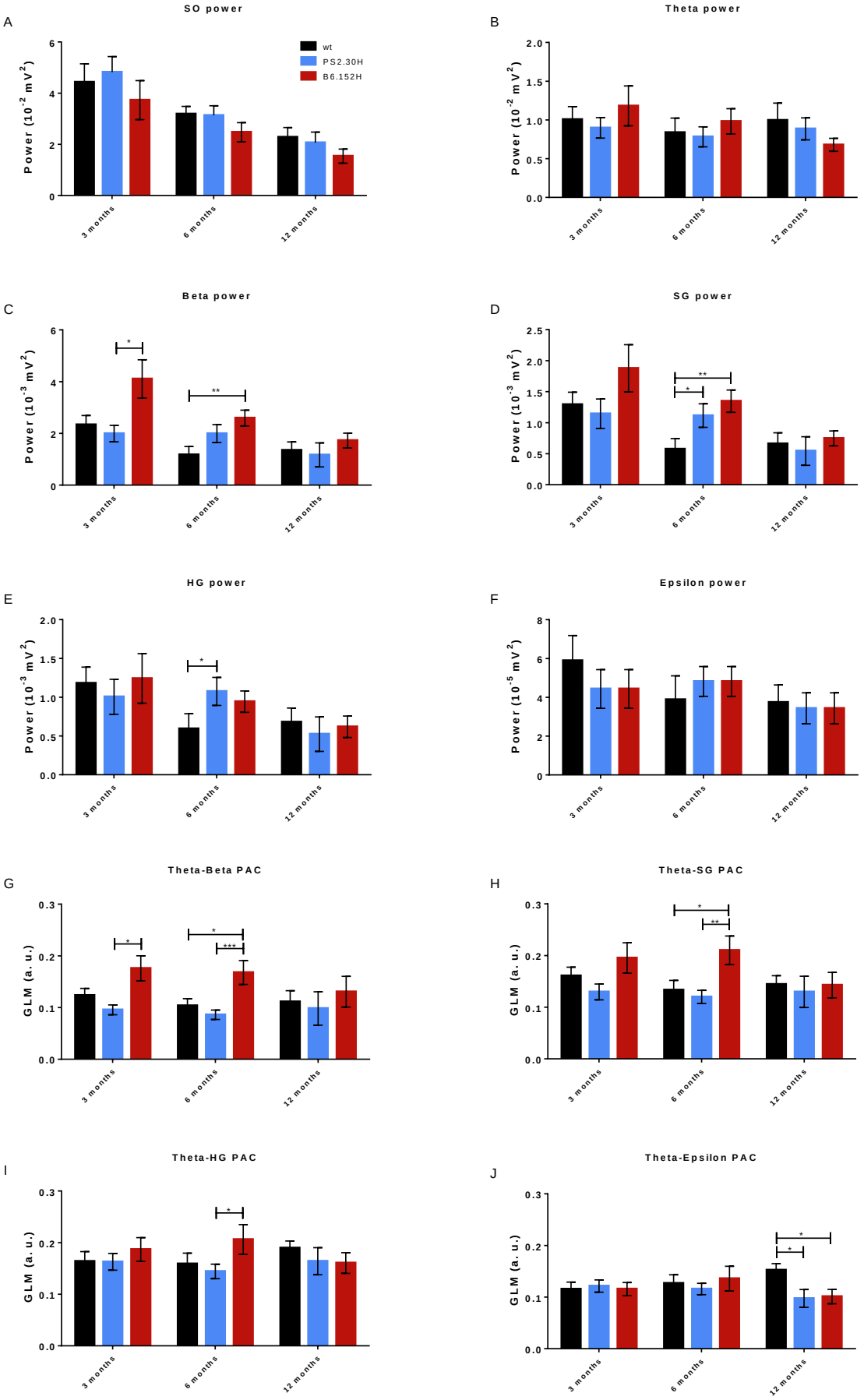
A
SO power
wt
PS2.30H
B6.152H
Power (10-2 mV2)
3 months
6 months
12 months
B
Theta power
Power (10-2 mV2)
C
Beta power
Power (10-3 mV2)
D
SG power
Power (10-3 mV2)
E
HG power
Power (10-3 mV2)
F
Epsilon power
Power (10-5 mV2)
G
Theta-Beta PAC
GLM (a. u.)
H
Theta-SG PAC
GLM (a. u.)
I
Theta-HG PAC
GLM (a. u.)
J
Theta-Epsilon PAC
GLM (a. u.)

Figure 17. Power and PAC. A-F, Bar graphs of mean power within individual oscillation bands, computed as the integral of PSD in the relative range. In B6.152H mice, power is significantly increased in the beta band at 3 months of age as well as in the beta and SG bands at 6 months of age. In PS2.30H mice, power is significantly increased in the SG and HG bands at 6 months of age. No power difference is present at 12 months of age among genotypes. **G-J**, Bar graphs of mean GLM index of PAC within individual classes. In the B6.152H line, PAC level is increased in the theta-beta and -SG classes at 6 months of age. Both B6.152H and PS2.30H lines present reduced theta-epsilon PAC at 12 months of age. In 3- and 6-month-old PS2.30H mice, in spite of no statistical difference with wt mice, PAC level is significantly lower than B6.152H mice in the theta-beta (3 and 6 months), theta-SG (6 months) and theta-HG classes (6 months). Error bars represent ± SEM. *, $p < 0.05$; **, $p < 0.01$; ***, $p < 0.001$. Mann-Whitney rank-sum test.

10, panels A – F) and we observed that all genotypes were statistically comparable ($p \geq 0.05$, Mann-Whitney rank-sum test), at all ages, in terms of SO and theta power as well as concerning the power in the very high frequency epsilon band. On the other hand, alterations of the beta and/or gamma band power emerged in both lines at the age of 6 months. In particular, B6.152H mice presented both beta (B6.152H, 2.592e-3 ± 0.305e-3 mV^2; wt, 1.177e-3 ± 0.317e-3 mV^2) and SG (B6.152H, 1.347e-3 ± 0.179e-3 mV^2; wt, 0.575e-3 ± 0.169e-3 mV^2) power increase ($p < 0.05$, Mann-Whitney rank-sum test) at 6 months of age with respect to wt mice. Similarly, in the PS2.30H line SG (PS2.30H, 1.115e-3 ± 0.190e-3 mV^2) and HG (PS2.30H, 1.075e-3 ± 0.181e-3 mV^2; wt, 0.593e-3 ± 0.193e-3 mV^2) power were significantly enhanced compared to wt mice. Additionally, beta power was enhanced in 3-month-old B6.152H mice with respect to age-matched PS2.30H mice (B6.152H, 2.592e-3 ± 0.305e-3 mV^2; PS2.30H, 1.993e-3 ± 0.344e-3 mV^2).

At 12 months of age, the last time point we considered, the amplitude of all oscillations was comparable across genotypes.

In conclusion, both PS2.30H and B6.152H lines present enhancement of the power in individual, yet not fully overlapping, bands encompassing the beta-gamma range, at 6 months of age. This variation from the wt phenotype results fully reversed at 12 months of age.

7.5 Theta-gamma Phase Amplitude Coupling

Finally, we asked whether the spectral alterations that we observed could be accompanied by changes at a higher level of oscillatory network behavior, namely the phenomenon of frequency nesting. In particular we addressed the CFC between the phase of the theta oscillation and amplitude of higher frequencies. We quantified the PAC in the theta-beta, -SG, -HG and -epsilon classes by computing the GLM index as described in Materials and Methods (see Figure 10, panels G - J). According to the recommendations developed by the work of Aru J. et al. (Aru et al. 2015) for CFC investigation, we ensured (i) that the lower, modulating, frequency band actually corresponded to an oscillatory activity (i.e., theta) and (ii) that the bandwidth of higher, modulated, frequency always was at least 2 times the frequency of the modulating band. Nevertheless, we wish to highlight that, owing to our experimental framework, which was intended for assessing spontaneous activity, we could not verify to what degree the CFC coupling that we observed was due to causal relationship between the theta and the higher frequency oscillations. Therefore, it is possible that the levels of CFC that we report here were determined, at least to a certain degree, by common drive onto the DG network (Aru et al. 2015).

In B6.152H mice, the pattern of alteration of PAC level in the different classes closely resembles that of power (see Figure 10, panels A – F). In fact, theta-beta (B6.152H, 0.168 ± 0.023; wt, 0.103 ± 0.013) as well as theta-SG (B6.152H, 0.210 ± 0.028; wt, 0.133 ± 0.018) PAC resulted

significantly enhanced ($p < 0.05$, Mann-Whitney rank-sum test) in this line compared to wt mice at 6 months of age. On the contrary PS2.30H mice did not present any difference ($p \geq 0.05$, Mann-Whitney rank-sum test) with respect to wt mice either at 3 or 6 months of age. Despite the increase of SG and HG power in 6-month-old PS2.30H mice, the level of PAC in the classes concerning those bands results unaffected or even, perhaps, slightly reduced, as suggested by the statistically significant difference existing with age-matched B6.152H mice in both the theta-SG (B6.152H, 0.210 ± 0.028; PS2.30H, 0.120 ± 0.013) and the theta-HG (B6.152H, 0.206 ± 0.029; PS2.30H, 0.144 ± 0.014) classes, as well as in the theta-beta class both at 3 (B6.152H, 0.176 ± 0.024; PS2.30H, 0.096 ± 0.009) and 6 (B6.152H, 0.168 ± 0.023; PS2.30H, 0.086 ± 0.009) months of age. Finally, both transgenic lines reported a diminished theta-epsilon PAC at 12 months (B6.152H, 0.101 ± 0.014; PS2.30H, 0.097 ± 0.017; wt, 0.152 ± 0.012).

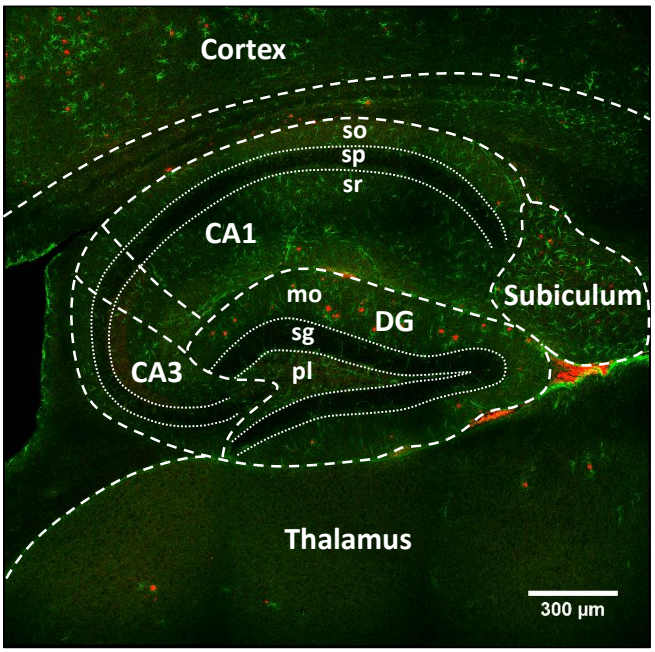

Figure 19. Cortical and hippocampal ROIs for amyloid plaques and astrogliosis analysis. Brain sagittal proximo-medial slice from a 6 month-old B6.152H mouse. The sub-regions of the HF and portion of cortex that we defined as ROIs for our IHC analysis are illustrated. Abbreviations: CA, *Cornu Ammonis*; so, *stratum oriens*; sp, piramidal layer; sr, *stratum radiatum*; DG, Dentate Gyrus; mo, molecular layer; sg, granule cell layer; pl, polymorphic layer. Aβ, red; GFAP, green. Brightness and contrast were adjusted for each colour channel for the sake of the illustration aim.

Taken together, these results indicate that the PS2.30H and B6.152H lines express markedly different alterations of network activity in terms of theta-higher frequency coupling at 3 and 6 months of age. In particular, at 6 months of age, the former displays significant overcoupling in two of the considered classes, as opposite to the latter that reports no difference in any class, compared to the wt line. Notwithstanding the differences existing between the transgenic lines in the first two ages of our study, PAC levels of PS2.30H and B6.152H mice converge to similar values at 12 months of age.

7.6 Amyloid plaque deposition and astrogliosis

Among the major histopathological hallmarks of AD are the extracellular deposition of amyloid plaques and the establishment of gliosis, i.e. the sustained inflammatory glial response to insulting conditions.

To provide histological disease correlates of the electrophysiological observations we obtained from our models, we evaluated the deposition of amyloid plaques as well as the presence of astrogliosis by IHC, at 3 and 6 months of age (see Materials and Methods).

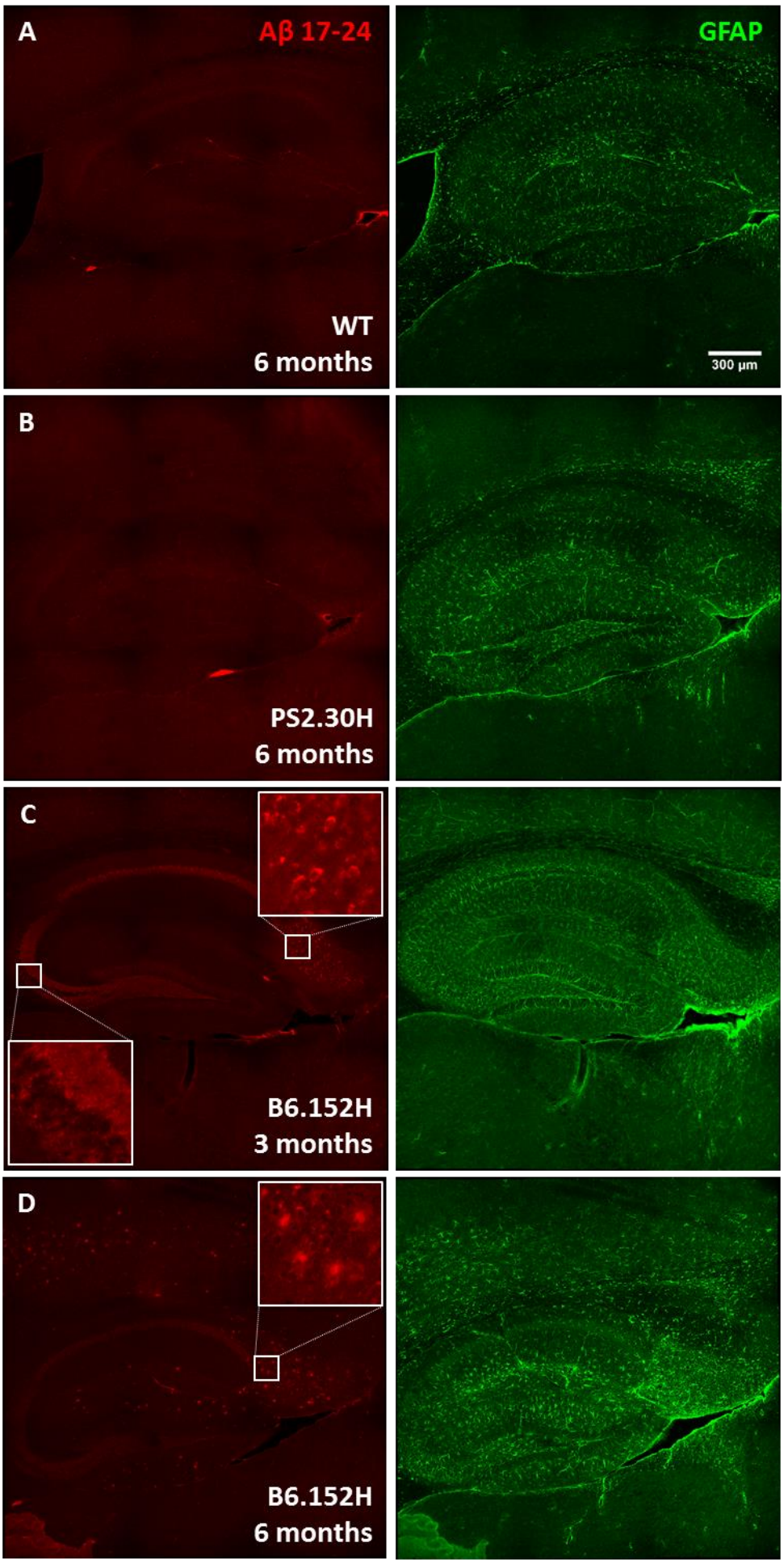
A
Aβ 17-24
GFAP
WT
6 months
300 µm
B
PS2.30H
6 months
C
B6.152H
3 months
D
B6.152H
6 months

Figure 21. Aβ load and astrogliosis. A-D, Representative images of slices from a 6-month-old wt mouse (**A**), a 6-month-old PS2.30H mouse (**B**), a 3-month-old B6.152H mouse (**C**) and a 6-month-old B6.152H mouse (**D**), where Aβ (left panels) and GFAP (right panels) were immunolabelled. Images in the same raw were acquired from the same slice. At 3 months of age, B6.152H mice display a strong intracellular accumulation of Aβ and/or Aβ-containing peptides, in particular in the subiculum and in the sp layer of CA1. The same layer in CA3 does not mirror the phenomenon. Conversely, in the CA3 subfield the sr layer appears diffusely labelled. Insets in **C**, magnification of a CA3 sp-sr and a subiculum detail, respectively. No deposition of amyloid plaques is observable in slices other than from the B6.152H line at 6 months of age (**D**). Plaques are mainly localized in the subiculum and, to a lesser extent, in the DG and in the cortex. Inset in **D**, magnification of a plaque-containing subiculum detail. GFAP labelling markedly increases in 6-month-old B6.152H mice (**D**) at the level of subiculum, DG and cortex.

The antibody that we employed to target Aβ – 4G8 – has been raised against the 17-24 epitope of the peptide. This latter is a portion of the APP extracellular domain - that is not buried within the lipid bilayer - before the secretase-operated cleavage. The 4G8 antibody labels both Aβ peptides, present in aggregates and amyloid plaques, as well as full-length APP and its β-carboxy-terminal fragment, at the membrane level.

We consistently found marked plaques deposition in the HF, especially in the *subiculum* and, to a lesser degree, in the DG, as well as in the cerebral cortex of the 6-month-old B6.152H compared to wt mice (n = 3, each group) (see Figure 12). These findings confirm and expand previous observations obtained in B6.152H mice by the Congo red approach, which mainly detects the fibril status of the deposits (Ozmen et al. 2009). On the contrary, extracellular amyloid aggregates were not observed in 3 month-old B6.152H mice (n = 3). However, a noticeable intracellular staining was detected in all considered territories (see magnification in inset of Figure 12, panel C), yet it was particularly strong in the *subiculum* and in the pyramidal layer (sp, *stratum pyramidalis*) of the CA1 region. Interestingly, as soon as the sp enters the CA3 sub-field, the intracellular labelling appears to drastically fade, in favor of a diffused staining of the CA3 *stratum radiatum* (sr) (see magnification in inset of Figure 12, panel C). Although we cannot affirm that the intracellular labelling that we observe represents Aβ accumulation, rather

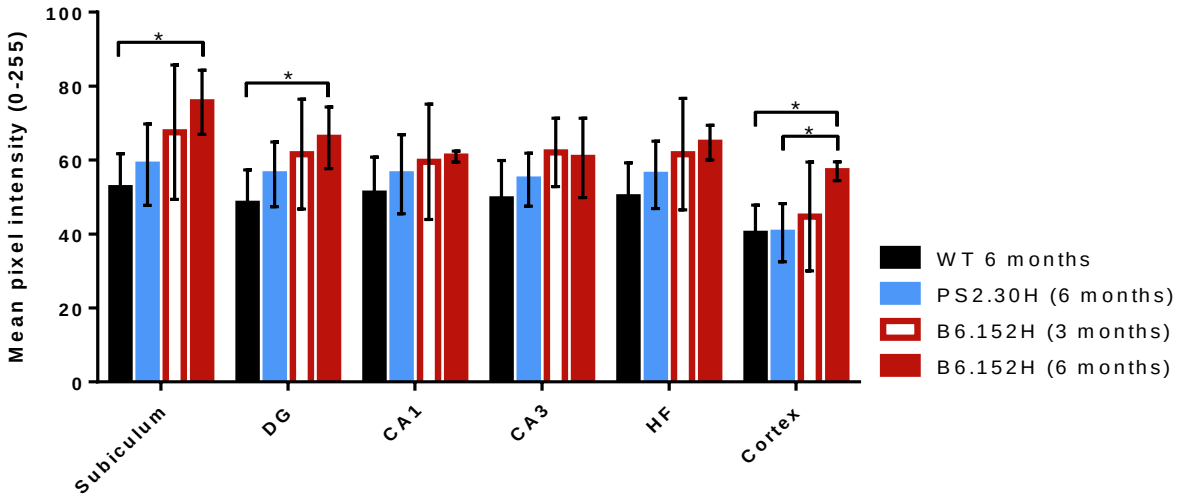

Figure 23. GFAP staining intensity. The degree of astrocytes reactivity in the HF and its sub-regions, as well as in the cortex, was evaluated through the intensity of GFAP staining, which was performed, imaged and analyzed under standardized parameters. Astrocytes reactivity results significantly enhanced, with respect to wt, only in the B6.152H line at 6 months. For all groups, n = 3. Error bars represent ± SEM. *, $p < 0.05$. Mann-Whitney rank-sum test.

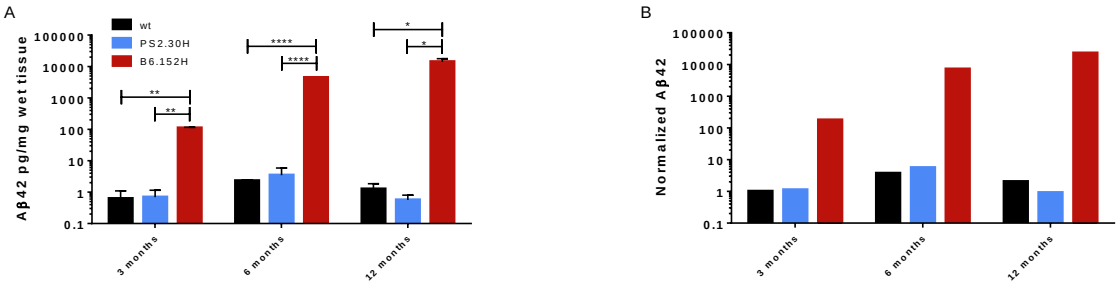

Figure 25. Hippocampal $A\beta_{42}$ quantification. The total amount of $A\beta_{42}$ was obtained by means of ELISA assays. **A**, Mean absolute quantity of $A\beta_{42}$. Error bars represent ± SEM. *, $p < 0.05$; **, $p < 0.01$; ****, $p < 0.0001$. Student's t-test. **B**, Mean $A\beta_{42}$ quantity normalized to the average in 3-month-old wt mice. In both graphs the y-axes is in log-scale. Only in the B6.152H line $A\beta_{42}$ levels are significantly higher compared to wt mice.

than APP overexpression, this would be in line with previous studies reporting that Aβ accumulates with the cells before plaques deposition (Gyure et al. 2001; Wirths et al. 2001).

Within the framework of the brain inflammatory condition that accompanies AD, astrocytes become reactive and increase the expression levels of the intermediate filament protein GFAP, this condition being known as astrogliosis (Steardo Jr et al. 2015). We quantified the expression of GFAP through the intensity of the staining fluorescent signal as shown in Figure 12. A quantitative analysis was carried out within specific regions as defined in Figure 11 and Materials and Methods, and summarized in Figure 13. We found a statistically significant increase ($p < 0.05$, Mann-Whitney rank-sum test) of mean intensity in the *subiculum* of 6-old-month B6.152H mice, compared to age-matched wt mice (B6.152H, 75.6 ± 6.1; wt, 52.4 ± 5.4), the DG (B6.152H, 66.0 ± 5.9; wt, 48.2 ± 5.3) and the cortex (B6.152H, 57.0 ± 1.8; wt, 40.0 ± 4.5).

7.7 Amyloid accumulation

It is now largely accepted that in AD synaptic loss and neuronal dysfunction are caused by accumulation of soluble forms of $A\beta_{42}$, especially small oligomers, rather than by amyloid plaques. The accumulation of $A\beta_{42}$ was thus evaluated at the hippocampal level by means of ELISA kits suited to measure both mouse and human $A\beta_{42}$ (see Materials and Methods). As shown in Figure 14, compared to wt mice, the PS2.30H mice have only slightly higher levels of $A\beta_{42}$, which are in the order of few pg/mg of wet tissue. In contrast, the B6.152H mice have about 100 times more $A\beta_{42}$ than wt mice at all the ages, in particular the 3-month-old B6.152H mice show $A\beta_{42}$ levels about 30 times higher than those found in 6-month-old PS2.30H mice.

8 DISCUSSION

In this work, we explored the electrophysiological alterations in the LFP activity of the DG network of two AD mouse models, PS2.30H and B6.152H, which harbor the N141I mutated form of PS2, respectively alone or in combination with the Swedish mutation of APP. We acquired the LFP signal in the condition of urethane anesthesia and extracted signal features, including amplitude, spectral steepness and theta-higher frequencies PAC by means of frequency and time-frequency methods. Importantly, to the end of assessing the temporal evolution of the features into exam, we investigated three age points, namely 3, 6 and 12 months, i.e before, during and after heavy plaque deposition, and we probed the time-matched presence of histological hallmarks, in the form of amyloid plaques and astrogliosis, as well as the degree of Aβ load. The electrophysiological alterations with respect to wt mice are summarized in Table 1. We first address the physiological significance of the observed alterations in the power, PAC and steepness categories and, next, we discuss these alterations in the context of the AD literature.

8.1 HYPER-SYNCHRONICITY: PSD AND PAC

The LFP, ECoG and EEG signals, when converted in the frequency domain by means of the Fourier transform, display a characteristic composition of a broad range of frequencies where, importantly, the amplitude exponentially decays as a function of the frequency. In agreement, the PSD function of a brain extracellular recording is often defined as $1/f^x$, where x is the scaling exponential of the decay. Concerning the nature of this behavior that is ubiquitously present in brain recordings, it has long been debated, whether the $1/f^x$ function decay is a mere background noise, differentially propagating as a function of the frequency owing to low-pass filtering properties of the tissue (Nunez 1981), or it is a component of brain functioning dynamics (Buzsaki 2006b). Only recently, the $1/f^x$ function has been led down to the size of the various

Table 1. Summary of the significant electrophysiological alterations in comparison with wt mice.

	3 months		6 months		12 months	
	PS2.30H	B6.152H	PS2.30H	B6.152H	PS2.30H	B6.152H
SO power	-	-	-	-	-	-
Theta power	-	-	-	-	-	-
Beta power	-	-	-	↑↑	-	-
SG power	-	-	↑	↑↑	-	-
HG power	-	-	↑	-	-	-
Epsilon power	-	-	-	-	-	-
Theta-beta PAC	-	-	-	↑	-	-
Theta-SG PAC	-	-	-	↑	-	-
Theta-HG PAC	-	-	-	-	-	-
Theta-Epsilon PAC	-	-	-	-	↓	↓
PSD slope coefficient	-	↑↑↑↑	-	↑↑	-	-

↑, increase, $p < 0.05$; ↑↑, increase, $p < 0.01$; ↑↑↑↑, increase, $p < 0.0001$; ↓, decrease, $p < 0.05$; Mann-Whitney test

frequency generators (Logothetis, Kayser, Oeltermann 2007) and has started to be widely recognized as a large scale representation of neural activity, thus, as a rich source of valuable information on the underlying network operations (Buzsáki, Logothetis, Singer 2013; He et al. 2010; He 2014).

The broad band power of extracellular brain recordings was shown to positively correlate with neuronal firing rate (Manning et al. 2009) but it is the slope coefficient of the PSD function that is funneling the most interest, mainly because it has been demonstrated to change depending on the behavioral task. For instance, the *x* exponential was reduced (i.e., the spectrum flattened) during a visual detection task when the subject was presented with an unpredictable stimulus (He et al. 2010) as well as in correspondence with sensory and motor responses in a manner that was consistent across modalities, yet with specific features (Podvalny et al. 2015). Further, it was linked to memory processing, since it diminished in the course of a working memory task with the increase of the cognitive load (He 2014).

Finally, attempts to understand the mechanisms underlying the decrease of the spectral steepness point to an enhancement of decoupled firing (Freeman and Zhai 2009; Podvalny et al. 2015; Voytek and Knight 2015). In this sense, the PSD slope coefficient (or the x exponential of $1/f^x$), provides a measure of neuronal firing synchronicity, with increased steepness indicating enhanced synchronicity.

Here, we assessed the steepness of the PSD function represented in the semi-log space as the slope coefficient of the PSD linear fitting in the 10 – 100 Hz range. We report an early increase of PSD steepness in the B6.152H line at 3 months of age with respect to wt mice. This finding is suggestive of a condition of hyper-synchronicity, spontaneously appearing in DG network activity under urethane anesthesia. The phenomenon persists at 6 months of age, though a progressive reduction of its degree as a function of age is observable. At 12 months of age, B6.152H and wt mice no longer differ in terms of spectral steepness.

Another notable feature of brain extracellular recordings is embodied by nested oscillations, where a slower rhythm influences a faster one in a dynamic fashion. CFC, i.e. the relation within each pair of nested oscillations, can occur on amplitude-amplitude, phase-phase or phase-amplitude basis (Canolty and Knight 2010). In the last decade, this latter type of CFC – PAC – has drawn much attention, in particular concerning the theta and gamma oscillations. Theta-gamma PAC has been consistently described in several regions, including the cortex (Canolty et al. 2006; Lee et al. 2005) and the hippocampus (Axmacher et al. 2010; Belluscio et al. 2012; Bragin et al. 1995). Most notably, theta-gamma PAC increased during a learning task and, further, predicticted learning performance (Tort et al. 2009). Finally, reduction of theta-gamma PAC also hampered memory performance (Shirvalkar, Rapp, Shapiro 2010). In light of all these observations, CFC, in general, and theta-gamma PAC, in particular, are progressively losing their connotate of epiphenomenon and becoming recognized as a functional mechanism fundamental for brain function.

We investigated the level CFC existing in our LFP signals between the theta phase and the amplitude of beta, SG, HG and epsilon band, respectively, as quantified by means of the GLM. At 6 months of age, B6.152H mice displayed enhanced PAC compared to wt mice in the theta-beta

and -SG classes. These observations indicate a condition of overcoupling in the B6.152H line with respect to wt mice, emerging at 6 months of age. Interestingly, while PAC in all classes resulted unaffected with respect to wt mice in the PS2.30H line at both 3 and 6 months of age, the two transgenic mouse lines reported the strongest difference. Indeed, B6.152H PAC was higher in comparison with the PS2.30H line in the theta-beta class both at 3 and 6 months of age and in the theta-SG class at the age of 6 months. Moreover, 6-month-old B6.152H mice had also a stronger theta-HG PAC than PS2.30H mice. Taken together, these findings possibly suggest a slightly lower level of coupling in the PS2.30H line compared to wt mice, that is not possible to statistically resolve with the sample size in our hands. Finally, at 12 months of age all classes of PAC, resulting altered in the preceding time points of our analysis, appeared realigned to the wt mouse levels. All in all, 3- and 6-month-old PS2.30H mice appear unaffected in terms of theta-higher frequency PAC, contrarily to B6.152H mice that present features of overcoupling at 6 months of age. An exception is embodied by the theta-epsilon PAC, which was significantly reduced in both PS2.30H and B6.152H mice compared to age-matched wt mice at 12 months of age. Both transgenic lines, in spite of a strikingly different evolution of their PAC levels within the individual classes, appear in line with wt mice at 12 months of age, although the decreased level of theta-epsilon PAC that they display might represent the beginning of a different aging pattern.

While both the PAC and the PSD steepness are referred to as indicators of synchronicity within the network, their alterations in the B6.152H line do not fully overlap. However, it is important to note that they are not believed to represent the same phenomenon. On the one hand, PAC describes the level of modulation that the phase of a carrier frequency exerts on the amplitude of faster one and, in other words, it represents the ability of the slower rhythm to affect the statistical temporal distribution of neuronal firing. On the other hand, the PSD steepness reflects the overall statistics of neuronal firing, with a steeper slope resulting from a shift of neuronal firing towards increased synchronicity, thus contributing to the power of the slower oscillations (Podvalny et al. 2015). In addition, although we limited our analysis to the modulation brought by theta on the higher frequencies oscillations, the LFP signal features a hierarchy of nested oscillations in an extensive progression throughout the frequency spectrum (He et al. 2010; Lakatos et al. 2005). Hence, the apparent discrepancy between the hyper-synchronicity evaluated by means of the PAC and the PSD slope, respectively, could perhaps be overcome if a larger combination of phase-frequency/amplitude-frequency pairs were taken into exam.

Surprisingly, at 3 and 6 months of age, analysis of the PSD steepness resulted in a highly significant difference between the B6.152H and the wt line, in spite of a far weaker difference resolving these two lines in terms of individual bands power or theta-higher frequency PAC. Yet this is somehow predicted by previous studies indicating that, within the same behavioral conditions and brain area of interest, the scaling of the PSD is remarkably invariant across subjects (Linkenkaer-Hansen et al. 2001; Podvalny et al. 2015).

In conclusion, PSD steepness, better than theta-higher frequency PAC, is a feature of the hippocampal LFP that reliably characterizes the stages of the AD-like pathology in the B6.152H mouse model.

8.2 HYPERACTIVITY: BETA AND GAMMA POWER

Quantification of the power within different frequency bands is a rather open and widely used approach. However, the physiological significance of power-content changes in a given band should be carefully addressed. The power of individual bands is estimated basing on the frequency-domain representation of the signal, i.e. the PSD function. As a matter of fact, the brain PSD is a combination of oscillatory as well as irregular activities and, as such, it is a complex and, unfortunately, poorly understood phenomenon (He 2014). Nevertheless, general consensus advocates that while real oscillations determine narrow-band peaks in the PSD, broad-band "bulges" represent the spectral counterpart of neuronal firing. This is particularly true at frequencies > 30 Hz, as demonstrated by studies reporting that gamma activity (~ 30 – 100 Hz) correlates with neuronal spiking (Csicsvari et al. 2003) and can even be exploited to infer spike trains (Rasch et al. 2008). On the other hand, true forms of oscillatory activities do exist even in the higher range of the LFP spectrum (> 100 Hz) (Scheffer-Teixeira et al. 2013). In particular, in the hippocampus, ripples (140 – 200 Hz) have long been known (Buzsáki et al. 2003) and, recently, high-frequency oscillations (HFO, 120 – 160 Hz) were described (Scheffer-Teixeira et al. 2012).

In the present study, we observed an alteration of the PSD function in the PS2.30H and B6.152H models that occurs as a shoulder of increased power in the spectrum encompassing the beta range in 3-month-old B6.152H mice and, respectively, the beta-SG and the SG-HG range in the B6.152H and PS2.30H lines, at 6 months of age. If the broadband power increase in the gamma range may be promptly read as an enhancement of neuronal firing, the same phenomenon in the beta range requires more caution.

Hippocampal beta oscillations are far less studied than SO, theta and gamma activities in this region and the interpretation of our observation in relation with them is not straightforward. Yet, beta band oscillations have been described in the murine hippocampus. On the one hand, they were detected in the range 23 – 30 Hz ("beta2"), in the context of novel object recognition. In general, they appear to be linked to the detection of novelty (França et al. 2014). On the other hand, burst of beta (~20 Hz) activity, relayed from the pyriform cortex (PC) specifically to the DG, were elicited in rats in correspondence with the presentation of odors either from predators or organic solvents (Lowry and Kay 2007; Vanderwolf 2001). Both these beta activities just described are narrowband and short-lived and do not fit with the broadband shoulder that we observe in the B6.152H line at both 3 and 6 months of age.

From another perspective, positive correlation between broadband power increase and neuronal firing activity is not limited to the gamma and higher frequencies bands and was described at < 30 Hz LFP frequencies, although to a smaller degree with respect to higher frequencies (Manning et al. 2009). In this light, this phenomenon, in spite of the relatively low frequency, is likely to reflect an increase of neuronal firing with respect to wt mice, i.e. hyperactivity.

All in all, the power spectrum alterations that we report suggest that both the AD mouse models in this study present a condition of neuronal hyperactivity at 6 months of age.

In the murine cortex *in vivo*, it was demonstrated that an optogenetically-operated enhancement of fast-spiking (FS) interneuron firing activity at a frequency ranging from 20 to 80 Hz results in a greater LFP power at the frequency corresponding to the stimulation. Lower stimulation frequencies yielded firing of FS interneurons but did not modulate LFP power. Conversely, opto-stimulation specifically targeting excitatory pyramidal cells produced an increase of LFP power only when provided at 8 - 24 Hz frequency. As for FS interneurons, the frequency of LFP power increase matched that of the stimulation (Cardin et al. 2009).

We speculate that the increase of power in the gamma range might be due to two, possibly combined, reasons: (i) an intrinsic hyperactivity and/or hyperexcitability of (FS) interneurons within the DG network and (ii) an increase of external drive onto FS interneurons in the DG. For instance, neurons in the nucleus basalis of Meynert, which provide a minor source of cholinergic input to the hippocampus, were reported to be metabolic hyperactive during MCI (Dubelaar et al. 2006). Future experiments aimed at interfering with the synaptic inputs of DG FS interneurons (mainly consisting of basket cells) brought by either external afferences or local excitatory granule cells will probably shed light on the mechanism/s underlying the increase of gamma power in the DG.

8.3 HYPERACTIVITY/HYPER-SYNCHRONICITY AND AD

The phenomena of hyperactivity and hyper-synchronicity are both well-known in the clinical field of AD.

Many works have investigated brain activity alterations in patients diagnosed with AD or MCI by means of functional imaging techniques, the most popular being the BOLD-fMRI. A stronger activation of the hippocampal region was reported in MCI patients while performing a recognition memory task. Interestingly, these subjects performed similarly to controls and presented no difference in terms of hippocampal volume. On the contrary, the same study showed that AD patients displayed fMRI-assessed hippocampal activation similar to controls while performing worse at the mnemonic task and exhibiting a reduced hippocampal volume (Dickerson et al. 2005) (see Introduction). Subsequent studies, although is the presence of a

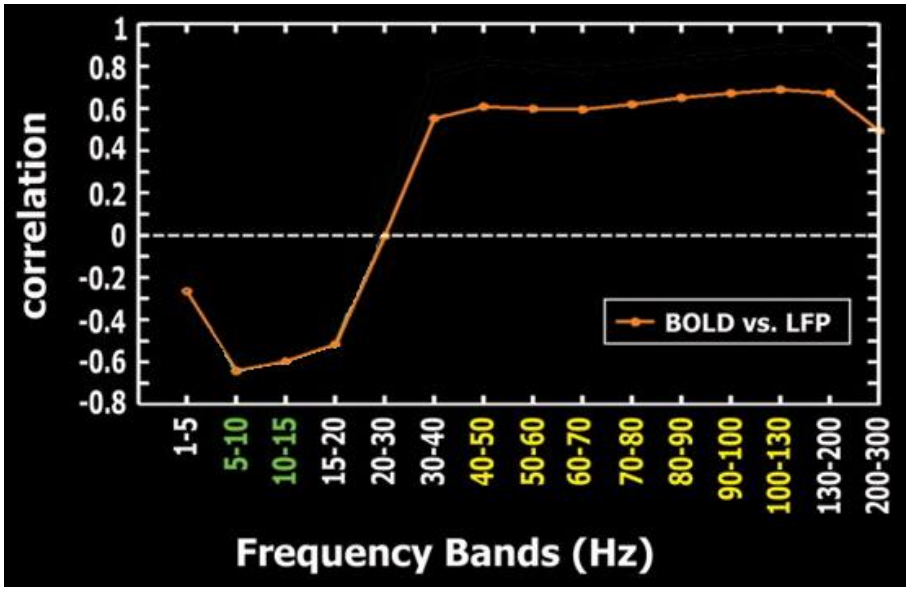

Figure 27. Correlation between BOLD-fMRI and LFP signals as a function of the frequency. The correlation between the average BOLD-fMRI signal in the auditory cortex during an auditory session (BOLD) and the fMRI signal predicted from the LFP activity in each range (LFP) recorded in the same location. The correlation is high and positive above 40 Hz, indicating that the fMRI signal modelled basing of the > 40 Hz LFP accurately correlates with the real signal. *Vice versa*, in the 5 – 15 Hz LFP range, the real signal strongly negatively correlates with the predictors. Adapted from (Mukamel et al. 2005).

certain variability in terms of results (Johnson et al. 2006; Machulda et al. 2003), have overall contributed to draw a picture where the beginning of the clinical phase of AD, corresponding to MCI, is marked by hyperactivity in the hippocampus as well as other cortical regions (Dickerson et al. 2005; Hämäläinen et al. 2007; Pihlajamaki, Jauhiainen, Soininen 2009). Interestingly, along with the activation of the hippocampus, a number of genes regulated by the synaptic activity were proved to follow the same pattern of early increased and late decreased transcription (Bossers et al. 2010; Lau et al. 2013). In particular, increased fMRI-assessed hippocampal activation was found in presymptomatic subjects harboring a PS1 FAD mutation. Also in this case, FAD mutation carriers performed similarly to control subjects (Quiroz et al. 2010).

The relation between the fMRI signal and the ongoing electrophysiological activity is not completely understood but it is being uncovered (He et al. 2008). The LFP signal recorded from the auditory cortex was shown to markedly correlate with fMRI-imaged activation in that same area in the course of an auditory task. Importantly, the correlation with the fMRI signal was positive for frequencies above 40 Hz and negative for frequencies below 15 Hz in the LFP recording. Additionally, correlation declined above 130 - 140 Hz (Mukamel et al. 2005; Nir et al. 2007). These observations bridge between the neuronal spiking rate in a given region and the degree of above-baseline activation of that area, imaged by the fMRI (see Figure 15).

Hyper-synchronicity, on the other hand, represents a common feature in AD, in the form of epilepsy. The incidence of seizures is higher in AD patients than in control groups (Lozsadi and Larner 2006) and it reaches even higher levels in the early-onset FAD subjects (Palop and Mucke 2009) with 32% of PS2-N141I-FAD patients showing seizures (Jayadev et al. 2010). Notably, epileptiform activity has been often observed as electroencephalographic seizures associated with transient epileptic amnesia (TEA) (Rabinowicz et al. 2000), raising the hypothesis of epileptic discharge to be an underestimated phenomenon (Mendes 2002; Palop et al. 2007). Finally, it is worth noting that epileptiform activity emerges at very young age in FAD early-onset subjects, long before the first cognitive symptoms are detected.

Taken together, the above described findings provide a framework for the interpretation of our results in regard both to the hyperactivity and the hyper-synchronicity. The former, that we statistically detect in both our transgenic lines at 6 months of age, is in line with previous studies indicating a condition of enhanced fMRI activity in MCI patients, while the latter correlates with higher incidence of epilepsy found in FAD families' pedigrees as well as with the consistent observation of TEA in AD patients.

8.4 Hyperactivity and AD mouse models

The neuronal hyperactivity that we found in both the transgenic lines investigated, adds to similar previous observations obtained from other AD models, in support to the hypothesis claiming early neuronal hyperactivity to be a biomarker of AD.

In particular, neuronal hyperexcitability was demonstrated at 3 – 4 months of age in different mice, including the hAPPJ20 line, expressing hAPP with various forms of FAD mutations and it was linked with the non-convulsive seizures spontaneously appearing in those mice (Palop et al. 2007). Subsequently, spontaneous hyperactivity, in terms of increased neuronal firing rate, was

reported in hAPPJ20 mice in baseline condition (Verret et al. 2012). Notably, this line is known to exhibit plaques deposition starting from 5 – 7 months of age. Further, hyperexcitability, as augmented rate of Ca^{2+} transients, was observed in cortical neurons in the APP23xPS45 line in mice 6- to 10-month-old (Busche et al. 2008) and was later reported to occur in the hippocampus as well (Busche et al. 2012). Interestingly, while in the cortex the hyperactivity was detectable only concomitantly with plaques and, furthermore, in close proximity with these latter (Busche et al. 2008), in the hippocampus it was observed also at the age of 1 - 2 months, before plaques deposition (Busche et al. 2012).

In a more direct relation to our study, enhancement of hippocampal gamma power in the range ~20 – 45 Hz was reported in freely behaving 4-month-old APP23 mice (Ittner et al. 2014), characterized by plaques deposition starting at 6 months of age (Sturchler-Pierrat et al. 1997) (but see also (Rubio et al. 2012)).

As it was already observed (Stargardt, Swaab, Bossers 2015), all the FAD transgenic mouse line in which neuronal hyperactivity was described are based on mutated forms of APP and produce very high levels of Aβ as well as they exhibit plaque deposition at a very early age. Hence, these lines are not suited for addressing the question as whether the hyperactivity per se could be responsible, at least partially, of the cascade of events that underlay AD pathology. Our B6.152H line makes no exception. However it is interesting to note that in our study B6.152H mice developed a condition of hippocampal hyperactivity at the same age of PS2.30H mice. This occurred despite of the drastically different levels of $A\beta_{42}$ production. In particular, at the time point where we found the increased SG-HG power, PS2.30H mice present Aβ levels that are only slightly higher than those found in age-matched wt mice, no plaques deposition and no significant sign of astrogliosis. In addition, the hyperactivity is no longer detectable in both transgenic lines at the late time point of our study. Thus, the hippocampal hyperactivity that we report does not seem to correlate with Aβ levels and, considering the mismatch with plaques and astrogliosis in the PS2.30H, we speculate not to be a compensatory mechanism (Stargardt, Swaab, Bossers 2015). Thus it better correlates to the expression of mutant PS2. Experiments on PS2KO mice would possibly shed light on this issue.

Nevertheless, B6.152H mice exhibit a pattern of alterations of the LFP activity that is more complex than in the PS2.30H line. Indeed, in conjunction with the hyperactivity, they also present hyper-synchronicity, detectable as early as 3 months of age in form of a steeper PSD function decay, or at 6 month age as enhanced theta-beta and theta-SG PAC. Since the hyper-synchronicity is not detectable in the PS2.30H line at any age, this aspect is possibly attributable to the much higher levels of Aβ (and/or astrogliosis) that add on the effects due to mutated PS2. Experiments on mice carrying the APP Swedish mutation alone would provide further insight on the individual contribution provided by APP and PS2 mutations to the B6.152H phenotype.

Our results further support the hypothesis of an enhanced neuronal activity to precede the first clinical symptoms.

8.5 HYPER-SYNCHRONICITY AND AD MOUSE MODELS

Although no previous report, to the best of our knowledge, addressed neuronal synchronicity as measured by the PSD steepness in AD mouse models, nonetheless many studies have pointed to an increased spiking synchronicity as a common feature of mouse lines expressing mutated forms of APP. Epileptiform activity has been consistently found in several mouse lines expressing mutated APP, including hAPPJ20 (Palop et al. 2007), APP23 (Ittner et al. 2014), Tg2576 (Westmark et al. 2008) and CRND8 (Del Vecchio et al. 2004). In particular, not only sporadic seizures were described to spontaneously appear in freely behaving animals (Ittner et al. 2014; Palop et al. 2007; Westmark et al. 2008) but, in addition, the hyper-synchronicity emerged as an enhanced tendency to the development of seizures after administration of riluzole (Ittner et al. 2014; Verret et al. 2012), a voltage gated sodium channel blocker, or pentylenetetrazol (Del Vecchio et al. 2004; Westmark et al. 2008), a GABA-A receptor antagonist.

As for the hyperactivity (see previous paragraph), all the mentioned AD models are based on the overexpression of APP and it is, thus, difficult to estimate the individual contribution of Aβ and APP overexpression to the observed hyper-synchronicity. Born and collaborators specifically addressed this issue by generating a controllable APP-transgenic model in which APP expression was under the control of the Tet-Off system and could be reduced by about 80% through the administration of doxycycline (DOX). They found that their Tet-Off APP line presented increased synchronicity and seizures and that APP knock-down by administration of DOX, decreased APP and Aβ levels and reversed the altered phenotype. Conversely, selective decrease of Aβ through the administration of a γ-secretase inhibitor, LY411575, did not rescue the phenotype in spite of the significant reduction of Aβ levels. Finally, the authors tested for the presence of seizures and hyper-synchronicity the EEG of the AD model APP/PS1, where APP levels are similar to the wt ones, yet Aβ levels are boosted and amyloid plaques are formed. In this latter case they found neither spontaneous occurrence of seizure nor spectral alterations. They concluded that the aberrant synchronicity and the susceptibility to seizures in the Tet-Off APP line, as well as in the other APP-overexpressing lines previously described, is possibly due to APP overexpression *per se* or to an APP fragment other than Aβ (Born et al. 2014).

In agreement with the previous studies just summarized, we found a marker of increased synchronicity only in our B6.152H line, which overexpresses APP.

Interestingly, in the B6.152H line we observed a significant astrogliosis at 6 months of age contextually with the appearance of the extracellular amyloid deposits. Very recently, a clinical study described astrogliosis to emerge and then decline in the preclinical phase of FAD. The extension of our GFAP-expression analysis to 12-month-old mice would allow to evaluate the degree to which this aspect of FAD is reproduced in the B6.152H line (Rodriguez-Vieitez et al. 2016).

8.6 CALCIUM DYSHOMEOSTASIS

We report a significant increase of neuronal activity in the DG of PS2.30H mice in spite of the lack of amyloid plaque deposition and astrogliosis and similar levels of total $A\beta_{42}$, with respect to age-matched wt mice. These results stand in favor of the mutant PS2 to play a role in network

activity alteration through, possibly, the documented dysregulation of Ca^{2+} homeostasis or other yet unknown effects, either dependent or independent on γ-secretase activity.

PS1 and PS2 mutations have been shown to directly affect the ER Ca^{2+} signaling, mainly by altering the IP_3R- and RyR-mediated Ca^{2+} release (Del Prete, Checler, Chami 2014). Moreover, PS2 enhances ER Ca^{2+} leakage (Brunello et al. 2009) and mitochondrial Ca^{2+} uptake. This latter aspect relies on the closer ER-mitochondria interaction realized by the mutant PS2 (Kipanyula et al. 2012; Zampese et al. 2011a). *In vivo*, enhanced Ca^{2+} activity has been reported only in mouse models expressing hAPP along with a mutant form of hPS1 (Busche et al. 2012; Kuchibhotla et al. 2008). Here, we show that the expression of the mutant N141I form of PS2 alone is sufficient for the development of a phenotype of neuronal hyperactivity. Although the relation between the hyperactivity that we observed and Ca^{2+} dyshomeostasis remains to be investigated, it is tempting to speculate a connection among our finding, the early ER/mitochondria Ca^{2+} dysregulation observed *in vitro* (Kipanyula et al. 2012) and the enhanced neuronal Ca^{2+} activity reported *in vivo* (Busche et al. 2008; Busche et al. 2012).

Notwithstanding, it should be noted that, in our PS2.30H mice, the mutant PS2 is expressed not only in neurons but also in astrocytes (unpublished data) and in the two mouse lines, both neurons and astrocytes display altered Ca^{2+} homeostasis (Kipanyula et al. 2012). Hence, a possible role of astrocytes in the hyperactivity described here is to be taken into account.

8.7 Respiration and hippocampal theta

As a last observation, we discuss here a peculiar aspect of the theta oscillations that we investigated.

Two types of hippocampal theta oscillations have classically been defined as type I (atropine-insensitive) or type II (atropine-sensitive) on the basing of their sensitivity to muscarinic acetylcholine receptor antagonists (Buzsáki 2002). The cholinergic theta rhythm is known to rely on muscarinic receptors involving phospholipase C (PLC) and, at least partially, the voltage-gated Ca^{2+} channel 2.3 (Cav2.3) (Müller et al. 2012; Shin et al. 2005). Moreover it is elicited in the hippocampus by MS-DBB cholinergic input and, importantly, used to be the only one acknowledged under urethane anesthesia (Kramis, Vanderwolf, Bland 1975). However, a new theta rhythm has been recently described in the hippocampus of urethane-anesthetized animals, after noxious stimulation (Yanovsky et al. 2014). This rhythm, called HRR, differs from the classical type II theta in that it is atropine-resistant. Most notably, HRR is entrained by nasal respiration and it is strongest in the hilus of the DG.

By recording the LFP signal from the DG of urethane-anesthetized mice, we observed a prominent oscillatory activity, generally peaking between 2 and 3 Hz. This rhythm had the same frequency of the respiratory activity and followed its same fluctuations. This observation is consistent with the atropine-resistant HRR described in the murine hippocampus under anesthesia after noxious stimulation (Yanovsky et al. 2014). However, being the oscillations in our study spontaneously generated, theta rhythm would be expected to be of the type II (atropine sensitive) (Kramis, Vanderwolf, Bland 1975).

In addition, under urethane anesthesia windows of theta oscillations have been described to alternate with moments dominated by SO (Kiss et al. 2013; Pagliardini, Gosgnach, Dickson 2013; Shin et al. 2005) and, on this ground, urethane has been proposed to induce a sleep-like condition (Clement et al. 2008; Pagliardini, Gosgnach, Dickson 2013). Conversely, not only we could not identify a clear alternation of theta versus SO phases but also the SO power often coherently followed the fluctuations of the theta rhythm.

Taken together, the fact that we acquired the LFP signal from the DG, where the HRR is most prominent, along with the observations that, in our data, the theta rhythm (i) had the same frequency of respiration, (ii) did not alternate with SO and (iii) was particularly low in terms of frequency, suggest that it could be a form of spontaneous HRR. Nevertheless, for HRR has so far been described only after noxious stimulation, it is not clear at this stage whether the spontaneous theta activity that we observed could be atropine sensitive or resistant. Pharmacological experiments with administration of muscarinic antagonists (e.g., atropine or scopolamine) will be needed to elucidate this specific aspect.

9 CONCLUSIONS AND PERSPECTIVES

In the hippocampus of the AD mouse models PS2.30H and B6152H, we report two different patterns of electrophysiological alterations occurring at the level of the spontaneous network activity in the hippocampus respectively of PS2.30H and B6152H mice (see Table 1).

In the PS2.30H line, which expresses the N141I mutant form of PS2, we found neuronal hyperactivity at 6 months of age, detected as an increased spectral power in the SG-HG range. This phenomenon occurs in the absence of amyloid plaque deposition and astrogliosis in mice which also exhibit levels of $A\beta_{42}$ only slightly higher than wt mice. Hence, this alteration appears to be caused by the mutant human *PSEN2* transgene through an Aβ-independent mechanism. From this perspective, the PS2.30H line results to be an appropriate model for studying the effects of the mutant PS2, i.e. Ca^{2+} dyshomeostasis and neuronal hyperactivity, separated from amyloidosis/gliosis. Further, it has been proved that other PS mutations behave as loss-of-function (Shen and Kelleher 2007). Hence, it will be of interest to investigate the presence of network hyperactivity in the PS2KO line, that is now also available to our group.

The B6.152H mice, which express the mutant PS2 in combination with the Swedish APP mutation, present neuronal hyperactivity in the beta-SG range at 6 months of age, overlapping with the PS2.30H line, although the frequency range was left-shifted. In addition, B6.152H mice were characterized by hyper-synchronicity in the form of both a theta-beta and -SG overcoupling and a steeper power spectrum. This latter, was observed as early as 3 months of age – the earliest time point of our study – preceding plaques deposition and astrogliosis. However, it emerged in a context of strong APP overexpression and $A\beta_{42}$ production. Likewise, neuronal hyper-synchronicity has been described in many models expressing FAD mutant forms of hAPP (Born et al. 2014; Verret et al. 2012). Therefore, we speculate that the hyper-synchronicity that we observed in our B6.152H mice, unlike the hyperactivity, is more directly due to the APP/ $A\beta_{42}$ overexpression. In future experiments, the inclusion of the single transgenic mouse line expressing only the Swedish hAPP will help elucidating this point. Finally, a study aimed at reducing the Aβ level reduction, for instance by acute γ-secretase inhibition according to (Lanz et al. 2003), will provide hints on the specific contribution of APP and Aβ (Born et al. 2014; Busche et al. 2012).

In the B6.152H line the hyper-synchronicity was an early marker as it preceded plaque formation and astrogliosis as well as it anticipated the known cognitive decline (Ozmen et al. 2009), which is first detected at 8 months of age. Yet, the most interesting aspect related to this finding is the robustness of the statistical resolution between B6.152H and wt mice basing on the spectral slope. The idea of assessing the PSD-function features as a way to address network-level alterations in the context of neurological disorder is vary recent (Podvalny et al. 2015; Voytek and Knight 2015; Voytek et al. 2015). By exploiting this concept in computing the PSD slope coefficient, we found that, in spite of the relatively small number of animals and the large variability exhibited by the other investigated parameter, the PSD steepness provides a very high statistical significance of the difference between the groups ($p < 0.0001$), indicating that it is highly invariant across subjects within the same group. The PSD slope coefficient is a very

straightforward parameter to compute from an LFP or EEG recording and might represent a valuable biomarker. The extension of this approach to other AD mouse models exhibiting hyper-synchronicity and/or seizures will permit to validate our conclusion. Moreover, further investigation of cortical recordings will allow to evaluate its ultimate utility in the EEG settings.

10 ACKNOWLEDGMENTS

We acknowledge L. Ozmen and F. Hoffmann-La Roche Ltd (Basel, Switzerland) for kindly donating the transgenic mice used in this study.

Many people have contributed to this work at different times: Mario Agostini, Gianluca Casagrande, Mufti Mahmud, Emanuele Murana, Maria Rubega, Elena Scremin, Giovanni Sparacino, Andrea Urbani and Stefano Vassanelli. They all take part in the “we” that I widely used in the text. Yet, I owe the most significant thanks to my supervisor, Cristina Fasolato, for the dedication and the efforts that she put in this project as well as for the help and support she generously provided me.

11 REFERENCES

Adeli H and Ghosh-Dastidar S. 2010. Automated EEG-based diagnosis of neurological disorders: Inventing the future of neurology. CRC Press.

Agostini M and Fasolato C. 2016. What players are taking part on Ca2+ homeostasis dysregulation in AD? In: The cellular players in alzheimer's disease: One for all and all for one. Solé M and Miñano-Molina AJ, editors. OMICS Group International.

Alzheimer A. 1911. Über eigenartige krankheitsfälle des späteren alters. Zeitschrift Für Die Gesamte Neurologie Und Psychiatrie 4(1):356-85.

Alzheimer A. 1907. Uber eine eigenartige erkrankung der hirnrinde. Allgemeine Zeitschrife Psychiatrie 64:146-8.

Alzheimer's Association,. 2015. 2015 alzheimer's disease facts and figures. Alzheimer's & Dementia: The Journal of the Alzheimer's Association 11(3):332-84.

Amatniek JC, Hauser WA, DelCastillo-Castaneda C, Jacobs DM, Marder K, Bell K, Albert M, Brandt J, Stern Y. 2006. Incidence and predictors of seizures in patients with alzheimer's disease. Epilepsia 47(5):867-72.

American Psychiatric Association. 2013. Diagnostic and statistical manual of mental disorders (DSM-5®). American Psychiatric Pub.

Andersen P, Morris R, Amaral D, Bliss T, O'Keefe J. 2006. The hippocampus book. Oxford University Press, USA.

Andreasen N and Zetterberg H. 2008. Amyloid-related biomarkers for alzheimer's disease. Curr Med Chem 15(8):766-71.

Aru J, Aru J, Priesemann V, Wibral M, Lana L, Pipa G, Singer W, Vicente R. 2015. Untangling cross-frequency coupling in neuroscience. Curr Opin Neurobiol 31:51-61.

Axmacher N, Henseler MM, Jensen O, Weinreich I, Elger CE, Fell J. 2010. Cross-frequency coupling supports multi-item working memory in the human hippocampus. Proc Natl Acad Sci U S A 107(7):3228-33.

Bakker A, Krauss GL, Albert MS, Speck CL, Jones LR, Stark CE, Yassa MA, Bassett SS, Shelton AL, Gallagher M. 2012. Reduction of hippocampal hyperactivity improves cognition in amnestic mild cognitive impairment. Neuron 74(3):467-74.

Bassett SS, Yousem DM, Cristinzio C, Kusevic I, Yassa MA, Caffo BS, Zeger SL. 2006. Familial risk for alzheimer's disease alters fMRI activation patterns. Brain 129(Pt 5):1229-39.

Belluscio MA, Mizuseki K, Schmidt R, Kempter R, Buzsaki G. 2012. Cross-frequency phase-phase coupling between theta and gamma oscillations in the hippocampus. J Neurosci 32(2):423-35.

Bennys K, Rondouin G, Vergnes C, Touchon J. 2001. Diagnostic value of quantitative EEG in alzheimer's disease. Neurophysiologie Clinique/Clinical Neurophysiology 31(3):153-60.

Bentahir M, Nyabi O, Verhamme J, Tolia A, Horré K, Wiltfang J, Esselmann H, Strooper B. 2006. Presenilin clinical mutations can affect γ-secretase activity by different mechanisms. J Neurochem 96(3):732-42.

Benzinger TL, Blazey T, Jack CR,Jr, Koeppe RA, Su Y, Xiong C, Raichle ME, Snyder AZ, Ances BM, Bateman RJ, et al. 2013. Regional variability of imaging biomarkers in autosomal dominant alzheimer's disease. Proc Natl Acad Sci U S A 110(47):E4502-9.

Berger H. 1929. Über das elektrenkephalogramm des menschen. Eur Arch Psychiatry Clin Neurosci 87(1):527-70.

Bertram L and Tanzi R. 2011. Genetics of alzheimer's disease. Neurodegeneration: The Molecular Pathology of Dementia and Movement Disorders :51-91.

Besthorn C, Zerfass R, Geiger-Kabisch C, Sattel H, Daniel S, Schreiter-Gasser U, Förstl H. 1997. Discrimination of alzheimer's disease and normal aging by EEG data. Electroencephalogr Clin Neurophysiol 103(2):241-8.

Bezprozvanny I. 2009. Calcium signaling and neurodegenerative diseases. Trends Mol Med 15(3):89-100.

Blennow K. 2004. Cerebrospinal fluid protein biomarkers for alzheimer's disease. NeuroRx 1(2):213-25.

Borchelt DR, Davis J, Fischer M, Lee MK, Slunt HH, Ratovitsky T, Regard J, Copeland NG, Jenkins NA, Sisodia SS. 1996. A vector for expressing foreign genes in the brains and hearts of transgenic mice. Genet Anal : Biomol Eng 13(6):159-63.

Born HA, Kim JY, Savjani RR, Das P, Dabaghian YA, Guo Q, Yoo JW, Schuler DR, Cirrito JR, Zheng H, et al. 2014. Genetic suppression of transgenic APP rescues hypersynchronous network activity in a mouse model of alzeimer's disease. J Neurosci 34(11):3826-40.

Bossers K, Wirz KT, Meerhoff GF, Essing AH, van Dongen JW, Houba P, Kruse CG, Verhaagen J, Swaab DF. 2010. Concerted changes in transcripts in the prefrontal cortex precede neuropathology in alzheimer's disease. Brain 133(Pt 12):3699-723.

Braak H and Braak E. 1998. Evolution of neuronal changes in the course of alzheimer's disease. Springer.

Braak H and Braak E. 1997. Frequency of stages of alzheimer-related lesions in different age categories. Neurobiol Aging 18(4):351-7.

Bragin A, Jando G, Nadasdy Z, Hetke J, Wise K, Buzsaki G. 1995. Gamma (40-100 hz) oscillation in the hippocampus of the behaving rat. J Neurosci 15(1 Pt 1):47-60.
Brunello L, Zampese E, Florean C, Pozzan T, Pizzo P, Fasolato C. 2009. Presenilin-2 dampens intracellular Ca2 stores by increasing Ca2 leakage and reducing Ca2 uptake. J Cell Mol Med 13(9b):3358-69.
Buckner RL, Snyder AZ, Shannon BJ, LaRossa G, Sachs R, Fotenos AF, Sheline YI, Klunk WE, Mathis CA, Morris JC, et al. 2005. Molecular, structural, and functional characterization of alzheimer's disease: Evidence for a relationship between default activity, amyloid, and memory. J Neurosci 25(34):7709-17.
Busche MA, Grienberger C, Keskin AD, Song B, Neumann U, Staufenbiel M, Förstl H, Konnerth A. 2015. Decreased amyloid-[beta] and increased neuronal hyperactivity by immunotherapy in alzheimer's models. Nat Neurosci .
Busche MA, Chen X, Henning HA, Reichwald J, Staufenbiel M, Sakmann B, Konnerth A. 2012. Critical role of soluble amyloid-beta for early hippocampal hyperactivity in a mouse model of alzheimer's disease. Proc Natl Acad Sci U S A 109(22):8740-5.
Busche MA, Eichhoff G, Adelsberger H, Abramowski D, Wiederhold KH, Haass C, Staufenbiel M, Konnerth A, Garaschuk O. 2008. Clusters of hyperactive neurons near amyloid plaques in a mouse model of alzheimer's disease. Science 321(5896):1686-9.
Buzsáki G, Buhl D, Harris K, Csicsvari J, Czeh B, Morozov A. 2003. Hippocampal network patterns of activity in the mouse. Neuroscience 116(1):201-11.
Buzsáki G, Czopf J, Kondakor I, Kellenyi L. 1986. Laminar distribution of hippocampal rhythmic slow activity (RSA) in the behaving rat: Current-source density analysis, effects of urethane and atropine. Brain Res 365(1):125-37.
Buzsaki G. 2006. Rhythms of the brain. Oxford University Press.
Buzsáki G. 2002. Theta oscillations in the hippocampus. Neuron 33(3):325-40.
Buzsáki G and Wang X. 2012. Mechanisms of gamma oscillations. Annu Rev Neurosci 35:203-25.
Buzsáki G and Draguhn A. 2004. Neuronal oscillations in cortical networks. Science 304(5679):1926-9.
Buzsáki G, Logothetis N, Singer W. 2013. Scaling brain size, keeping timing: Evolutionary preservation of brain rhythms. Neuron 80(3):751-64.
Buzsáki G, Anastassiou CA, Koch C. 2012. The origin of extracellular fields and currents—EEG, ECoG, LFP and spikes. Nature Reviews Neuroscience 13(6):407-20.
Camandola S and Mattson MP. 2011. Aberrant subcellular neuronal calcium regulation in aging and alzheimer's disease. Biochimica Et Biophysica Acta (BBA)-Molecular Cell Research 1813(5):965-73.
Canolty RT and Knight RT. 2010. The functional role of cross-frequency coupling. Trends Cogn Sci (Regul Ed) 14(11):506-15.
Canolty RT, Edwards E, Dalal SS, Soltani M, Nagarajan SS, Kirsch HE, Berger MS, Barbaro NM, Knight RT. 2006. High gamma power is phase-locked to theta oscillations in human neocortex. Science 313(5793):1626-8.
Cardin JA, Carlén M, Meletis K, Knoblich U, Zhang F, Deisseroth K, Tsai L, Moore CI. 2009. Driving fast-spiking cells induces gamma rhythm and controls sensory responses. Nature 459(7247):663-7.
Caroni P. 1997. Overexpression of growth-associated proteins in the neurons of adult transgenic mice. J Neurosci Methods 71(1):3-9.
Celone KA, Calhoun VD, Dickerson BC, Atri A, Chua EF, Miller SL, DePeau K, Rentz DM, Selkoe DJ, Blacker D, et al. 2006. Alterations in memory networks in mild cognitive impairment and alzheimer's disease: An independent component analysis. J Neurosci 26(40):10222-31.
Chen X, Li M, Wang S, Zhu H, Xiong Y, Liu X. 2014. Pittsburgh compound B retention and progression of cognitive status–a meta-analysis. European Journal of Neurology 21(8):1060-7.
Chin J., Ling HP, Comery T., Pangalos M., Reinhart P. and Wood A. 2008. Chronic imbalance in neuronal activity and compensatory plasticity are associated with cognitive impairment in Tg2576 and PS1/APP mouse models of alzheimer’s disease. International conference on alzheimer’s disease.
Clement EA, Richard A, Thwaites M, Ailon J, Peters S, Dickson CT. 2008. Cyclic and sleep-like spontaneous alternations of brain state under urethane anaesthesia. PLoS One 3(4):e2004.
Colgin LL and Moser EI. 2010. Gamma oscillations in the hippocampus. Physiology (Bethesda) 25(5):319-29.
Craig MT and McBain CJ. 2015. Navigating the circuitry of the brain's GPS system: Future challenges for neurophysiologists. Hippocampus .
Crystal HA, Dickson DW, Sliwinski MJ, Lipton RB, Grober E, Marks-Nelson H, Antis P. 1993. Pathological markers associated with normal aging and dementia in the elderly. Ann Neurol 34(4):566-73.
Csicsvari J, Jamieson B, Wise KD, Buzsáki G. 2003. Mechanisms of gamma oscillations in the hippocampus of the behaving rat. Neuron 37(2):311-22.
Cui Y, Liu B, Luo S, Zhen X, Fan M, Liu T, Zhu W, Park M, Jiang T, Jin JS. 2011. Identification of conversion from mild cognitive impairment to alzheimer’s disease using multivariate predictors. PloS One 6(7):e21896.

Dauwels J, Vialatte F, Cichocki A. 2010. Diagnosis of alzheimer's disease from EEG signals: Where are we standing? Current Alzheimer Research 7(6):487-505.
Davis D, Schmitt F, Wekstein D, Markesbery W. 1999. Alzheimer neuropathologic alterations in aged cognitively normal subjects. Journal of Neuropathology & Experimental Neurology 58(4):376-88.
Del Prete D, Checler F, Chami M. 2014. Ryanodine receptors: Physiological function and deregulation in alzheimer disease. Mol.Neurodegener 9:21.
Del Vecchio RA, Gold LH, Novick SJ, Wong G, Hyde LA. 2004. Increased seizure threshold and severity in young transgenic CRND8 mice. Neurosci Lett 367(2):164-7.
Depuy SD, Kanbar R, Coates MB, Stornetta RL, Guyenet PG. 2011. Control of breathing by raphe obscurus serotonergic neurons in mice. J Neurosci 31(6):1981-90.
Di Fede G, Catania M, Morbin M, Rossi G, Suardi S, Mazzoleni G, Merlin M, Giovagnoli AR, Prioni S, Erbetta A, et al. 2009. A recessive mutation in the APP gene with dominant-negative effect on amyloidogenesis. Science 323(5920):1473-7.
Dickerson BC, Salat DH, Greve DN, Chua EF, Rand-Giovannetti E, Rentz DM, Bertram L, Mullin K, Tanzi RE, Blacker D, et al. 2005. Increased hippocampal activation in mild cognitive impairment compared to normal aging and AD. Neurology 65(3):404-11.
Dubelaar EJ, Mufson EJ, ter Meulen WG, Van Heerikhuize JJ, Verwer RW, Swaab DF. 2006. Increased metabolic activity in nucleus basalis of meynert neurons in elderly individuals with mild cognitive impairment as indicated by the size of the golgi apparatus. J Neuropathol Exp Neurol 65(3):257-66.
Duyckaerts C, Potier M, Delatour B. 2008. Alzheimer disease models and human neuropathology: Similarities and differences. Acta Neuropathol 115(1):5-38.
Ewers M, Sperling RA, Klunk WE, Weiner MW, Hampel H. 2011. Neuroimaging markers for the prediction and early diagnosis of alzheimer's disease dementia. Trends Neurosci 34(8):430-42.
Fedele E, Rivera D, Marengo B, Pronzato MA, Ricciarelli R. 2015. Amyloid β: Walking on the dark side of the moon. Mech Ageing Dev 152:1-4.
Fell J, Ludowig E, Staresina BP, Wagner T, Kranz T, Elger CE, Axmacher N. 2011. Medial temporal theta/alpha power enhancement precedes successful memory encoding: Evidence based on intracranial EEG. J Neurosci 31(14):5392-7.
Fischer P. 1907. Miliare nekrosen mit drusigen wucherungen der neurofibrillen, eine regelmässige veränderung der hirnrinde bei seniler demenz. Eur Neurol 22(4):361-72.
Forlenza OV, Diniz BS, Gattaz WF. 2010. Diagnosis and biomarkers of predementia in alzheimer's disease. BMC Med 8:89,7015-8-89.
França AS, Nascimento GC, Lopes-dos-Santos V, Muratori L, Ribeiro S, Lobão-Soares B, Tort AB. 2014. Beta2 oscillations (23–30 hz) in the mouse hippocampus during novel object recognition. Eur J Neurosci 40(11):3693-703.
Freeman WJ. 2007. Definitions of state variables and state space for brain-computer interface. Cognitive Neurodynamics 1(1):3-14.
Freeman WJ and Zhai J. 2009. Simulated power spectral density (PSD) of background electrocorticogram (ECoG). Cognitive Neurodynamics 3(1):97-103.
Gandy S. 2005. The role of cerebral amyloid beta accumulation in common forms of alzheimer disease. J Clin Invest 115(5):1121-9.
Giacomello M, Barbiero L, Zatti G, Squitti R, Binetti G, Pozzan T, Fasolato C, Ghidoni R, Pizzo P. 2005. Reduction of ca 2 stores and capacitative ca 2 entry is associated with the familial alzheimer's disease presenilin-2 T122R mutation and anticipates the onset of dementia. Neurobiol Dis 18(3):638-48.
Giannakopoulos P, Herrmann FR, Bussiere T, Bouras C, Kovari E, Perl DP, Morrison JH, Gold G, Hof PR. 2003. Tangle and neuron numbers, but not amyloid load, predict cognitive status in alzheimer's disease. Neurology 60(9):1495-500.
Glenner G and Wong C. 1984. Alzheimer's disease: Initial report of the purification andcharacterization of a novel cerebrovascular amyloid protein. biochem. biophys. res. com-mun. 120, 885-890. Glenner885120Biochem.Biophys.Res.Commun .
Goate A, Chartier-Harlin M, Mullan M, Brown J, Crawford F, Fidani L, Giuffra L, Haynes A, Irving N, James L. 1991. Segregation of a missense mutation in the amyloid precursor protein gene with familial alzheimer's disease. Nature 349(6311):704-6.
Goedert M, Wischik CM, Crowther RA, Walker JE, Klug A. 1988. Cloning and sequencing of the cDNA encoding a core protein of the paired helical filament of alzheimer disease: Identification as the microtubule-associated protein tau. Proc Natl Acad Sci U S A 85(11):4051-5.

Golde TE, Schneider LS, Koo EH. 2011. Anti-aβ therapeutics in alzheimer's disease: The need for a paradigm shift. Neuron 69(2):203-13.
Gosche KM, Mortimer JA, Smith CD, Markesbery WR, Snowdon DA. 2002. Hippocampal volume as an index of alzheimer neuropathology: Findings from the nun study. Neurology 58(10):1476-82.
Graeber M, Kösel S, Grasbon-Frodl E, Möller H, Mehraein P. 1998. Histopathology and APOE genotype of the first alzheimer disease patient, auguste D. Neurogenetics 1(3):223-8.
Grunwald M, Busse F, Hensel A, Kruggel F, Riedel–Heller S, Wolf H, Arendt T, Gertz H. 2001. Correlation between cortical θ activity and hippocampal volumes in health, mild cognitive impairment, and mild dementia. Journal of Clinical Neurophysiology 18(2):178-84.
Guerreiro R and Hardy J. 2014. Genetics of alzheimer's disease. Neurotherapeutics 11(4):732-7.
Gyure KA, Durham R, Stewart WF, Smialek JE, Troncoso JC. 2001. Intraneuronal abeta-amyloid precedes development of amyloid plaques in down syndrome. Arch Pathol Lab Med 125(4):489.
Hämäläinen A, Pihlajamäki M, Tanila H, Hänninen T, Niskanen E, Tervo S, Karjalainen PA, Vanninen RL, Soininen H. 2007. Increased fMRI responses during encoding in mild cognitive impairment. Neurobiol Aging 28(12):1889-903.
Hampel H, Teipel S, Fuchsberger T, Andreasen N, Wiltfang J, Otto M, Shen Y, Dodel R, Du Y, Farlow M. 2004. Value of CSF β-amyloid1–42 and tau as predictors of alzheimer's disease in patients with mild cognitive impairment. Mol Psychiatry 9(7):705-10.
Hara K and Harris RA. 2002. The anesthetic mechanism of urethane: The effects on neurotransmitter-gated ion channels. Anesthesia & Analgesia 94(2):313-8.
Hardy J. 2006. A hundred years of alzheimer's disease research. Neuron 52(1):3-13.
Hardy JA and Higgins GA. 1992. Alzheimer's disease: The amyloid cascade hypothesis. Science 256(5054):184.
Hardy J and Selkoe DJ. 2002. The amyloid hypothesis of alzheimer's disease: Progress and problems on the road to therapeutics. Science 297(5580):353-6.
Harrison JR and Owen MJ. 2016. Alzheimer's disease: The amyloid hypothesis on trial. Br J Psychiatry 208(1):1-3.
Hass Matthew R., Sato Chihiro, Kopan Raphael and Zhao Guojun. 2009. Presenilin: RIP and beyond. Seminars in cell & developmental biologyElsevier. 201 p.
Hayrapetyan V, Rybalchenko V, Rybalchenko N, Koulen P. 2008. The N-terminus of presenilin-2 increases single channel activity of brain ryanodine receptors through direct protein–protein interaction. Cell Calcium 44(5):507-18.
He BJ. 2014. Scale-free brain activity: Past, present, and future. Trends Cogn Sci (Regul Ed) 18(9):480-7.
He BJ, Zempel JM, Snyder AZ, Raichle ME. 2010. The temporal structures and functional significance of scale-free brain activity. Neuron 66(3):353-69.
He BJ, Snyder AZ, Zempel JM, Smyth MD, Raichle ME. 2008. Electrophysiological correlates of the brain's intrinsic large-scale functional architecture. Proc Natl Acad Sci U S A 105(41):16039-44.
Herrup K. 2015. The case for rejecting the amyloid cascade hypothesis. Nat Neurosci :794-9.
Holscher C, Anwyl R, Rowan MJ. 1997. Stimulation on the positive phase of hippocampal theta rhythm induces long-term potentiation that can be depotentiated by stimulation on the negative phase in area CA1 in vivo. J Neurosci 17(16):6470-7.
Honarnejad K and Herms J. 2012. Presenilins: Role in calcium homeostasis. Int J Biochem Cell Biol 44(11):1983-6.
Huang C, Wahlund L, Dierks T, Julin P, Winblad B, Jelic V. 2000. Discrimination of alzheimer's disease and mild cognitive impairment by equivalent EEG sources: A cross-sectional and longitudinal study. Clinical Neurophysiology 111(11):1961-7.
Huang Y, Yang S, Hu Z, Liu G, Zhou W, Zhang Y. 2012. A new approach to location of the dentate gyrus and perforant path in rats/mice by landmarks on the skull. Acta Neurobiol Exp 72:468-72.
International Federation of Societies for Electroencephalography and Clinical Neurophysiology. 1974. Electroencephalography and Clinical Neurophysiology 37:521-3.
Ittner AA, Gladbach A, Bertz J, Suh LS, Ittner LM. 2014. p38 MAP kinase-mediated NMDA receptor-dependent suppression of hippocampal hypersynchronicity in a mouse model of alzheimer's disease. Acta Neuropathologica Communications 2(1):1-17.
Jack CR,Jr, Albert MS, Knopman DS, McKhann GM, Sperling RA, Carrillo MC, Thies B, Phelps CH. 2011. Introduction to the recommendations from the national institute on aging-alzheimer's association workgroups on diagnostic guidelines for alzheimer's disease. Alzheimers Dement 7(3):257-62.
Jagust W. 2016. Is amyloid-beta harmful to the brain? insights from human imaging studies. Brain 139(Pt 1):23-30.
James W. 1890. The principles of psychology. .
Jayadev S, Leverenz JB, Steinbart E, Stahl J, Klunk W, Yu CE, Bird TD. 2010. Alzheimer's disease phenotypes and genotypes associated with mutations in presenilin 2. Brain 133(Pt 4):1143-54.

Jelic V, Johansson S, Almkvist O, Shigeta M, Julin P, Nordberg A, Winblad B, Wahlund L. 2000. Quantitative electroencephalography in mild cognitive impairment: Longitudinal changes and possible prediction of alzheimer's disease. Neurobiol Aging 21(4):533-40.

Johnson S, Schmitz T, Moritz C, Meyerand M, Rowley H, Alexander A, Hansen K, Gleason C, Carlsson C, Ries M. 2006. Activation of brain regions vulnerable to alzheimer's disease: The effect of mild cognitive impairment. Neurobiol Aging 27(11):1604-12.

Jonsson T, Atwal JK, Steinberg S, Snaedal J, Jonsson PV, Bjornsson S, Stefansson H, Sulem P, Gudbjartsson D, Maloney J. 2012. A mutation in APP protects against alzheimer/'s disease and age-related cognitive decline. Nature 488(7409):96-9.

Kahana MJ, Seelig D, Madsen JR. 2001. Theta returns. Curr Opin Neurobiol 11(6):739-44.

Kang J, Lemaire H, Unterbeck A, Salbaum JM, Masters CL, Grzeschik K, Multhaup G, Beyreuther K, Müller-Hill B. 1987. The precursor of alzheimer's disease amyloid A4 protein resembles a cell-surface receptor. .

Katzman R. 1976. The prevalence and malignancy of alzheimer disease: A major killer. Arch Neurol 33(4):217-8.

Kay LM and Lazzara P. 2010. How global are olfactory bulb oscillations? J Neurophysiol 104(3):1768-73.

Khachaturian ZS. 1987. Hypothesis on the regulation of cytosol calcium concentration and the aging brain. Neurobiol Aging 8(4):345-6.

Khan UA, Liu L, Provenzano FA, Berman DE, Profaci CP, Sloan R, Mayeux R, Duff KE, Small SA. 2014. Molecular drivers and cortical spread of lateral entorhinal cortex dysfunction in preclinical alzheimer's disease. Nat Neurosci 17(2):304-11.

Kipanyula MJ, Contreras L, Zampese E, Lazzari C, Wong AK, Pizzo P, Fasolato C, Pozzan T. 2012. Ca2 dysregulation in neurons from transgenic mice expressing mutant presenilin 2. Aging Cell 11(5):885-93.

Kirwan CB and Stark CE. 2004. Medial temporal lobe activation during encoding and retrieval of novel face-name pairs. Hippocampus 14(7):919-30.

Kiss T, Feng J, Hoffmann W, Shaffer C, Hajós M. 2013. Rhythmic theta and delta activity of cortical and hippocampal neuronal networks in genetically or pharmacologically induced N-methyl-D-aspartate receptor hypofunction under urethane anesthesia. Neuroscience 237:255-67.

Knopman D, Parisi J, Salviati A, Floriach-Robert M, Boeve B, Ivnik R, Smith G, Dickson D, Johnson K, Petersen L. 2003. Neuropathology of cognitively normal elderly. Journal of Neuropathology & Experimental Neurology 62(11):1087-95.

Kramis R, Vanderwolf C, Bland BH. 1975. Two types of hippocampal rhythmical slow activity in both the rabbit and the rat: Relations to behavior and effects of atropine, diethyl ether, urethane, and pentobarbital. Exp Neurol 49(1):58-85.

Kuchibhotla KV, Goldman ST, Lattarulo CR, Wu H, Hyman BT, Bacskai BJ. 2008. Aβ plaques lead to aberrant regulation of calcium homeostasis in vivo resulting in structural and functional disruption of neuronal networks. Neuron 59(2):214-25.

Lai MT, Chen E, Crouthamel MC, DiMuzio-Mower J, Xu M, Huang Q, Price E, Register RB, Shi XP, Donoviel DB, et al. 2003. Presenilin-1 and presenilin-2 exhibit distinct yet overlapping gamma-secretase activities. J Biol Chem 278(25):22475-81.

Lakatos P, Shah AS, Knuth KH, Ulbert I, Karmos G, Schroeder CE. 2005. An oscillatory hierarchy controlling neuronal excitability and stimulus processing in the auditory cortex. J Neurophysiol 94(3):1904-11.

Lanz TA, Himes CS, Pallante G, Adams L, Yamazaki S, Amore B, Merchant KM. 2003. The gamma-secretase inhibitor N-[N-(3,5-difluorophenacetyl)-L-alanyl]-S-phenylglycine t-butyl ester reduces A beta levels in vivo in plasma and cerebrospinal fluid in young (plaque-free) and aged (plaque-bearing) Tg2576 mice. J Pharmacol Exp Ther 305(3):864-71.

Lau P, Bossers K, Janky R, Salta E, Frigerio CS, Barbash S, Rothman R, Sierksma AS, Thathiah A, Greenberg D, et al. 2013. Alteration of the microRNA network during the progression of alzheimer's disease. EMBO Mol Med 5(10):1613-34.

Lawson VH and Bland BH. 1993. The role of the septohippocampal pathway in the regulation of hippocampal field activity and behavior: Analysis by the intraseptal microinfusion of carbachol, atropine, and procaine. Exp Neurol 120(1):132-44.

Lee H, Simpson GV, Logothetis NK, Rainer G. 2005. Phase locking of single neuron activity to theta oscillations during working memory in monkey extrastriate visual cortex. Neuron 45(1):147-56.

Lega BC, Jacobs J, Kahana M. 2012. Human hippocampal theta oscillations and the formation of episodic memories. Hippocampus 22(4):748-61.

Lega B, Burke J, Jacobs J, Kahana MJ. 2016. Slow-theta-to-gamma phase-amplitude coupling in human hippocampus supports the formation of new episodic memories. Cereb Cortex 26(1):268-78.

Lesné S, Kotilinek L, Ashe KH. 2008. Plaque-bearing mice with reduced levels of oligomeric amyloid-β assemblies have intact memory function. Neuroscience 151(3):745-9.
Lesné S, Koh MT, Kotilinek L, Kayed R, Glabe CG, Yang A, Gallagher M, Ashe KH. 2006. A specific amyloid-β protein assembly in the brain impairs memory. Nature 440(7082):352-7.
Leuchter AF, Spar JE, Walter DO, Weiner H. 1987. Electroencephalographic spectra and coherence in the diagnosis of alzheimer's-type and multi-infarct dementia: A pilot study. Arch Gen Psychiatry 44(11):993-8.
Lima FR, Arantes CP, Muras AG, Nomizo R, Brentani RR, Martins VR. 2007. Cellular prion protein expression in astrocytes modulates neuronal survival and differentiation. J Neurochem 103(6):2164-76.
Linkenkaer-Hansen K, Nikouline VV, Palva JM, Ilmoniemi RJ. 2001. Long-range temporal correlations and scaling behavior in human brain oscillations. J Neurosci 21(4):1370-7.
Lisman JE and Jensen O. 2013. The theta-gamma neural code. Neuron 77(6):1002-16.
Lista S, Garaci FG, Ewers M, Teipel S, Zetterberg H, Blennow K, Hampel H. 2014. CSF Aβ1-42 combined with neuroimaging biomarkers in the early detection, diagnosis and prediction of alzheimer's disease. Alzheimer's & Dementia 10(3):381-92.
Locatelli T, Cursi M, Liberati D, Franceschi M, Comi G. 1998. EEG coherence in alzheimer's disease. Electroencephalogr Clin Neurophysiol 106(3):229-37.
Logothetis NK, Kayser C, Oeltermann A. 2007. In vivo measurement of cortical impedance spectrum in monkeys: Implications for signal propagation. Neuron 55(5):809-23.
Lowry CA and Kay LM. 2007. Chemical factors determine olfactory system beta oscillations in waking rats. J Neurophysiol 98(1):394-404.
Lozsadi DA and Larner AJ. 2006. Prevalence and causes of seizures at the time of diagnosis of probable alzheimer's disease. Dement Geriatr Cogn Disord 22(2):121-4.
Machulda MM, Ward HA, Borowski B, Gunter JL, Cha RH, O'Brien PC, Petersen RC, Boeve BF, Knopman D, Tang-Wai DF, et al. 2003. Comparison of memory fMRI response among normal, MCI, and alzheimer's patients. Neurology 61(4):500-6.
Manly JJ, Tang M, Schupf N, Stern Y, Vonsattel JG, Mayeux R. 2008. Frequency and course of mild cognitive impairment in a multiethnic community. Ann Neurol 63(4):494-506.
Manning JR, Jacobs J, Fried I, Kahana MJ. 2009. Broadband shifts in local field potential power spectra are correlated with single-neuron spiking in humans. J Neurosci 29(43):13613-20.
Markowska AL, Olton DS, Givens B. 1995. Cholinergic manipulations in the medial septal area: Age-related effects on working memory and hippocampal electrophysiology. J Neurosci 15(3 Pt 1):2063-73.
Maskri L, Zhu X, Fritzen S, Kuhn K, Ullmer C, Engels P, Andriske M, Stichel CC, Lubbert H. 2004. Influence of different promoters on the expression pattern of mutated human alpha-synuclein in transgenic mice. Neurodegener Dis 1(6):255-65.
Masliah E, Terry RD, Mallory M, Alford M, Hansen LA. 1990. Diffuse plaques do not accentuate synapse loss in alzheimer's disease. Am J Pathol 137(6):1293-7.
Masters CL, Simms G, Weinman NA, Multhaup G, McDonald BL, Beyreuther K. 1985. Amyloid plaque core protein in alzheimer disease and down syndrome. Proc Natl Acad Sci U S A 82(12):4245-9.
Mattsson N, Zetterberg H, Hansson O, Andreasen N, Parnetti L, Jonsson M, Herukka S, van der Flier, Wiesje M, Blankenstein MA, Ewers M. 2009. CSF biomarkers and incipient alzheimer disease in patients with mild cognitive impairment. Jama 302(4):385-93.
Mattsson N and Zetterberg H. 2009. Future screening for incipient alzheimer's disease--the influence of prevalence on test performance. Eur Neurol 62(4):200-3.
Maurer K, Volk S, Gerbaldo H. 1997. Auguste D and alzheimer's disease. The Lancet 349(9064):1546-9.
McKhann G, Drachman D, Folstein M, Katzman R, Price D, Stadlan EM. 1984. Clinical diagnosis of alzheimer's disease: Report of the NINCDS-ADRDA work group under the auspices of department of health and human services task force on alzheimer's disease. Neurology 34(7):939-44.
Mendes MHF. 2002. Transient epileptic amnesia: An under-diagnosed phenomenon? three more cases. Seizure 11(4):238-42.
Miller SL, Fenstermacher E, Bates J, Blacker D, Sperling RA, Dickerson BC. 2008. Hippocampal activation in adults with mild cognitive impairment predicts subsequent cognitive decline. J Neurol Neurosurg Psychiatry 79(6):630-5.
Minkeviciene R, Rheims S, Dobszay MB, Zilberter M, Hartikainen J, Fulop L, Penke B, Zilberter Y, Harkany T, Pitkanen A, et al. 2009. Amyloid beta-induced neuronal hyperexcitability triggers progressive epilepsy. J Neurosci 29(11):3453-62.
Mitchell AJ, Monge-Argiles JA, Sanchez-Paya J. 2010. Do CSF biomarkers help clinicians predict the progression of mild cognitive impairment to dementia? Pract Neurol 10(4):202-7.

Moretti D, Miniussi C, Frisoni G, Zanetti O, Binetti G, Geroldi C, Galluzzi S, Rossini P. 2007. Vascular damage and EEG markers in subjects with mild cognitive impairment. Clinical Neurophysiology 118(8):1866-76.
Moser M, Colello RJ, Pott U, Oesch B. 1995. Developmental expression of the prion protein gene in glial cells. Neuron 14(3):509-17.
Mukamel R, Gelbard H, Arieli A, Hasson U, Fried I, Malach R. 2005. Coupling between neuronal firing, field potentials, and FMRI in human auditory cortex. Science 309(5736):951-4.
Müller R, Struck H, Ho M, Brockhaus-Dumke A, Klosterkötter J, Broich K, Hescheler J, Schneider T, Weiergräber M. 2012. Atropine-sensitive hippocampal theta oscillations are mediated by ca v 2.3 R-type ca 2 channels. Neuroscience 205:125-39.
Muller U, Winter P, Graeber MB. 2013. A presenilin 1 mutation in the first case of alzheimer's disease. Lancet Neurol 12(2):129-30.
Namgung U, Valcourt E, Routtenberg A. 1995. Long-term potentiation in vivo in the intact mouse hippocampus. Brain Res 689(1):85-92.
Nielson DM, Smith TA, Sreekumar V, Dennis S, Sederberg PB. 2015. Human hippocampus represents space and time during retrieval of real-world memories. Proc Natl Acad Sci U S A 112(35):11078-83.
Nir Y, Fisch L, Mukamel R, Gelbard-Sagiv H, Arieli A, Fried I, Malach R. 2007. Coupling between neuronal firing rate, gamma LFP, and BOLD fMRI is related to interneuronal correlations. Current Biology 17(15):1275-85.
Nunez P. 1981. Electric fields of the brain. 1981. .
Oh H, Steffener J, Razlighi QR, Habeck C, Liu D, Gazes Y, Janicki S, Stern Y. 2015. Aβ-related hyperactivation in frontoparietal control regions in cognitively normal elderly. Neurobiol Aging 36(12):3247-54.
Ozmen L, Albientz A, Czech C, Jacobsen H. 2009. Expression of transgenic APP mRNA is the key determinant for beta-amyloid deposition in PS2APP transgenic mice. Neurodegener Dis 6(1-2):29-36.
Pagliardini S, Gosgnach S, Dickson CT. 2013. Spontaneous sleep-like brain state alternations and breathing characteristics in urethane anesthetized mice. PloS One 8(7):e70411.
Palop JJ and Mucke L. 2009. Epilepsy and cognitive impairments in alzheimer disease. Arch Neurol 66(4):435-40.
Palop JJ, Chin J, Mucke L. 2006. A network dysfunction perspective on neurodegenerative diseases. Nature 443(7113):768-73.
Palop JJ, Chin J, Roberson ED, Wang J, Thwin MT, Bien-Ly N, Yoo J, Ho KO, Yu G, Kreitzer A. 2007. Aberrant excitatory neuronal activity and compensatory remodeling of inhibitory hippocampal circuits in mouse models of alzheimer's disease. Neuron 55(5):697-711.
Penny W, Duzel E, Miller K, Ojemann J. 2008. Testing for nested oscillation. J Neurosci Methods 174(1):50-61.
Penttonen M and Buzsáki G. 2003. Natural logarithmic relationship between brain oscillators. Thalamus & Related Systems 2(02):145-52.
Pernía-Andrade AJ and Jonas P. 2014. Theta-gamma-modulated synaptic currents in hippocampal granule cells in vivo define a mechanism for network oscillations. Neuron 81(1):140-52.
Perusini G. 1909. Über klinisch und histologisch eigenartige psychische erkrankungen des späteren lebensalters. Histologische Und Histopathologische Arbeiten.Jena: Verlag G Fischer :297-351.
Petersen RC, Doody R, Kurz A, Mohs RC, Morris JC, Rabins PV, Ritchie K, Rossor M, Thal L, Winblad B. 2001. Current concepts in mild cognitive impairment. Arch Neurol 58(12):1985-92.
Pihlajamaki M, Jauhiainen AM, Soininen H. 2009. Structural and functional MRI in mild cognitive impairment. Current Alzheimer Research 6(2):179-85.
Podvalny E, Noy N, Harel M, Bickel S, Chechik G, Schroeder CE, Mehta AD, Tsodyks M, Malach R. 2015. A unifying principle underlying the extracellular field potential spectral responses in the human cortex. J Neurophysiol :jn. 00943.2014.
Poil S, De Haan W, van der Flier, Wiesje M, Mansvelder HD, Scheltens P, Linkenkaer-Hansen K. 2013. Integrative EEG biomarkers predict progression to alzheimer's disease at the MCI stage. Frontiers in Aging Neuroscience 5.
Poirier R, Veltman I, Pflimlin MC, Knoflach F, Metzger F. 2010. Enhanced dentate gyrus synaptic plasticity but reduced neurogenesis in a mouse model of amyloidosis. Neurobiol Dis 40(2):386-93.
Price JL and Morris JC. 1999. Tangles and plaques in nondemented aging and" preclinical" alzheimer's disease. Ann Neurol 45(3):358-68.
Price JL, Davis P, Morris J, White D. 1991. The distribution of tangles, plaques and related immunohistochemical markers in healthy aging and alzheimer's disease. Neurobiol Aging 12(4):295-312.
Pucci E, Belardinelli N, Cacchio G, Signorino M, Angeleri F. 1999. EEG power spectrum differences in early and late onset forms of alzheimer's disease. Clinical Neurophysiology 110(4):621-31.
Purves D. 2004. Neuroscience. Sinauer Associates Inc.

Putcha D, Brickhouse M, O'Keefe K, Sullivan C, Rentz D, Marshall G, Dickerson B, Sperling R. 2011. Hippocampal hyperactivation associated with cortical thinning in alzheimer's disease signature regions in non-demented elderly adults. J Neurosci 31(48):17680-8.

Puzzo D, Gulisano W, Arancio O, Palmeri A. 2015. The keystone of alzheimer pathogenesis might be sought in aβ physiology. Neuroscience 307:26-36.

Quiroz YT, Budson AE, Celone K, Ruiz A, Newmark R, Castrillón G, Lopera F, Stern CE. 2010. Hippocampal hyperactivation in presymptomatic familial alzheimer's disease. Ann Neurol 68(6):865-75.

Rabinowicz AL, Starkstein SE, Leiguarda RC, Coleman AE. 2000. Transient epileptic amnesia in dementia: A treatable unrecognized cause of episodic amnestic wandering. Alzheimer Disease & Associated Disorders 14(4):231-3.

Rasch MJ, Gretton A, Murayama Y, Maass W, Logothetis NK. 2008. Inferring spike trains from local field potentials. J Neurophysiol 99(3):1461-76.

Ray WJ and Cole HW. 1985. EEG alpha activity reflects attentional demands, and beta activity reflects emotional and cognitive processes. Science 228(4700):750-2.

Richards JG, Higgins GA, Ouagazzal AM, Ozmen L, Kew JN, Bohrmann B, Malherbe P, Brockhaus M, Loetscher H, Czech C, et al. 2003. PS2APP transgenic mice, coexpressing hPS2mut and hAPPswe, show age-related cognitive deficits associated with discrete brain amyloid deposition and inflammation. J Neurosci 23(26):8989-9003.

Riley KP, Snowdon DA, Markesbery WR. 2002. Alzheimer's neurofibrillary pathology and the spectrum of cognitive function: Findings from the nun study. Ann Neurol 51(5):567-77.

Roberson ED, Scearce-Levie K, Palop JJ, Yan F, Cheng IH, Wu T, Gerstein H, Yu GQ, Mucke L. 2007. Reducing endogenous tau ameliorates amyloid beta-induced deficits in an alzheimer's disease mouse model. Science 316(5825):750-4.

Rodríguez-Arellano J, Parpura V, Zorec R, Verkhratsky A. 2015. Astrocytes in physiological aging and alzheimer's disease. Neuroscience .

Rodriguez-Vieitez E, et al. 2016. Diverging longitudinal changes in astrocytosis and amyloid PET in autosomal dominant alzheimer's disease. Brain : A Journal of Neurology JID - 0372537 OTO - NOTNLM .

Rogaev E, Sherrington R, Rogaeva E, Levesque G, Ikeda M, Liang Y, Chi H, Lin C, Holman K, Tsuda T. 1995. Familial alzheimer's disease in kindreds with missense mutations in a gene on chromosome 1 related to the alzheimer's disease type 3 gene. Nature 376(6543):775-8.

Rossini P, Del Percio C, Pasqualetti P, Cassetta E, Binetti G, Dal Forno G, Ferreri F, Frisoni G, Chiovenda P, Miniussi C. 2006. Conversion from mild cognitive impairment to alzheimer's disease is predicted by sources and coherence of brain electroencephalography rhythms. Neuroscience 143(3):793-803.

Rubio SE, Vega-Flores G, Martinez A, Bosch C, Perez-Mediavilla A, del Rio J, Gruart A, Delgado-Garcia JM, Soriano E, Pascual M. 2012. Accelerated aging of the GABAergic septohippocampal pathway and decreased hippocampal rhythms in a mouse model of alzheimer's disease. Faseb J 26(11):4458-67.

Rupp C, Beyreuther K, Maurer K, Kins S. 2014. A presenilin 1 mutation in the first case of alzheimer's disease: Revisited. Alzheimer's & Dementia 10(6):869-72.

Ryan NS, Rossor MN, Fox NC. 2015. Alzheimer's disease in the 100 years since alzheimer's death. Brain :awv316.

Sanchez PE, Zhu L, Verret L, Vossel KA, Orr AG, Cirrito JR, Devidze N, Ho K, Yu G, Palop JJ. 2012. Levetiracetam suppresses neuronal network dysfunction and reverses synaptic and cognitive deficits in an alzheimer's disease model. Proceedings of the National Academy of Sciences 109(42):E2895-903.

Saunders AM, Strittmatter WJ, Schmechel D, George-Hyslop PH, Pericak-Vance MA, Joo SH, Rosi BL, Gusella JF, Crapper-MacLachlan DR, Alberts MJ. 1993. Association of apolipoprotein E allele epsilon 4 with late-onset familial and sporadic alzheimer's disease. Neurology 43(8):1467-72.

Sceniak MP and MacIver MB. 2006. Cellular actions of urethane on rat visual cortical neurons in vitro. J Neurophysiol 95(6):3865-74.

Scheffer-Teixeira R, Belchior H, Leao RN, Ribeiro S, Tort AB. 2013. On high-frequency field oscillations (>100 hz) and the spectral leakage of spiking activity. J Neurosci 33(4):1535-9.

Scheffer-Teixeira R, Belchior H, Caixeta FV, Souza BC, Ribeiro S, Tort AB. 2012. Theta phase modulates multiple layer-specific oscillations in the CA1 region. Cereb Cortex 22(10):2404-14.

Schmidt R, Kienbacher E, Benke T, Dal-Bianco P, Delazer M, Ladurner G, Jellinger K, Marksteiner J, Ransmayr G, Schmidt H, et al. 2008. Sex differences in alzheimer's disease. Neuropsychiatr 22(1):1-15.

Schoonenboom NS, Mulder C, Van Kamp GJ, Mehta SP, Scheltens P, Blankenstein MA, Mehta PD. 2005. Amyloid β 38, 40, and 42 species in cerebrospinal fluid: More of the same? Ann Neurol 58(1):139-42.

Sederberg PB, Schulze-Bonhage A, Madsen JR, Bromfield EB, Litt B, Brandt A, Kahana MJ. 2007a. Gamma oscillations distinguish true from false memories. Psychol Sci 18(11):927-32.

Sederberg PB, Schulze-Bonhage A, Madsen JR, Bromfield EB, McCarthy DC, Brandt A, Tully MS, Kahana MJ. 2007b. Hippocampal and neocortical gamma oscillations predict memory formation in humans. Cereb Cortex 17(5):1190-6.
Selkoe DJ. 1991. The molecular pathology of alzheimer's disease. Neuron 6(4):487-98.
Selkoe DJ and Wolfe MS. 2007. Presenilin: Running with scissors in the membrane. Cell 131(2):215-21.
Shankar GM, Li S, Mehta TH, Garcia-Munoz A, Shepardson NE, Smith I, Brett FM, Farrell MA, Rowan MJ, Lemere CA. 2008. Amyloid-β protein dimers isolated directly from alzheimer's brains impair synaptic plasticity and memory. Nat Med 14(8):837-42.
Shankar GM, Bloodgood BL, Townsend M, Walsh DM, Selkoe DJ, Sabatini BL. 2007. Natural oligomers of the alzheimer amyloid-beta protein induce reversible synapse loss by modulating an NMDA-type glutamate receptor-dependent signaling pathway. J Neurosci 27(11):2866-75.
Shen J and Kelleher RJ,3rd. 2007. The presenilin hypothesis of alzheimer's disease: Evidence for a loss-of-function pathogenic mechanism. Proc Natl Acad Sci U S A 104(2):403-9.
Shilling D, Mak DO, Kang DE, Foskett JK. 2012. Lack of evidence for presenilins as endoplasmic reticulum Ca2+ leak channels. J Biol Chem 287(14):10933-44.
Shin J, Kim D, Bianchi R, Wong RK, Shin HS. 2005. Genetic dissection of theta rhythm heterogeneity in mice. Proc Natl Acad Sci U S A 102(50):18165-70.
Shirvalkar PR, Rapp PR, Shapiro ML. 2010. Bidirectional changes to hippocampal theta-gamma comodulation predict memory for recent spatial episodes. Proc Natl Acad Sci U S A 107(15):7054-9.
Smith SJ. 2005. EEG in neurological conditions other than epilepsy: When does it help, what does it add? J Neurol Neurosurg Psychiatry 76 Suppl 2:ii8-12.
Sperling R and Johnson K. 2013a. Biomarkers of alzheimer disease: Current and future applications to diagnostic criteria. CONTINUUM: Lifelong Learning in Neurology 19(2, Dementia):325-38.
Sperling R, Mormino E, Johnson K. 2014. The evolution of preclinical alzheimer's disease: Implications for prevention trials. Neuron 84(3):608-22.
Sperling RA, LaViolette PS, O'Keefe K, O'Brien J, Rentz DM, Pihlajamaki M, Marshall G, Hyman BT, Selkoe DJ, Hedden T. 2009. Amyloid deposition is associated with impaired default network function in older persons without dementia. Neuron 63(2):178-88.
Sperling R and Johnson K. 2013b. Biomarkers of alzheimer disease: Current and future applications to diagnostic criteria. Continuum (Minneap Minn) 19(2 Dementia):325-38.
Sporns O. 2011. Networks of the brain. MIT press.
Squire LR, Stark CE, Clark RE. 2004. The medial temporal lobe*. Annu Rev Neurosci 27:279-306.
Stargardt A, Swaab DF, Bossers K. 2015. The storm before the quiet: Neuronal hyperactivity and aβ in the presymptomatic stages of alzheimer's disease. Neurobiol Aging 36(1):1-11.
Steardo Jr L, Bronzuoli MR, Iacomino A, Esposito G, Steardo L, Scuderi C. 2015. Does neuroinflammation turn on the flame in alzheimer's disease? focus on astrocytes. Frontiers in Neuroscience 9.
Steriade M and Deschenes M. 1984. The thalamus as a neuronal oscillator. Brain Res Rev 8(1):1-63.
Steriade M, Gloor P, Llinas R, Da Silva FL, Mesulam M. 1990. Basic mechanisms of cerebral rhythmic activities. Electroencephalogr Clin Neurophysiol 76(6):481-508.
Steriade M, Nunez A, Amzica F. 1993. A novel slow (< 1 hz) oscillation of neocortical neurons in vivo: Depolarizing and hyperpolarizing components. J Neurosci 13(8):3252-65.
Strozyk D, Blennow K, White LR, Launer LJ. 2003. CSF abeta 42 levels correlate with amyloid-neuropathology in a population-based autopsy study. Neurology 60(4):652-6.
Sturchler-Pierrat C, Abramowski D, Duke M, Wiederhold KH, Mistl C, Rothacher S, Ledermann B, Burki K, Frey P, Paganetti PA, et al. 1997. Two amyloid precursor protein transgenic mouse models with alzheimer disease-like pathology. Proc Natl Acad Sci U S A 94(24):13287-92.
Stutzmann GE, Caccamo A, LaFerla FM, Parker I. 2004. Dysregulated IP3 signaling in cortical neurons of knock-in mice expressing an alzheimer's-linked mutation in presenilin1 results in exaggerated Ca2+ signals and altered membrane excitability. J Neurosci 24(2):508-13.
Stutzmann GE, Smith I, Caccamo A, Oddo S, Laferla FM, Parker I. 2006. Enhanced ryanodine receptor recruitment contributes to Ca2+ disruptions in young, adult, and aged alzheimer's disease mice. J Neurosci 26(19):5180-9.
Suzuki N, Cheung TT, Cai XD, Odaka A, Otvos L,Jr, Eckman C, Golde TE, Younkin SG. 1994. An increased percentage of long amyloid beta protein secreted by familial amyloid beta protein precursor (beta APP717) mutants. Science 264(5163):1336-40.
Tanila J., Minkeviciene R. and Dobszay MB. 2008. Fibrillar beta-amyloid associates with epileptic seizures in APPswe/PS1de9 mice and changes excitability in cortical and hippocampal neurons. Society for neuroscience annual meeting.

Terry RD, Masliah E, Salmon DP, Butters N, DeTeresa R, Hill R, Hansen LA, Katzman R. 1991. Physical basis of cognitive alterations in alzheimer's disease: Synapse loss is the major correlate of cognitive impairment. Ann Neurol 30(4):572-80.

Tomiyama T, Nagata T, Shimada H, Teraoka R, Fukushima A, Kanemitsu H, Takuma H, Kuwano R, Imagawa M, Ataka S. 2008. A new amyloid β variant favoring oligomerization in alzheimer's-type dementia. Ann Neurol 63(3):377-87.

Tomlinson B, Blessed G, Roth M. 1970. Observations on the brains of demented old people. J Neurol Sci 11(3):205-42.

Tort AB, Komorowski R, Eichenbaum H, Kopell N. 2010. Measuring phase-amplitude coupling between neuronal oscillations of different frequencies. J Neurophysiol 104(2):1195-210.

Tort AB, Komorowski RW, Manns JR, Kopell NJ, Eichenbaum H. 2009. Theta–gamma coupling increases during the learning of item–context associations. Proceedings of the National Academy of Sciences 106(49):20942-7.

Trambaiolli LR, Lorena AC, Fraga FJ, Kanda PA, Anghinah R, Nitrini R. 2011. Improving alzheimer's disease diagnosis with machine learning techniques. Clin EEG Neurosci 42(3):160-5.

Tu H, Nelson O, Bezprozvanny A, Wang Z, Lee S, Hao Y, Serneels L, De Strooper B, Yu G, Bezprozvanny I. 2006. Presenilins form ER ca 2 leak channels, a function disrupted by familial alzheimer's disease-linked mutations. Cell 126(5):981-93.

Van Vugt MK, Schulze-Bonhage A, Litt B, Brandt A, Kahana MJ. 2010. Hippocampal gamma oscillations increase with memory load. The Journal of Neuroscience 30(7):2694-9.

Vandecasteele M, Varga V, Berenyi A, Papp E, Bartho P, Venance L, Freund TF, Buzsaki G. 2014. Optogenetic activation of septal cholinergic neurons suppresses sharp wave ripples and enhances theta oscillations in the hippocampus. Proc Natl Acad Sci U S A 111(37):13535-40.

Vanderwolf CH. 1969. Hippocampal electrical activity and voluntary movement in the rat. Electroencephalogr Clin Neurophysiol 26(4):407-18.

Vanderwolf C. 2001. The hippocampus as an olfacto-motor mechanism: Were the classical anatomists right after all? Behav Brain Res 127(1):25-47.

Verret L, Mann EO, Hang GB, Barth AM, Cobos I, Ho K, Devidze N, Masliah E, Kreitzer AC, Mody I. 2012. Inhibitory interneuron deficit links altered network activity and cognitive dysfunction in alzheimer model. Cell 149(3):708-21.

Vidal M, Morris R, Grosveld F, Spanopoulou E. 1990. Tissue-specific control elements of the thy-1 gene. Embo J 9(3):833-40.

Villemagne VL, Burnham S, Bourgeat P, Brown B, Ellis KA, Salvado O, Szoeke C, Macaulay SL, Martins R, Maruff P. 2013. Amyloid β deposition, neurodegeneration, and cognitive decline in sporadic alzheimer's disease: A prospective cohort study. The Lancet Neurology 12(4):357-67.

Voytek B and Knight RT. 2015. Dynamic network communication as a unifying neural basis for cognition, development, aging, and disease. Biol Psychiatry 77(12):1089-97.

Voytek B, Kramer MA, Case J, Lepage KQ, Tempesta ZR, Knight RT, Gazzaley A. 2015. Age-related changes in 1/f neural electrophysiological noise. J Neurosci 35(38):13257-65.

Wang Z, Tan L, Liu J, Yu J. 2015. The essential role of soluble aβ oligomers in alzheimer's disease. Mol Neurobiol :1-20.

Webster SJ, Bachstetter AD, Nelson PT, Schmitt FA, Van Eldik LJ. 2014. Using mice to model alzheimer's dementia: An overview of the clinical disease and the preclinical behavioral changes in 10 mouse models. Frontiers in Genetics 5.

Westmark CJ, Westmark PR, Beard AM, Hildebrandt SM, Malter JS. 2008. Seizure susceptibility and mortality in mice that over-express amyloid precursor protein. Int J Clin Exp Pathol 1(2):157-68.

Winson J. 1978. Loss of hippocampal theta rhythm results in spatial memory deficit in the rat. Science 201(4351):160-3.

Wirths O, Multhaup G, Czech C, Blanchard V, Moussaoui S, Tremp G, Pradier L, Beyreuther K, Bayer TA. 2001. Intraneuronal aβ accumulation precedes plaque formation in β-amyloid precursor protein and presenilin-1 double-transgenic mice. Neurosci Lett 306(1):116-20.

Wolansky T, Clement EA, Peters SR, Palczak MA, Dickson CT. 2006. Hippocampal slow oscillation: A novel EEG state and its coordination with ongoing neocortical activity. J Neurosci 26(23):6213-29.

World Health Organization,. 2015. Fact sheet N°362, march 2015. .

Yanovsky Y, Ciatipis M, Draguhn A, Tort AB, Brankack J. 2014. Slow oscillations in the mouse hippocampus entrained by nasal respiration. J Neurosci 34(17):5949-64.

Younkin SG. 1995. Evidence that Aβ42 is the real culprit in alzheimer's disease. Ann Neurol 37(3):287-8.

Yuk DY, Lee YK, Nam SY, Yun YW, Hwang DY, Choi DY, Oh KW, Hong JT. 2009. Reduced anxiety in the mice expressing mutant (N141I) presenilin 2. J Neurosci Res 87(2):522-31.

Zahs KR and Ashe KH. 2010. 'Too much good news'–are alzheimer mouse models trying to tell us how to prevent, not cure, alzheimer's disease? Trends Neurosci 33(8):381-9.

Zampese E, Fasolato C, Pozzan T, Pizzo P. 2011a. Presenilin-2 modulation of ER-mitochondria interactions: FAD mutations, mechanisms and pathological consequences. Communicative & Integrative Biology 4(3):357-60.

Zampese E, Fasolato C, Kipanyula MJ, Bortolozzi M, Pozzan T, Pizzo P. 2011b. Presenilin 2 modulates endoplasmic reticulum (ER)-mitochondria interactions and Ca2+ cross-talk. Proc Natl Acad Sci U S A 108(7):2777-82.

Zatti G, Burgo A, Giacomello M, Barbiero L, Ghidoni R, Sinigaglia G, Florean C, Bagnoli S, Binetti G, Sorbi S. 2006. Presenilin mutations linked to familial alzheimer's disease reduce endoplasmic reticulum and golgi apparatus calcium levels. Cell Calcium 39(6):539-50.

Zeineh MM, Engel SA, Thompson PM, Bookheimer SY. 2003. Dynamics of the hippocampus during encoding and retrieval of face-name pairs. Science 299(5606):577-80.

Zetterberg H, Tullhog K, Hansson O, Minthon L, Londos E, Blennow K. 2010. Low incidence of post-lumbar puncture headache in 1,089 consecutive memory clinic patients. Eur Neurol 63(6):326-30.

Zhang C, Wang H, Wang H, Wu M. 2013. EEG-based expert system using complexity measures and probability density function control in alpha sub-band. Integrated Computer-Aided Engineering 20(4):391-405.